The Thesis Committee for Yushan Li
Certifies that this is the approved version of the following Thesis

ASSESSING AN OFFSHORE CARBON STORAGE OPPORTUNITY AT CHANDELEUR SOUND, LOUISIANA

APPROVED BY
SUPERVISING COMMITTEE:

Dr. Susan Hovorka, Supervisor

Dr. Carlos Uroza, Reader

Ramon Gil-Egui, Reader

ASSESSING AN OFFSHORE CARBON STORAGE OPPORTUNITY AT CHANDELEUR SOUND, LOUISIANA

by

Yushan Li

Thesis

Presented to the Faculty of the Graduate School of

The University of Texas at Austin

in Partial Fulfillment

of the Requirements

for the Degree of

Master of Science in Energy and Earth Resources

The University of Texas at Austin

May 2023

Dedication

This paper is dedicated to my family who are thousand miles away in China, thank you for the unlimited love and support, I have missed y'all very much.

Acknowledgements

Disclaimer: "This report was prepared as an account of work sponsored by an agency of the United States Government. Neither the United States Government nor any agency thereof, nor any of their employees, makes any warranty, express or implied, or assumes any legal liability or responsibility for the accuracy, completeness, or usefulness of any information, apparatus, product, or process disclosed, or represents that its use would not infringe privately owned rights. Reference herein to any specific commercial product, process, or service by trade name, trademark, manufacturer, or otherwise does not necessarily constitute or imply its endorsement, recommendation, or favoring by the United States Government or any agency thereof. The views and opinions of authors expressed herein do not necessarily state or reflect those of the United States Government or any agency thereof." This material is based upon work supported by the Department of Energy under Award Number DE- FE0031558.

I would like to express my sincere gratitude to the Gulf Coast Carbon Center for granting me the opportunity to work as a graduate research assistant. I extend my appreciation to my thesis committee members, especially Dr. Susan Hovorka, my supervisor, for her unwavering dedication in ensuring the success of her students. Her enthusiasm for CCS has been a great source of motivation for me to deepen my understanding of this field. I am also deeply grateful to Dr. Carlos Uroza, my reader, for imparting valuable knowledge in geology and for his mentorship throughout my research. I am indebted to him for his guidance and for always being willing to lend a helping hand, not to mention the coffee. I would like to express my appreciation to Ramon Gil-Egui for his support and encouragement, as well as for providing me with opportunities to present posters, and to play ping-pong.

I am grateful to Marcie Purkey Phillips for introducing me to the Chandeleur project and for her diligent efforts in bringing it to fruition. I also want to acknowledge the outstanding technical support provided by Dallas Dunlap, my ultimate technical support, who was always available to assist me with any software-related issues. I extend my gratitude to Charlie for his assistance with well log interpretation, which was instrumental in moving my research forward. I would also like to thank Dr. Shuvajit Bhattacharya for his invaluable contribution in petrophysical analysis, and Dr. Hongliu Zeng for teaching me the theoretical aspects of stratal slicing, which have been immensely helpful. Lastly, I would like to express my appreciation to Ramon Trevino, Dr. Alex Bump, Dr. Seyyed Hosseini, Mike DeAngelo, Dr. Hailun Ni, and all the staff at GCCC who have contributed significantly to my growth and learning in this field.

I also want to thank my friends Hazal, Angela, Edna, Katherine, Shadya, Ismail, Dan, Tara, Maria, William, and many more of them, for struggling together, but always having consistent lunch plans. Lastly, I am grateful to my boyfriend Bryan, who providing me with daily encouragement that helped me stay motivated and focused.

Abstract

ASSESSING AN OFFSHORE CARBON STORAGE OPPORTUNITY AT CHANDELEUR SOUND, LOUISIANA

Yushan Li, M.S. E.E.R.

The University of Texas at Austin, 2023

Supervisor: Susan D. Hovorka

Carbon Capture and Storage (CCS) is considered a crucial technology for climate change mitigation. Its primary objective is to reduce CO_2 emissions caused by human activities by capturing gas from large point sources or from direct air capture and injecting it into deep geologic formations. This study focuses on the geological characterization and CO_2 storage capacity estimation for an offshore state water site – Chandeleur Sound, Louisiana. Form literature review, the storage window is narrowed to Middle and Upper Miocene. 3-D seismic data was used for fault and horizon picking, stratal slicing and attribute mapping. Three attributes/methods were used in the stratal slices: Sum Negative Amplitude, RMS amplitude, and Spectral Decomposition. The slices give a qualitative overview of the depositional trends and faulting in Chandeleur Sound and concluded that the ideal storage intervals include the Upper Miocene in the southern area, the upper part of Middle Miocene, and a massive channel system near the top of Upper Miocene which is likely to be a deposit from the paleo Tennessee River. Well log correlation was used to identify seven reservoir zones. Detailed reservoir properties were defined for these zones.

The thickest net sand interval within the Chandeleur Sound area is found in the center. Static and dynamic storage capacity calculations estimate a total storage capacity

of 306 to 2,000 million metric tons. of CO_2, depending on boundary condition. The value of 306 Mt is the most realistic and is used for source-sink matching.

Chandeleur Sound is close to Louisiana Chemical Corridor (LCC) and has plenty of point sources for CO_2 supply. The costs associated with carbon capture, transport and storage and were considered. Pipeline is the only transport scenario considered for large volumes that must be transported on land and then into shallow marine settings. CO_2 pipeline regulations include both federal and state level jurisdiction. Pipeline costs estimation using FECM/NETL CO_2 Transport Cost Model and Terrain-based approach concluded that a 20 inches pipeline from the carbon gathering hub to the injection site would have a construction cost from $140 million to $1.16 billion in 2023's dollars.

Table of Contents

List of Tables

List of Figures

1. Introduction

1.1. Overview of Carbon Capture and Storage

Carbon Capture and Storage (CCS) has been proposed by many groups as a promising solution to mitigate climate change by providing a secure and permanent mechanism to store carbon dioxide in deep underground formations (National Petroleum Council (NPC), 2019; Global CCS Institute, 2022). The goal of CCS is to capture CO_2 from both the atmosphere and from stationary sources of emissions - such as power generation plants that burn fossil fuels - to prevent the gas from entering the atmosphere. NPC in 2019 concluded that around 50% of U.S. greenhouse gas emissions came from 6,500 large stationary emitters, which produced 2.6 billion metric tons of CO_2 per year (NPC, 2019). In the short term, CCS can contribute to a reduction in the amount of carbon dioxide released into the atmosphere. In the long term, after CO_2 emissions are able to be significantly reduced, CCS technologies would allow the annual amount extracted from the atmosphere to be greater than the amount released, contributing to 'negative emissions' (NPC, 2019; Global CCS Institute, 2022).

Under the Paris Agreement, the International Energy Agency (IEA) outlines two different scenarios: The States Policy Scenario and the Sustainable Development Scenario. Stated Policy Scenario (STEPS) scenario, which aims for a 55% carbon dioxide emission reduction by 2030 compared to 1990s levels, assumes the energy demand will rise by 1% per year to 2040 (IEA, 2019). In the Sustainable Development Scenario (SDS), IEA concluded that CCS will account for 15% of the carbon reduction by the end of 2070 compared to STEPS (IEA, 2019). With the continuous increase in global population there is an inherent necessity for more energy production, and CCS provides a solution to reduce stationary emissions (NPC, 2019). The Intergovernmental Panel on Climate Change

(IPCC) concluded that the costs of maintaining atmospheric CO_2 levels consistent with holding average global temperatures at 2°C above pre-industrial levels, decreased by 50% with CCS implementation (IPCC, 2014). However, there were only 10 CCS facilities with a CO_2 storage capacity of 25 million metric tons per annum (Mtpa), which means they offset less than 1% of the emissions from large stationary sources (NPC, 2019). More CCS projects will be needed to sustain the demand of energy from fossil fuels while achieving carbon reduction under IEA's guidelines.

A CCS supply chain includes three major components: capture and separation, transport, and geological storage (NPC, 2019). The first step, carbon capture, involves capturing CO_2 from point sources or directly from the air followed by separation and purification. Then, during transportation, compressed CO_2 is sent to storage sites via pipeline, ship, truck, or other modes. Finally, supercritical CO_2 is injected into a permeable reservoir (Figure 1). Each of these steps require detailed engineering, financial evaluations, and environmental considerations as they are technologically sophisticated and expensive.

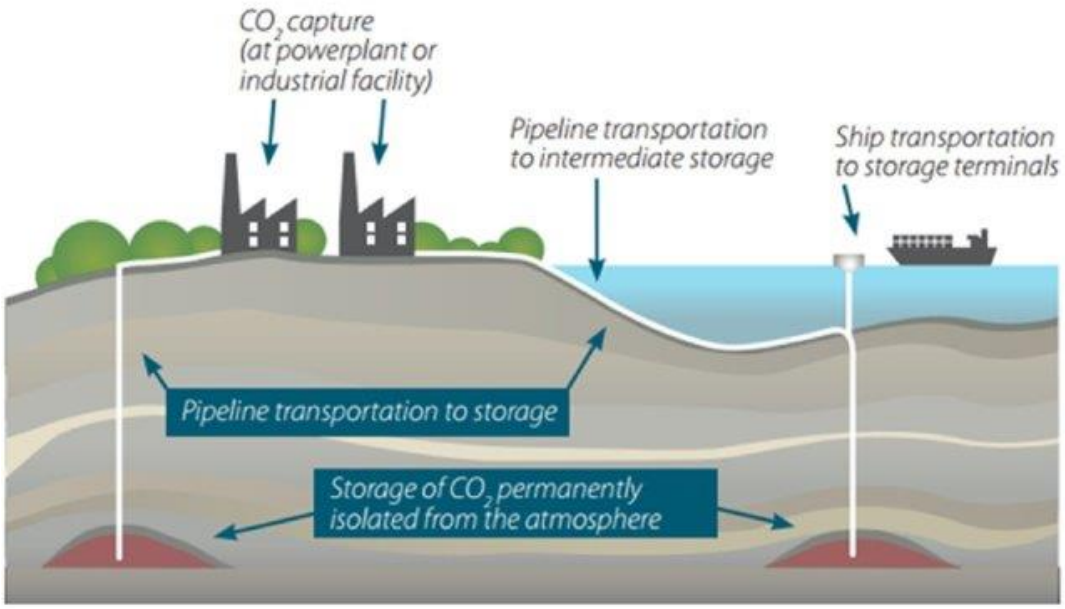

Figure 1. Illustration for CCS (Choudhary, 2016).

Nearly 45 million tonnes of CO_2 have been captured in the year 2021 (IEA, 2022). NPC concluded that capture, the first step, is the most expensive portion of the whole CCS project due to the equipment needed for gas separation (NPC, 2019). The DOE categorizes carbon capture for power plants into post-combustion, pre-combustion, and oxy-combustion capture. Post-combustion is the most widely used and applicable to low CO_2 concentration exhaust from natural gas and coal-fired plants. Pre-combustion and oxy-combustion have higher capital costs but offer advantages such as higher reduction of NOx emissions and purer CO_2 stream, respectively (DOE, n.d.; NPC, 2019).

After the CO_2 is captured, it would be liquefied and transported to the storage site for injection. As mentioned above, methods used for transport include pipeline, ship, rail, and truck. Pipelines are the most common way for CO_2 transport and will be discussed further in this research. Ships are proposed for use in offshore CCS projects, especially in Norway. Rail may be used for longer distances as a more cost-effective method of transport

while trucks may be preferred in shorter distances, but using these methods may not yield profits when transporting large volumes. Ultimately, the choice of transportation will vary depending on many factors such as distance, volume, availability of existing infrastructure, disturbance to nearby communities.

Finally, the carbon dioxide will be sequestered in its supercritical state. Supercritical CO_2 is a state in which the CO_2 exists in both a liquid and gas like state making it highly compressible, less viscous, and denser than gas. In this state, CO_2 takes up less space than gas and will allow for more efficient injection and storage. In order to maintain the supercritical state, CO_2 must be stored where the temperature is greater than T_c =31.1 °C and pressure greater than P_c =7.38 MPa (critical point) under normal atmospheric conditions (Bachu, 2003). With a geothermal gradient of 20 - 25 °C/km (Holloway and Savage, 1993; Nagihara and Smith, 2008; Christie and Nigihara, 2016), the reservoir should be at least 800 meters (~ 2,700 feet) deep. Target injection reservoirs include subsurface saline formations, coal beds, depleted oil and gas fields, and mature oil production fields for enhanced oil recovery (EOR) (Global CCS Institute, 2018). Features a reservoir must have include good porosity and permeability for CO_2 to flow; reasonable volume for a large amount of CO_2 to be stored, adequate features to ensure containment of CO_2.

In the US, as accordance with the Environmental Protection Agency (EPA), a Class VI permit needs to be obtained for the wells used for geological CO_2 storage. The main goal of a Class VI permit is to protect the underground sources of drinking water (USDW) and prevent any risk related to the storage. Monitoring is conducted during and after the injection with technologies such as soil gas detection, remote sensing, and 4-D geophysical surveys proposed (Jenkins et al., 2015). For offshore storage sites, which do not affect USDW, monitoring CO_2 plume and pressure shall still be required.

Interest in CCS has increased in recent years as a technology for climate change mitigation which requires detailed analysis of site-specific characteristics that would affect the storage value of each project. The goal for this research is to assess the geological viability of CCS in a previously unstudied location – Chandeleur Sound, Louisiana, by using well log and seismic data to identify suitable intervals in order to estimate the total capacity for CO_2 storage, and to evaluate the economic viability by estimating capital costs of the CO_2 transport via pipeline, a crucial step in the CCS supply chain.

1.2. PREVIOUS WORK

Many studies have been done on CO_2 storage capacity estimations specific to a single site or to a depositional environment (Dismukes et al., 2017; Beckham, 2018; Ruiz, 2019; Garcia, 2019; Ulfah, 2021). Capacity is estimated in two ways: static, which makes a simple calculation of the pore volume from physical properties based on an assumed pore volume occupancy, and dynamic, which takes into consideration pressure and injection rate limitations. Here I am giving a few examples of capacity studies near the Chandeleur Sound study area. Dismukes et al. (2017) proposed an onshore CCS project which integrated sources from the Louisiana Chemical Corridor (LCC) to Bayou Sorrel and Paradis fields. They estimated a dynamic storage capacity range of 94 to 132 million metric tons in both fields (Dismukes et al., 2017). They also investigated carbon sources, transportation, economic feasibility and legal issues. Beckham (2018) used a high-resolution geologic model, along with outcrop and subsurface data to analyze the CCS potential in deltaic depositional environments. Ruiz (2019) and Garcia (2019) analyzed two sites located at High Island field, offshore Texas State waters. They both conducted in depth research on geological characterizations, seismic and well log analysis, geo-cellular modeling, and calculated the storage capacity for both fields (Ruiz, 2019; Garcia, 2019).

Ulfah (2021) also used 3D seismic and well log data for an anticline structure located in offshore Texas and used sophisticated models to make capacity estimations and modeled the pressure plume.

I have followed a similar approach on an offshore storage site in Chandeleur Sound. Chandeleur Sound is located in state waters offshore Southeast Louisiana (Figure 2), along the Gulf of Mexico (GoM).

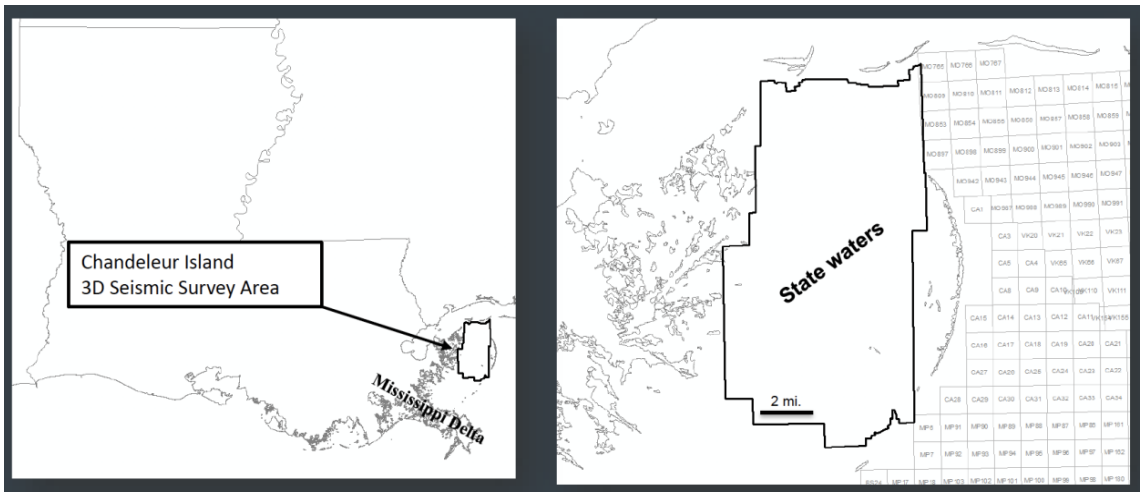

Figure 2. The location of study area – Chandeleur Sound 3-D seismic volume (Phillips, 2022).

2. Research Background

2.1. Geological Setting of the Chandeleur Study Area

Chandeleur Sound is located within the northern Gulf of Mexico Basin continental shelf. The origin of the Gulf of Mexico basin dates back to the late Triassic period, around 200 million years ago, when the supercontinent Pangaea began to break apart as the North American and South American plates pulled away from each other (rifting) (Martin, 1978; Salvador, 1987). As a result, a series of extensional faults developed in the region which contributed to create the basin with sediment input from the surrounding land. The basin has undergone many changes over its geological history, including infilling, subsidence, uplift, and salt withdrawal that created numerous faults and folds.

The Gulf of Mexico Basin is an important source of oil and natural gas, as well as minerals such as salt and sulfur. With the growth of the CCS industry, the shelf area of the Gulf of Mexico basin represents an attractive region to store vast amounts of CO_2 in sand-prone reservoirs (Meckel et al., 2018).

In the northern Gulf of Mexico, sediments were sourced from erosion of the North American continent, transported by rivers and deposited in fluvial, deltaic, shelf, slope and deep-water environments and consist of interbedded sands and shales (Snedden and Galloway, 2019). Throughout the Cenozoic era, large volumes of sediments brought by eight major fluvial systems (Figure 3) entered the Gulf of Mexico Basin from the North American Continent, resulting in large fluvial and deltaic systems, and thicker sediment accumulation (Galloway, 2008; Galloway et al., 2011). Sediments form wedge-shaped bodies that are shingled, with younger wedges deposited seaward of older wedges (Figure 4; Snedden and Galloway, 2019).

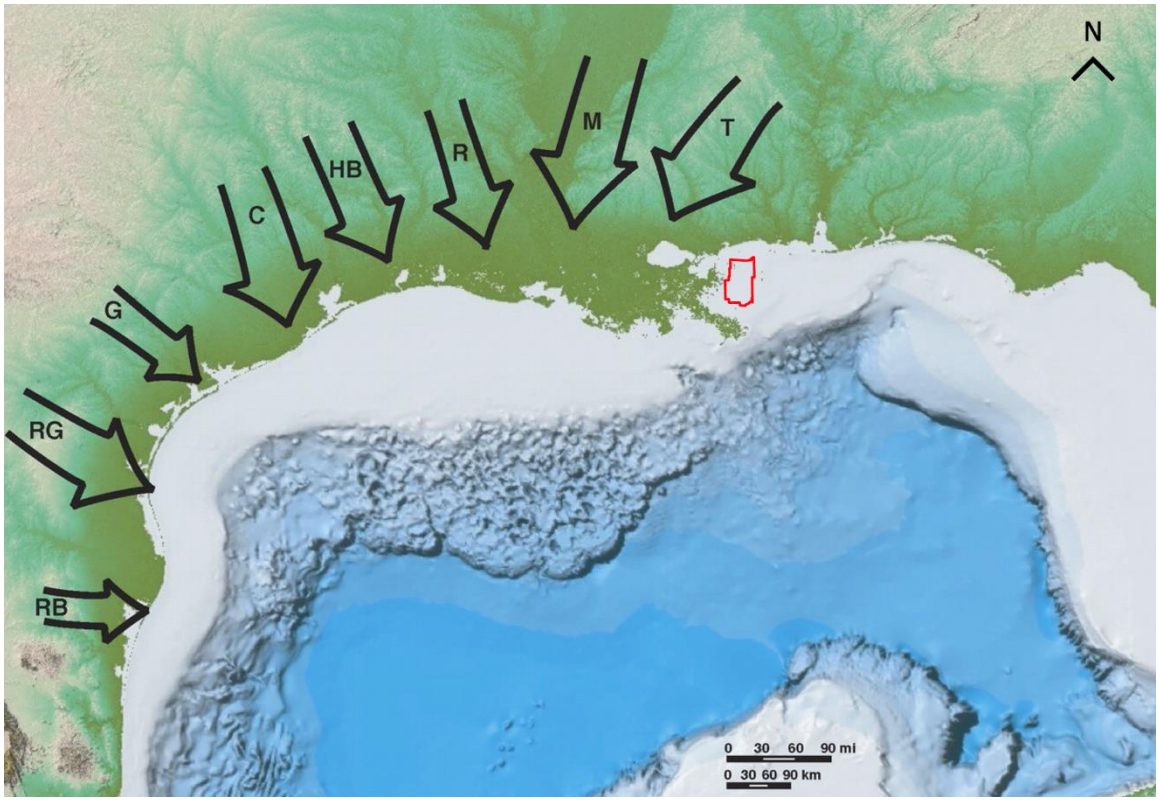

Figure 3. Geographic location of the Cenozoic fluvial input axes around the northern Gulf of Mexico (Galloway, 2008). Modified from Galloway et al., 2011. RB–Rio Bravo; RG–Rio Grande; G–Guadalupe; C–Colorado; HB–Houston-Brazos; R–Red; M–Mississippi, T–Tennessee.

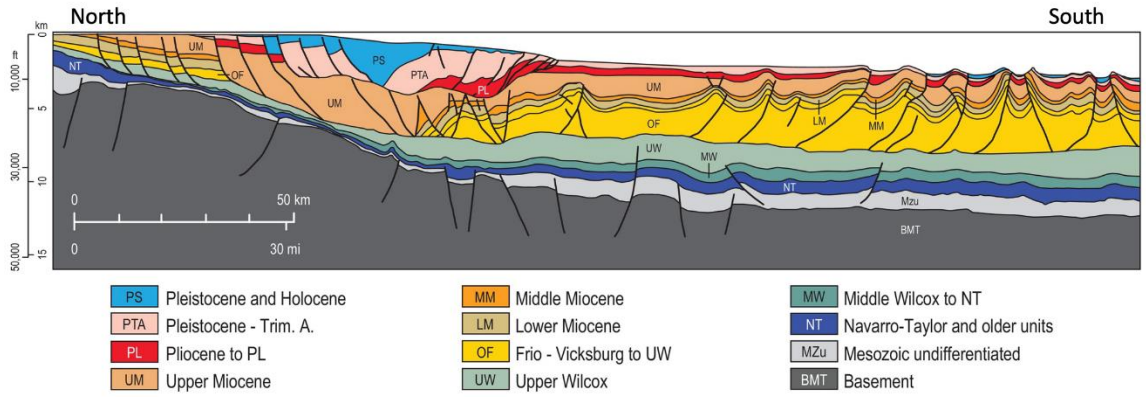

Figure 4. Gulf of Mexico Cenozoic cross section (Snedden and Galloway, 2019).

Considering the CO_2 supercritical depth, the ideal storage window in much of the GoM shelf region has been narrowed down to the Miocene probably Upper Oligocene in some areas While Chandeleur Sound is located east to the eight fluvial systems in Figure 3, the possible sediment supplier would be paleo Mississippi and Tennessee River.

The Lower Miocene (LM) is divided by two maximum flooding surfaces, into two lower sequences LM1 and LM2 (Snedden and Galloway, 2019). During the early Miocene, a substantial amount of sediment was brought by the paleo Rio Grande, Mississippi River and Red River, creating North Padre Delta, Calcasieu and Mississippi Delta, and Central Gulf Basin Floor Apron (Galloway et al., 2000). However, these fluvial systems mainly fed the northwest Gulf of Mexico Basin, leaving southeast Louisiana (where Chandeleur Sound located) starved. During both LM1 and LM2, shelf margin directly cut through Chandeleur study (Snedden and Galloway, 2019). Shore zone system and progradational slope apron contribute to the depositional facies in Southeast Louisiana during LM1, with muddy carbonate shelf and slope ramp intersecting Chandeleur Sound (Snedden and Galloway, 2019). Therefore, for Chandeleur Sound, Lower Miocene is not ideal for CO_2 storage. Figure 5 shows the map of paleogeography and facies of LM2.

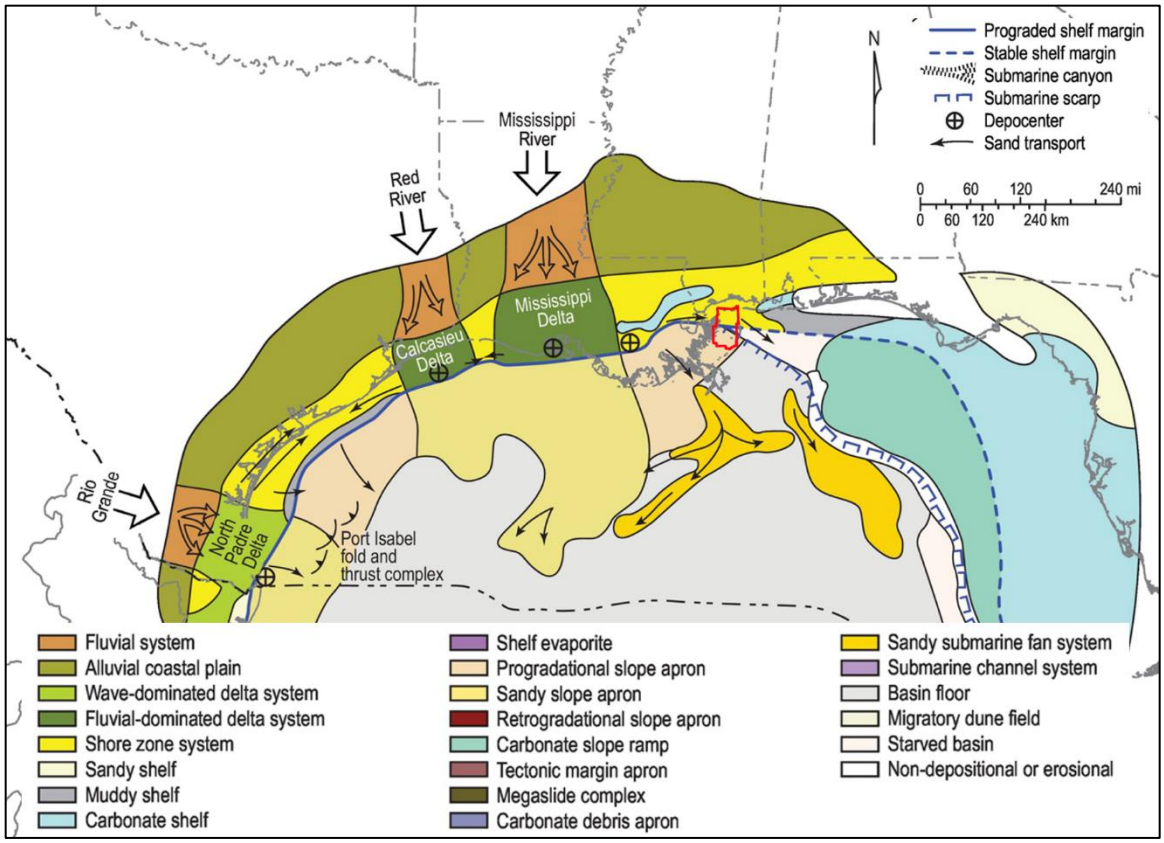

Figure 5. Paleogeography and facies of Lower Miocene 2, northern Gulf of Mexico. Red rectangle indicates Chandeleur Sound study area. Modified from Snedden and Galloway (2019).

It is believed that during the deposition of the Middle Miocene (MM), three major rivers – Guadalupe, Mississippi and Tennessee entered the gulf and a large depocenter was formed at the northern Gulf of Mexico (Galloway et al., 2011; Snedden and Galloway, 2019). The shelf margin was still positioned within the Chandeleur seismic survey area but has prograded basin-ward (Figure 6). The regional study also shows that during MM, Chandeleur overlapped with the shore zone, sandy shelf system and shelf-fed depositional coastal plain (Snedden and Galloway, 2019). The sandy zone would be favorable for CO_2 storage.

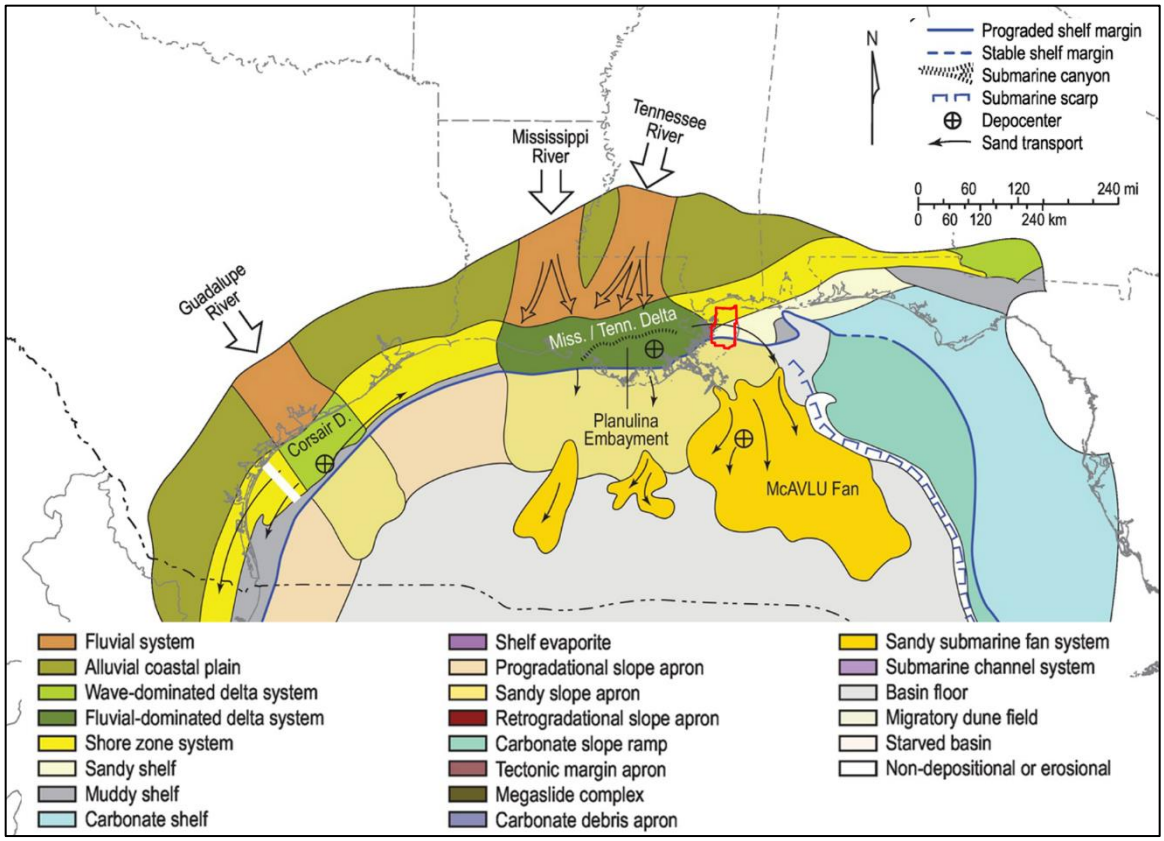

Figure 6. Paleogeography and facies of Middle Miocene, northern Gulf of Mexico. Red rectangle indicates Chandeleur Sound study area. Modified from Snedden and Galloway (2019).

During the Upper Miocene (UM), the shelf margin continued prograding basinward to south of the Chandeleur seismic survey (Figure 7) (Snedden and Galloway, 2019). Two principal fluvial axes (Mississippi and Tennessee River) persisted through the entire Upper Miocene deposode and provided a substantial amount of the sediment that infilled the central Gulf of Mexico. The slope and apron at the south of the survey transformed into a fluvial-dominated delta system, while the north side is still part of the shore zone (Wu, 2004; Snedden and Galloway, 2019). It is expected to see sandy deltaic features within UM in the southern Chandeleur Sound, and these features could be reservoirs for CO_2 storage.

Therefore, the storage window has been narrowed down to Middle and Upper Miocene. Despite the possibility of sand-prone reservoirs formed by fluvial deltaic systems, CO_2 storage in MM and UM is likely to be feasible because of following conditions:

1. The Middle and Upper Miocene are characterized as sand-rich deltaic have interbedded mudstones which could be used for seals. (Snedden and Galloway, 2019; Bump et al., 2021). Numerous oil and gas fields have been discovered in the areas near Chandeleur Sound, where the main production interval is Miocene (IHS Markit, n.d.). Oil and gas discovery likely indicate good reservoir quality and capable seals. Within the Chandeleur Sound seismic survey, many wells were drilled and provides good well control for seismic interpretation and reservoir quality evaluation.

2. The top of the overpressure in the Chandeleur area (Figure 8) has also been defined using the regional distribution of depth contours of the 0.70 psi/ft pressure gradient proposed by Burke et al. (2012). In addition to the depositional advantages, Most of the Upper Miocene and Middle Miocene are not overlapped with the overpressure region, which leaves most of the intervals available for CO_2 storage analysis.

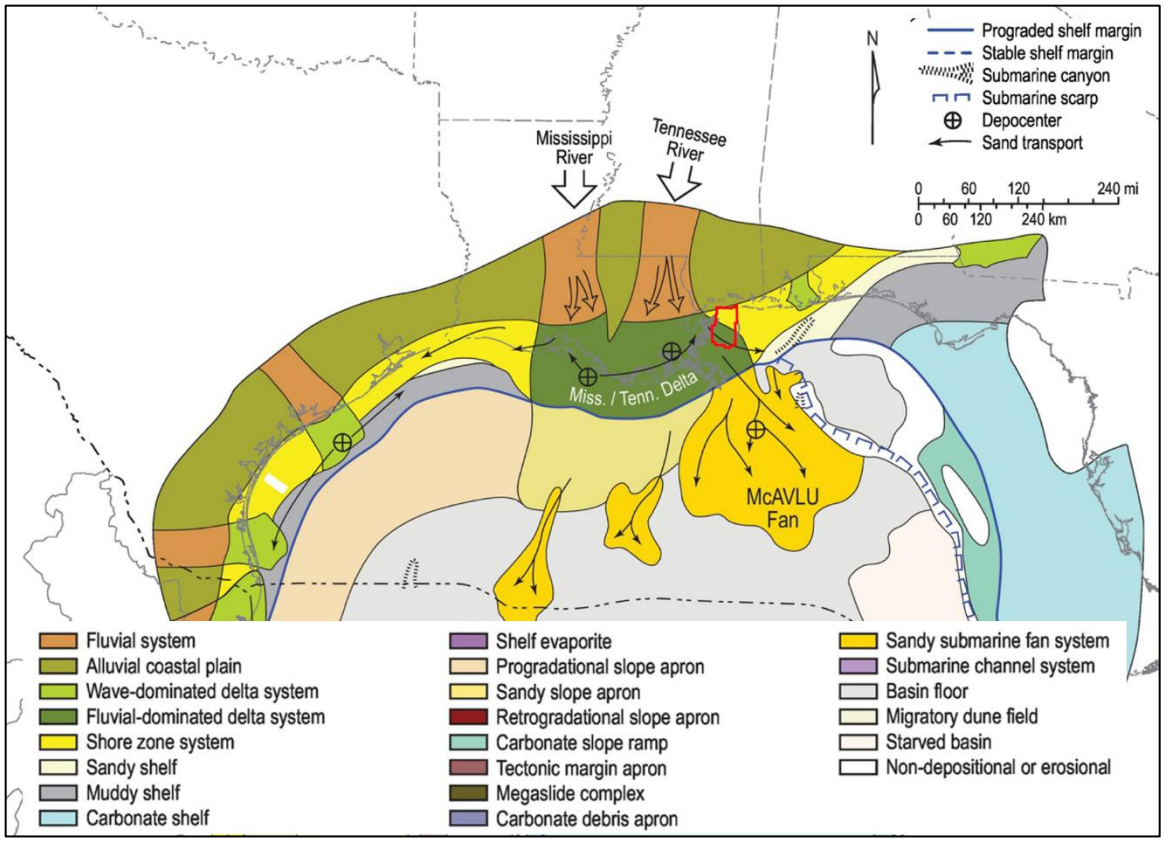

Figure 7. Paleogeography and facies of Upper Miocene, northern Gulf of Mexico. Red rectangle indicates Chandeleur Sound study area. Modified from Snedden and Galloway (2019).

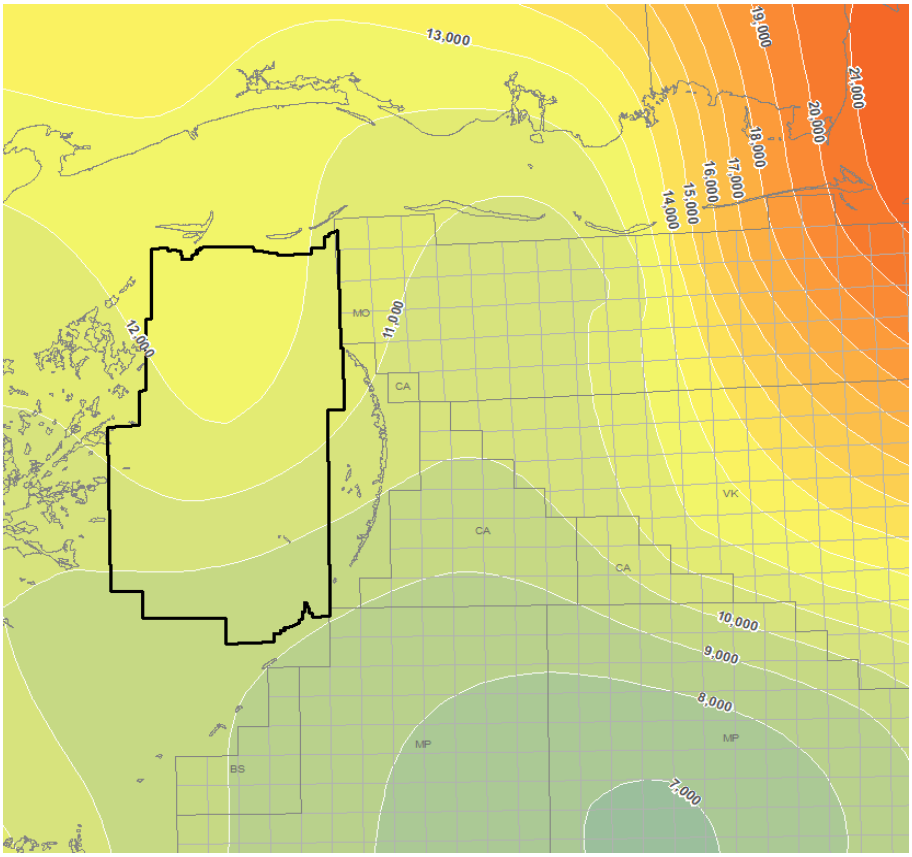

Figure 8. Map of overpressure, modified by Phillips (2022) from Burke et al., 2012.

2.2 Recent Findings on Chandeleur Sound

Carbon storage in Chandeleur Sound is favorable due to the abundance of CO_2 sources. According to the EPA, the state of Louisiana reported 128 million metric tons of CO_2 emission throughout 396 facilities in 2020 (EPA, 2021). The top 4 emitters, and their respective amounts of CO_2 emitted, were reported as follows: chemical plants (39 million metric tons), power plants (34 million metric tons), refineries (26 million metric tons), petroleum and natural gas systems (21 million metric tons) (EPA, 2021). Among all the facilities, two chemical plants have collected and reused the CO_2 on-site for other productions. Two other facilities have collected the emitted gas and transferred it to other

locations for reusing or for sequestration. One facility did both (EPA 2021). Geographically, the emitters clustered in New Orleans – Metairie, Baton Rouge, Lafayette, and Lake Charles metropolitan areas in Southern Louisiana. Located within the New Orleans – Metairie metropolitan area, Chandeleur Sound is close to the major emitters along the Louisiana Chemical Corridor (LCC), which makes it a good storage site. However, LCC is not the only industrial cluster for stationary carbon sources. The emitters in the whole state of Louisiana, as well as nearby sources in Mississippi, are all taken into consideration.

The stratigraphy of Chandeleur Sound during the Cenozoic era has been interpreted by the Gulf Basin Depositional Synthesis (GBDS) researcher Marcie Philips (Figure 9). From the seismic cross section, it is clear that the Paleocene and Eocene are undifferentiated. The Lower Miocene (LM1 and LM2) is condensed while the Middle and Upper Miocene intervals are sand prone. Recently, a submarine canyon, named Chandeleur Canyon, was discovered in Chandeleur Sound within the Middle Miocene (Phillips, 2022). Submarine Canyons are sediment conduits from the shelf to the slope and basin floor, where some are associated with fluvial channel systems up-dip of the canyons (Fisher et a., 2021). In our case, the canyon is likely created by sediment instability at the shelf margin (Uroza, personal communication, 2022; Coleman et al., 1983). Within the canyon fill, sediment moved by mass wasting was deposited from the shelf margin area to fill the canyon. This type of depositional setting could result in a mix of lithologies with high heterogeneity in the stratigraphic section of interest, making the estimation of porosity, permeability, and CO_2 storage capacity more difficult. Wells that penetrated through the Upper and Middle Miocene canyons also show shaly features with less sand compared to the non-canyon environments. Therefore, the stratigraphic section covered by Chandeleur

Canyon in the Middle Miocene is not under consideration as a storage reservoir in this research.

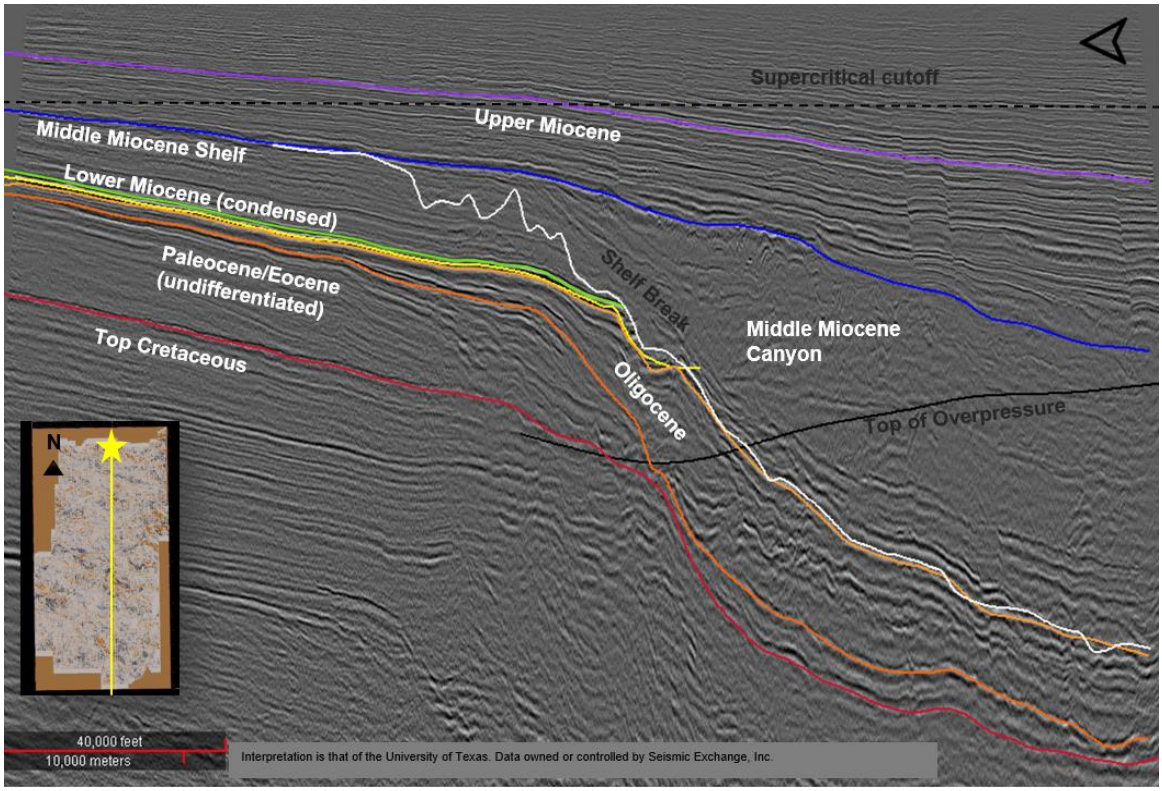

Figure 9. Stratigraphy interpretation on Chandeleur Sound 3-D seismic survey inline cross section during Cenozoic (Phillips, 2022). Data owned and controlled by SEI Inc, Interpretation by University of Texas at Austin.

2.3. HYDROCARBON PRODUCTION OVERVIEW

Chandeleur Sound is located in Louisiana's State waters with 170 wells drilled within the Chandeleur Sound seismic survey area from the 1960s to early 2000s. Among them, 34 wells have natural gas production and 29 of them produced from the Middle or Upper Miocene while 5 wells produced from Pleistocene or Pliocene (IHS Markit, n.d.). The total production from the 34 wells was 57.7 BCF (billion cubic feet) which means on

average, the cumulative production from each well was 1.7 BCF. Figure 10 shows the gas fields distributions. Well 17727204200000 has the largest gas production of 5.79 BCF, which is nearly three times greater than the average estimated value of 1.7 BCF from above, and 1,172 BBLs of oil. Annual gas production (Figure 11) shows that the annual production rate for the whole Chandeleur Seismic Survey was less than 5 BCF/yr from late 1960s to 2002 but peaked in Year 2003 at around 13 BCF/yr, and then decreased rapidly until depletion in 2011 (IHS Markit, n. d.).

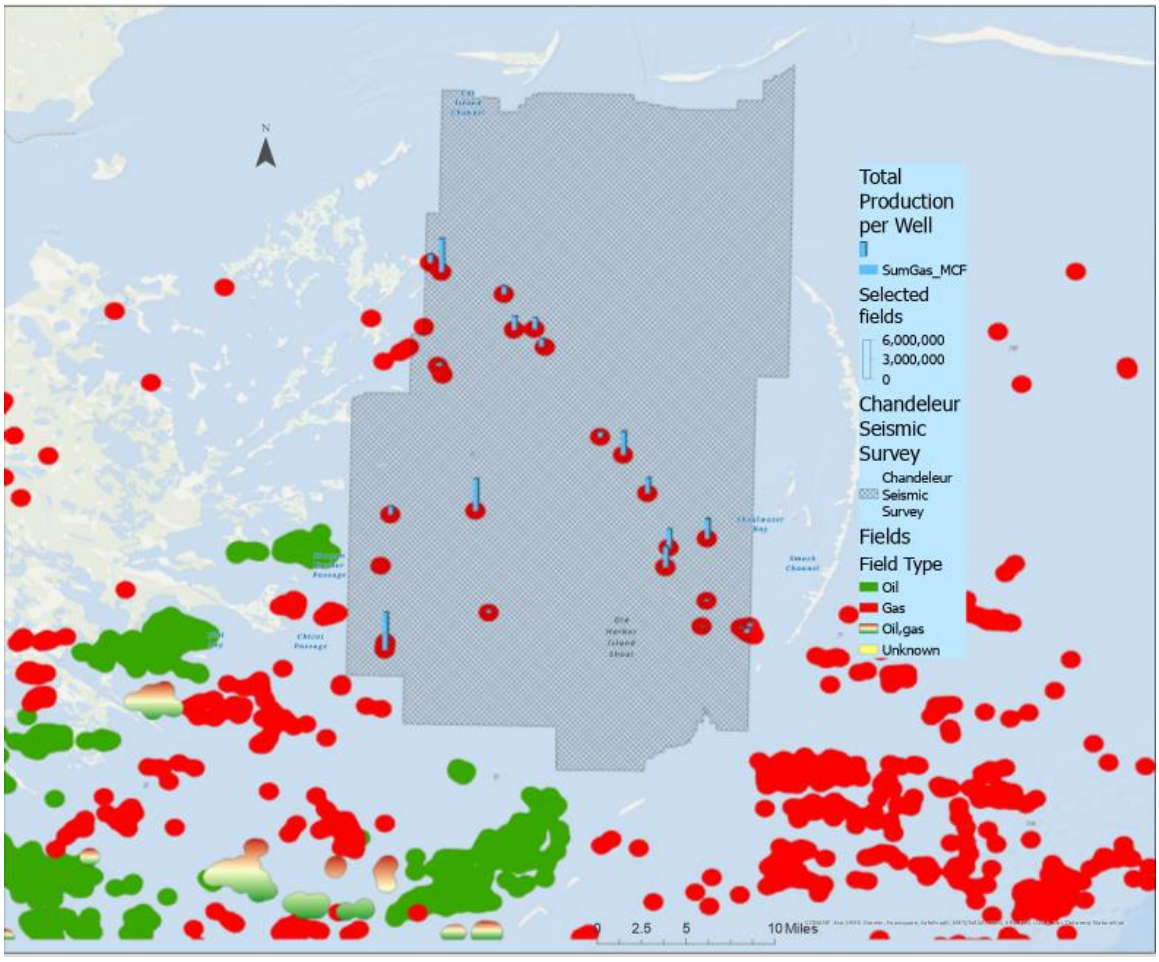

Figure 10. Hydrocarbon production within and near Chandeleur Sound seismic survey (Data from IHS Markit).

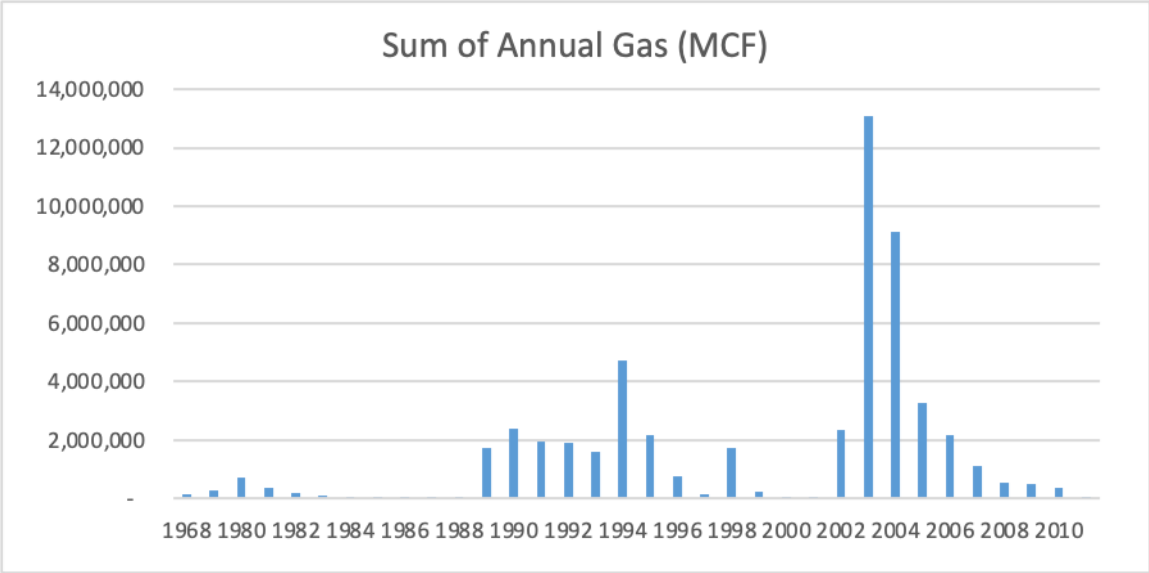

Figure 11. Annual natural gas production trend of Chandeleur Sound from 1968 to 2010 (IHS Markit, n.d.)

The hydrocarbon production within the Chandeleur seismic survey area is considered low compared to nearby fields such as the Eloi field, Chandeleur Sound Block 25, and Stuart Bluff. The presence of gas production proves that the petroleum system works, at least in the regions with proven gas production, within Chandeleur Sound. Prior to 1999, it was assumed that hydrocarbon exploration within Chandeleur Sound relied on 2-D seismic lines and well logs. 2-D seismic data lacks the ability to capture fine details and often fails to show out-of-plane structures. Considering this and the number of dry holes in Chandeleur Sound, it is possible that the sparse accumulation of gas production is the result of the lack of the structural traps, or lack of high-quality seals that are extensive enough to retain large amounts of gas from vertical leakage. Additionally, from the initial seismic analysis from Phillips (2022), there are no proven stratigraphic traps or structural boundaries within the seismic survey. There has been no analysis on the offset of the faults. Chandeleur Sound in the Middle Miocene Shelf and Upper Miocene shows a gently basin-

ward-dipping structure which leaves the possibility that hydrocarbon may have migrated landward until encountering a structural trap which is not under the Chandeleur seismic survey. These are risks that need to be carefully evaluated to ensure a well contained carbon storage project and will be further discussed in Section 3.3, Trapping Mechanism.

3. Geological Characterization and Storage Capacity Estimation

The first main goal for this research is to estimate the storage capacity for Chandeleur Sound. Two datasets - 3D seismic survey and well logs are being studied and interpreted following the workflow:

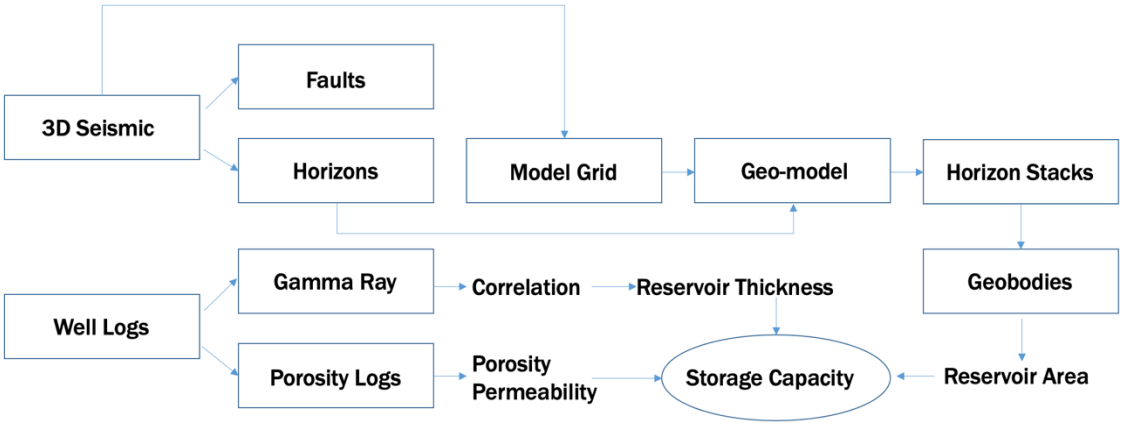

Figure 12. Workflow for storage capacity estimation (this work).

Several software was used for this section. Horizons and faults picking, and well logs correlation was done using Landmark Decision Space® (Haliburton software). Eliis's PaleoScan was used for creating a Model Grid, a Geo-model, Horizon Stacks, and Geobodies. Noted that the Geo-model was a Relative Geological Time Model, auto generated from seismic volume in PaleoScan to perform horizon stacking on, it is not a 3-D Geological Model. The dynamic storage capacity sensitivity analysis was run on EASiTool, a tool developed by GCCC (Hosseini and Ganjdanesh, 2018).

3.1. 3D Seismic Analysis

The 3-D seismic survey in time within the Chandeleur Sound area was leased from Seismic Exchange, Inc (SEI), it was converted to depth-structured models and interpreted by previous researchers in BEG. Faults and stratigraphic horizons were interpreted by

Marcie Philips and Dallas Dunlap from BEG. The interpretations were then used in this work to locate geological horizons (i.e., Top of Miocene, etc.). The whole survey is around 660 square miles in size. I have used the time-structured seismic volume for interpretations used depth-structured model to tie with the wells. The volume can be viewed at inline and crossline.

3.1.1. Faults and Horizon Picking

28 faults have been picked within the Chandeleur 3D seismic survey (Figure 13). All of them are interpreted as normal faults and cluster at the shelf edge. There are also faults on the south side of the survey. Most of the faults are stretching alongside the shelf break (Northwest to Southeast). Like many other faults in Gulf of Mexico, faults in Chandeleur Sound tend to be parallel with the shoreline.

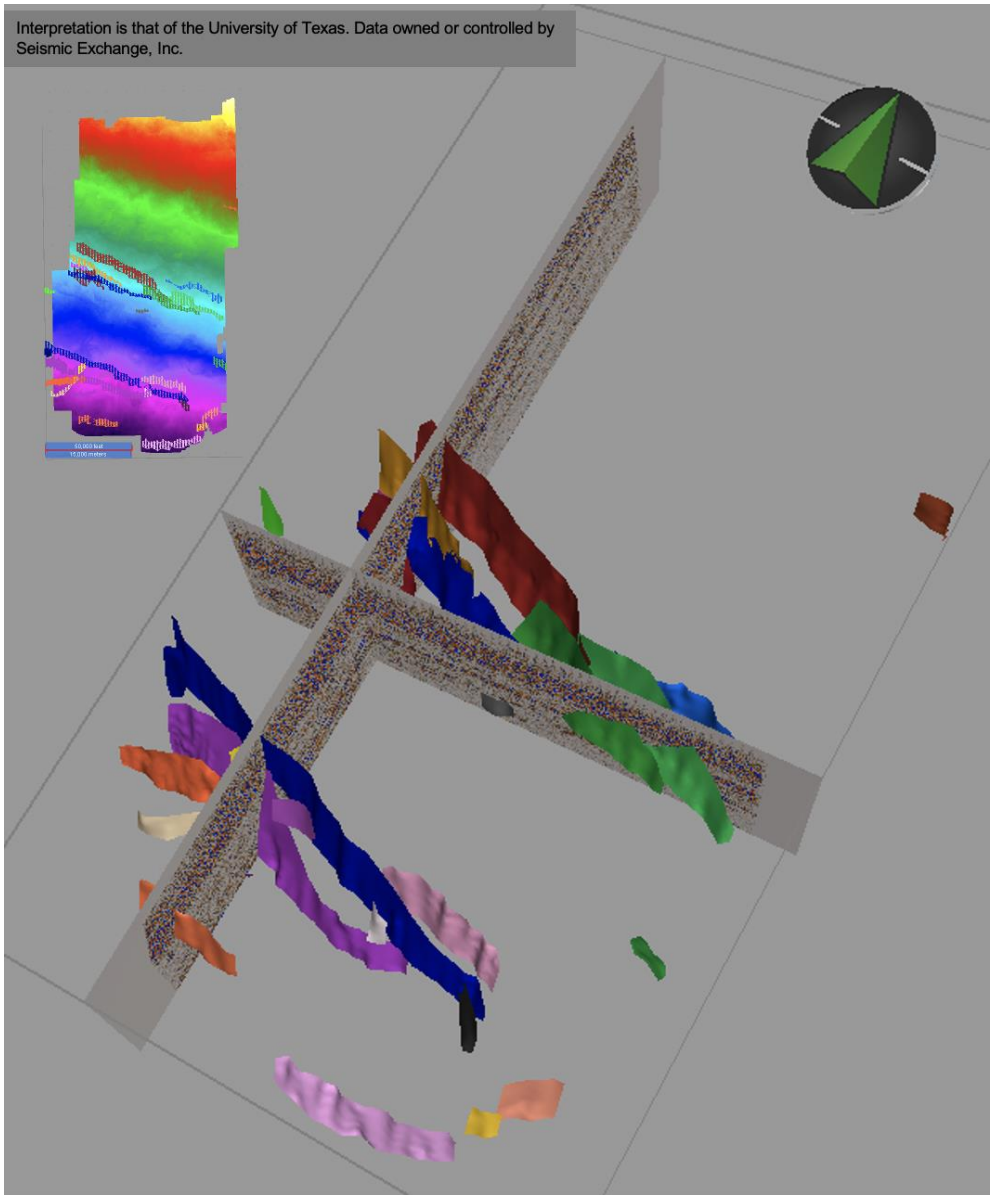

Figure 13. Faults within Chandeleur Sound Seismic Survey. Data owned and controlled by SEI Inc, Interpretation by University of Texas at Austin.

Three horizons were picked based on biostratigraphic zonation in ten wells. Ten wells with biostratigraphic markers were used for age definition interpretations (Phillips, personal communication, 2022) (Table i- Appendix). The Lower and Middle Miocene has distinctive fossil assemblages indicating the age of these surfaces while Upper Miocene

surface does not have a specific fossil indicator. Phillips (2022) used the youngest fossil *Bigenerina A* at well 17727204900000, which has an age slightly older than the top of Upper Miocene and picked the UM top 100 feet above the *Bigenerina A* marker. *Textularia W* can be used as an indicating fossil for defining top of Middle Miocene (Galloway et al., 2000). In this research I refer to surfaces: Top of UM, Top of MM, and Top of UM (Figure 14). Techniques used in horizon picking include manual-picking and auto-tracking while auto-tracking was used when reflectors were continuous, and manual-picking was used when encountering faults.

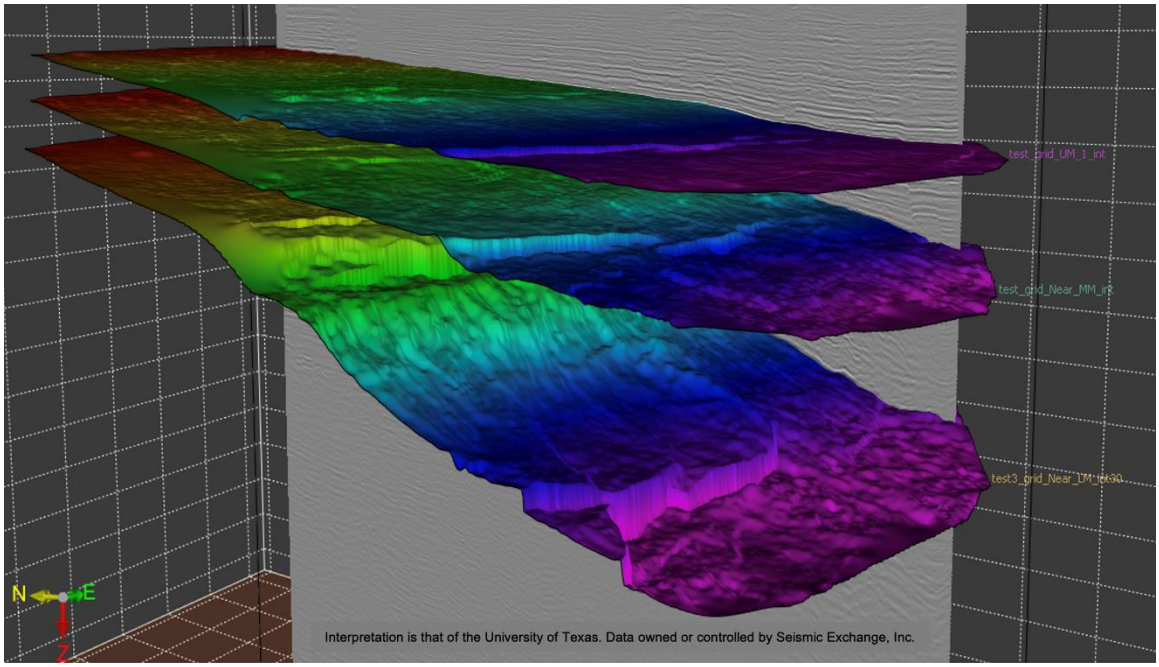

Figure 14. Three horizons interpreted (top to bottom: top of Upper Miocene, top of Middle Miocene, top of Lower Miocene). Data owned and controlled by SEI Inc, Interpretation by University of Texas at Austin.

3.1.2. Stratal Slicing and Attribute Mapping

Stratal slicing is a technique used on 3D seismic surveys to obtain attribute maps on selected stratum. This method was first introduced by Zeng (1994), giving considerations that traditional horizon and time slices were not perfect because the realistic stratal surfaces (time-transgressive) are not necessarily reflected on amplitude and impedance in the seismic volume (Zeng, 1994; Vail, 1977). It is a tool for interpreting horizontal seismic surfaces and can be applied with a linear interpolation algorithm between two reference events (Zeng, 2010). To best represent a stratal slice, frequency-based techniques such as phantom mapping (Zeng et al., 1998) can be used. Unfortunately, the slicing process in this research is limited because the 3 horizons that were picked and used in PaleoScan geo-model creation is based are seismic phases (peak and trough).

The interpreted seismic horizons were imported to PaleoScan for the stratal slicing process. This software can recognize faults when encountering a discontinuous horizon. With the 3D seismic volume and the horizons, a model grid was created showing the merged seismic patches that represents the similar wavelets and relative distance. The correlation threshold is 30%, which is the default value that allows patches with correlation factor above 30% to be linked (Eliis, 2021). After that, I increased horizon constraint by adding the three horizons and then imported to the model grid, providing the grid the reference from the interpretations. Finally, a Relative Geological Time Model (RGT Model) was computed from the model grid. This model was used in the stratal slicing process with several attributes including Sum Negative Amplitude, Root Mean Square (RMS) Amplitude, and Spectral Decomposition. Stratal slicing from each attribute was performed mainly on the storage interval of interest: Middle and Upper Miocene, which are bounded by two horizons: top of Lower Miocene and top of Upper Miocene. I extended the interval slightly beyond MM and UM in order to see other possible prospects.

3.1.2.1. Sum Negative Amplitude

550 stratal slices between the top of Upper Miocene (UM) and the top of Lower Miocene (LM) have been created using the attribute Sum Negative Amplitude. Five major sand-prone geobodies have been found, most of them located on the south side of the Chandeleur area, mainly located within the UM interval (Figure 15). It is likely that the sand was brought by a channel system from the northwest of the seismic survey which possibly was related to the paleo Mississippi or Tennessee River.

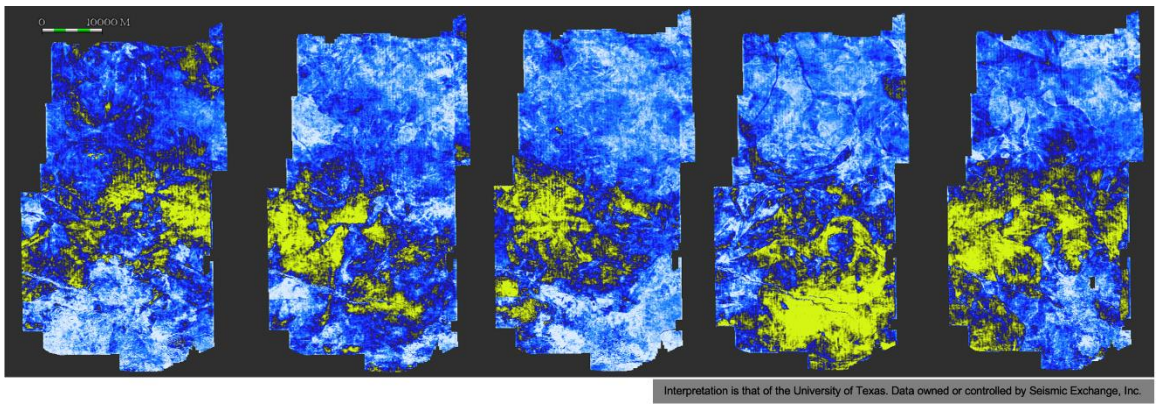

Figure 15. Sum Negative Amplitude stratal slices within Upper Miocene. Left to right: Lower UM to Upper UM. Yellow indicates large absolute negative values while white indicates positive amplitude values. Bright amplitudes are likely associated with sand-prone areas. Data owned and controlled by SEI Inc, Interpretation by University of Texas at Austin.

Sum Negative Amplitude, in PaleoScan, is the attribute for Horizon Stacking which sums over the vertical analyzed window and maps for each point of the current horizon. In this case, the window size is 7 samples. This method gives an overview of the general distribution of sand-prone geometries since the negative amplitudes reflect a trough in our polarity, which could indicate the presence of a low-velocity layer (sand-prone in Miocene case). The horizon stacks only provide a qualitative concept to map the approximate

location of the sands, instead of giving the exact value of reservoir properties, like porosity or net sand, for instance. This method has not been studied much like the more conventional attributes like RMS and Spectral Decomposition. We are confident to say that the yellow areas in Figure 15 are sand-prone, not only because of the amplitude characteristics but also because of the calibration with sand-prone intervals in well logs. The well log analysis would provide the values for sand thickness and porosity.

3.1.2.2. RMS Amplitude

Another batch of horizon stacks was created, displaying RMS Amplitude in 600 slices within the tops of UM and LM. In geology, RMS amplitude is a measure of the strength of seismic waves that are recorded by geophones or seismometers. It stands for "root mean square" amplitude and is calculated as the square root of the average of the squared values of the amplitude of the seismic wave over a specified time window. It can be expressed numerically as (Eliis, 2021):

$$x_{xRMS} = \sqrt{\frac{1}{n}\sum_{i=1}^{n} x_1^2}\sqrt{\frac{1}{n}\sum_{i=1}^{n} x_1^2} \quad (1)$$

RMS amplitude is an important parameter for seismic data analysis as it can provide information about the subsurface geological structure and the properties of the rock layers through which the seismic waves have traveled. The amplitude of the seismic wave is influenced by the density, velocity, and thickness of the different layers of rocks, and by the presence of faults, fractures, fluids in the pore space and other geological features that can reflect or absorb the seismic waves. In particular, the analysis of RMS amplitude can help geologists to identify potential hydrocarbon reservoirs, as the presence of porous and

permeable rocks filled with oil or gas can cause a significant increase in the amplitude of the seismic signal.

In our case, the sample size in one window (n) is 7. This method is favorable when distinguishing the high amplitudes and low amplitudes, where high amplitude indicates a significant change in relative rock impedance and low amplitude indicates less changes. RMS stratal slices correspond to the Sum Negative Amplitude slices showing the approximate sand-prone areas. The stratal slices are mostly grey in the northern part of the seismic survey, including Middle and Upper Miocene, where RMS Amplitude is less than 1. The high-amplitude bright spots tend to appear at the central to southern Chandeleur Sound (Figure 16). Bright sand-prone areas were spotted right below the top of MM horizon, which could be sand cumulation on top of the mass transport complex.

After making slices from RMS Amplitude attribute, six bright reflections were picked and seems to be continuous reservoirs. The high-amplitude areas (RMS Amplitude value > 1.5) were painted over and extracted as geo-bodies (Figure 17).

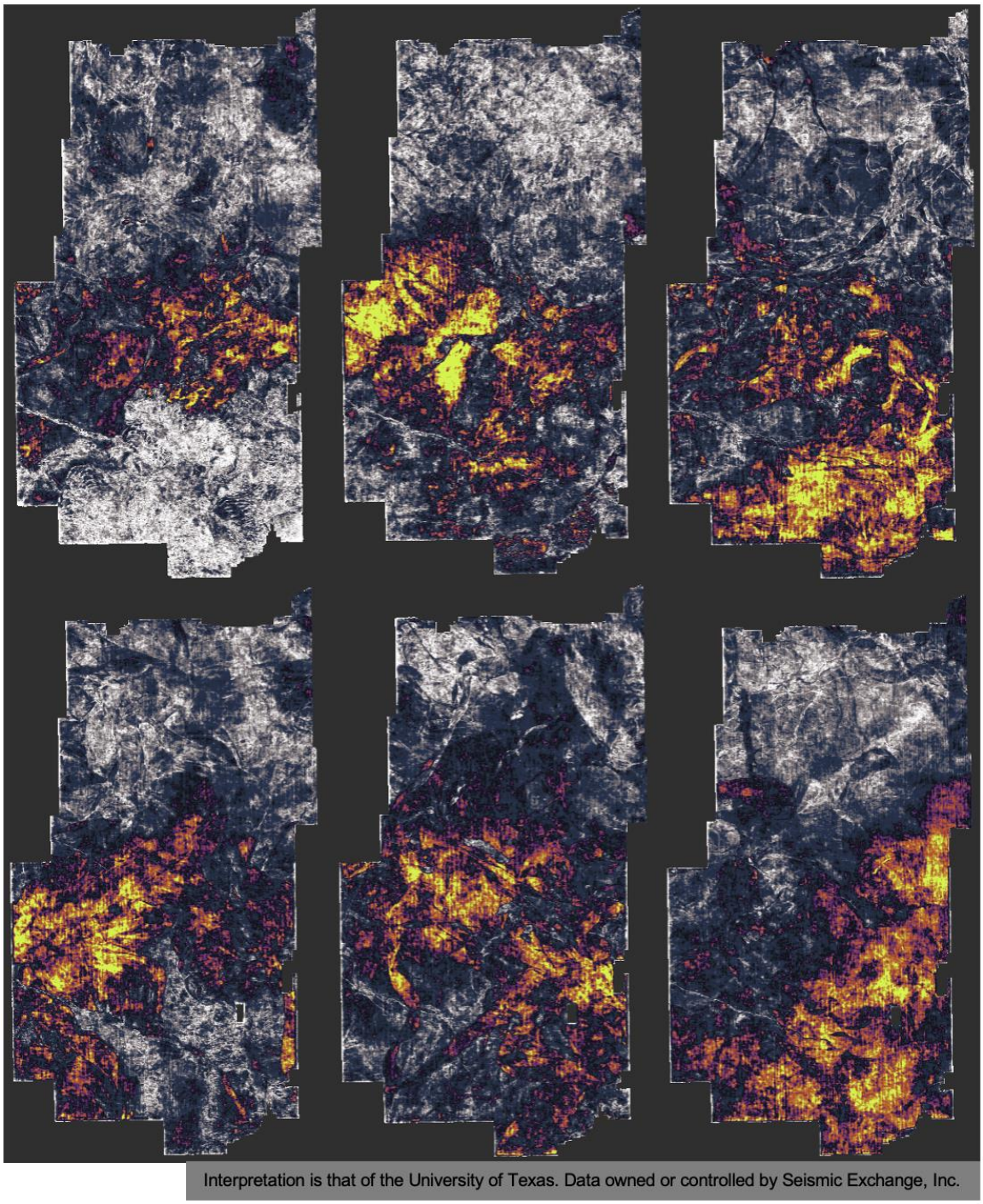

Figure 16. RMS Amplitude stratal slices within Upper Miocene. Top left to bottom right: Lower UM to Upper UM. Bright areas indicate sand-prone reservoirs. Data owned and controlled by SEI Inc, Interpretation by University of Texas at Austin.

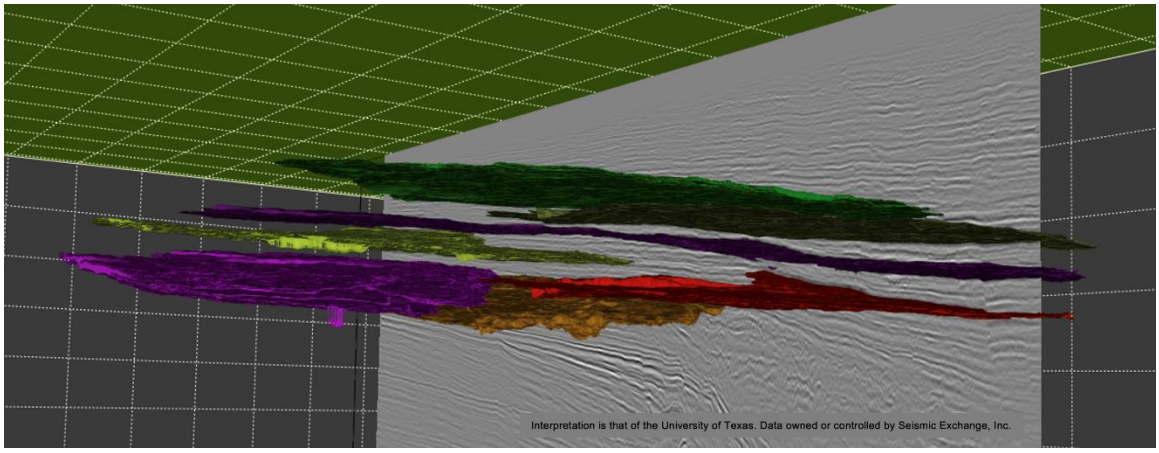

Figure 17. Extracted geo-bodies based on high amplitude areas. Data owned and controlled by SEI Inc, Interpretation by University of Texas at Austin.

3.1.2.3. Spectral Decomposition

Spectral Decomposition in reservoir characterization was first illustrated by Partyka et al. in 1999. Unlike the other two methods, it allows users to analyze the stratal slices based on frequency. It is a powerful way to determine the geomorphology in a stratal slice in terms of bed thickness. It is also good for identifying channel systems. Laughlin et al. (2002) applied this method for illustrating the heterogeneity in the channels and the overbanks (Figure 18) and found that the thinner bed was tuned in higher frequency and the thicker bed was highlighted under low frequency. Hossain (2020) used 20 Hz and successfully mapped out the sands and mud-filled channels in the Moragot field of Pattani Basin, Gulf of Thailand.

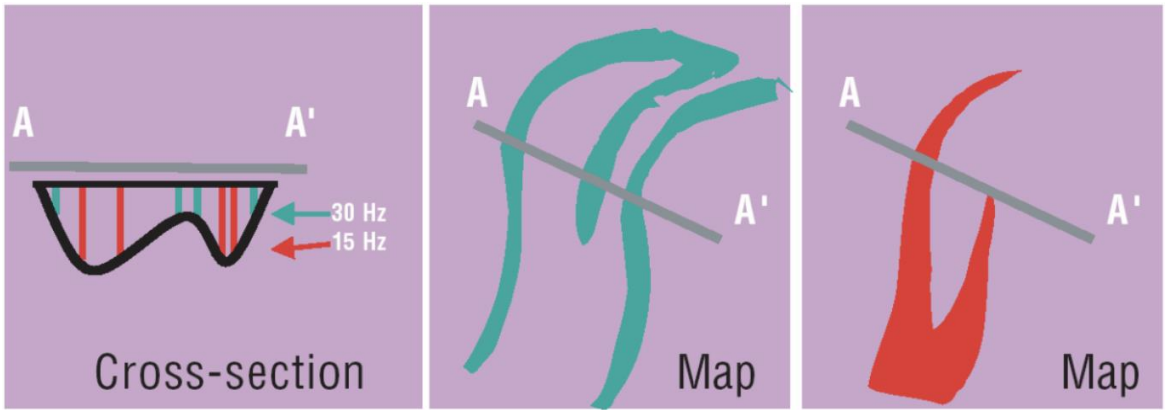

Figure 18. Illustration of spectral decomposition (Laughlin et al., 2002)

Before decomposing, frequency domain analysis was done using the Frequency Spectrum chart in Decision Space software. Two intervals of interest were selected within Middle-Upper Miocene. The frequency distributions are different in MM and UM (Figure 19) that MM appears to be more high amplitude-dominated while UM is relatively higher amplitude-dominated. Despite the difference in amplitude, it has appeared that the lower frequencies (< 30 Hz) can show both very high and very low amplitudes.

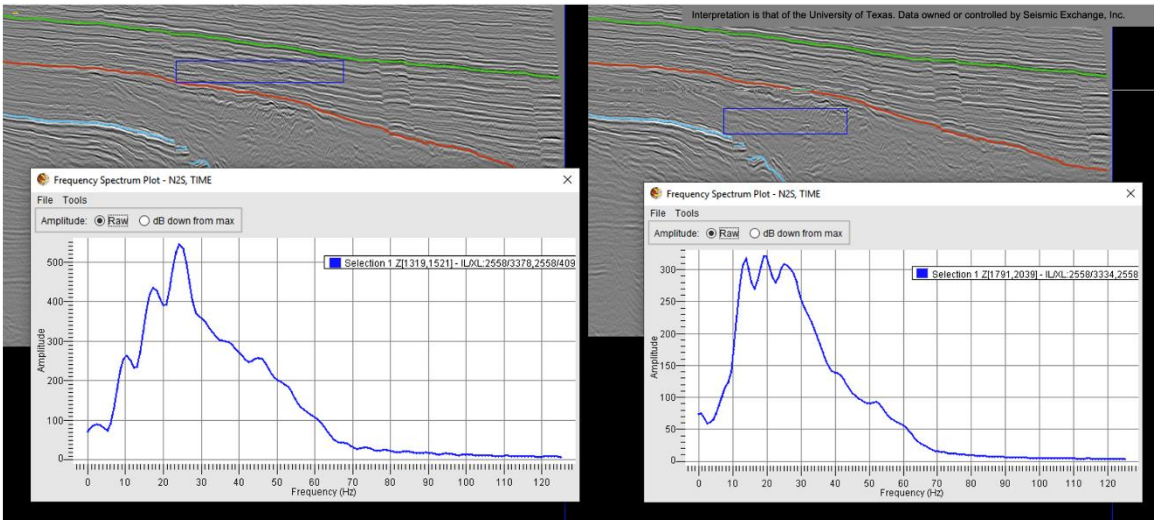

Figure 19 a; 19 b. Frequency spectrum plots of Upper (left) and Middle Miocene (right). Data owned and controlled by SEI Inc, Interpretation by University of Texas at Austin.

Figure 20 gives a perfect comparison of different frequencies (15 Hz and 40 Hz) on the same stratal slice. With 15 Hz we can identify the sand body located to the south, which was also identified by Sum Negative Amplitude and RMS Amplitude maps, while with 40 Hz we cannot identify such sand body.

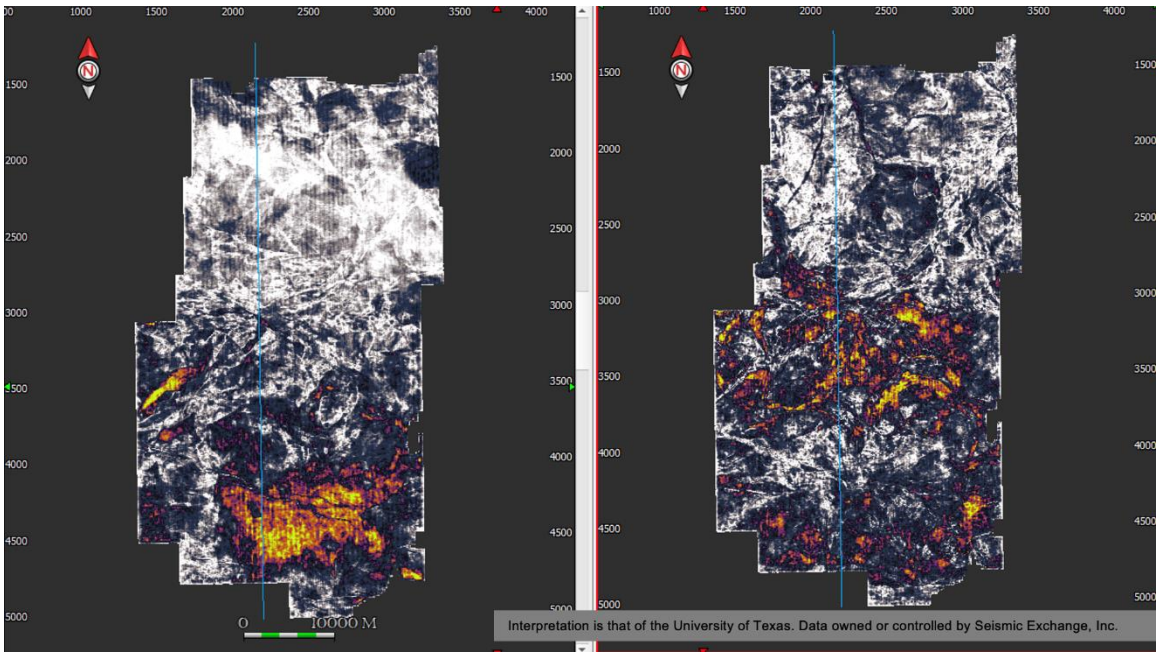

Figure 20 a; 20 b. Comparison of 15 Hz and 40 Hz in frequency on one stratal slice. Data owned and controlled by SEI Inc, Interpretation by University of Texas at Austin.

The seismic volume was decomposed into 25, 45, and 65Hz. A blending view was created by overlaying three frequencies together. The biggest finding from this approach is that above the Top of Upper Miocene horizon, a massive sand-filled channel system shows up under the 25 Hz frequency view (Figure 21). The lobate feature could be delta

front. This channel system is not seen within UM and MM, possibly due to channel shifting, but it is an example that shows that the overall channel fluvial system was flowing NW to SE into Chandeleur Sound. During Late Miocene, Tennessee River entered the Gulf of Mexico Basin from Cumberland Plateau and Appalachian terrains with large volumes of sand-rich sediment (Galloway et al., 2011). The channel system found from the stratal slice (Figure 21) is likely to be one of the paleo Tennessee River large distributaries. Fluvial systems are favorable for CO_2 storage (Sun et al., 2023), hence, a geo-body was extracted, and the delta front feature was included in the reservoir candidates.

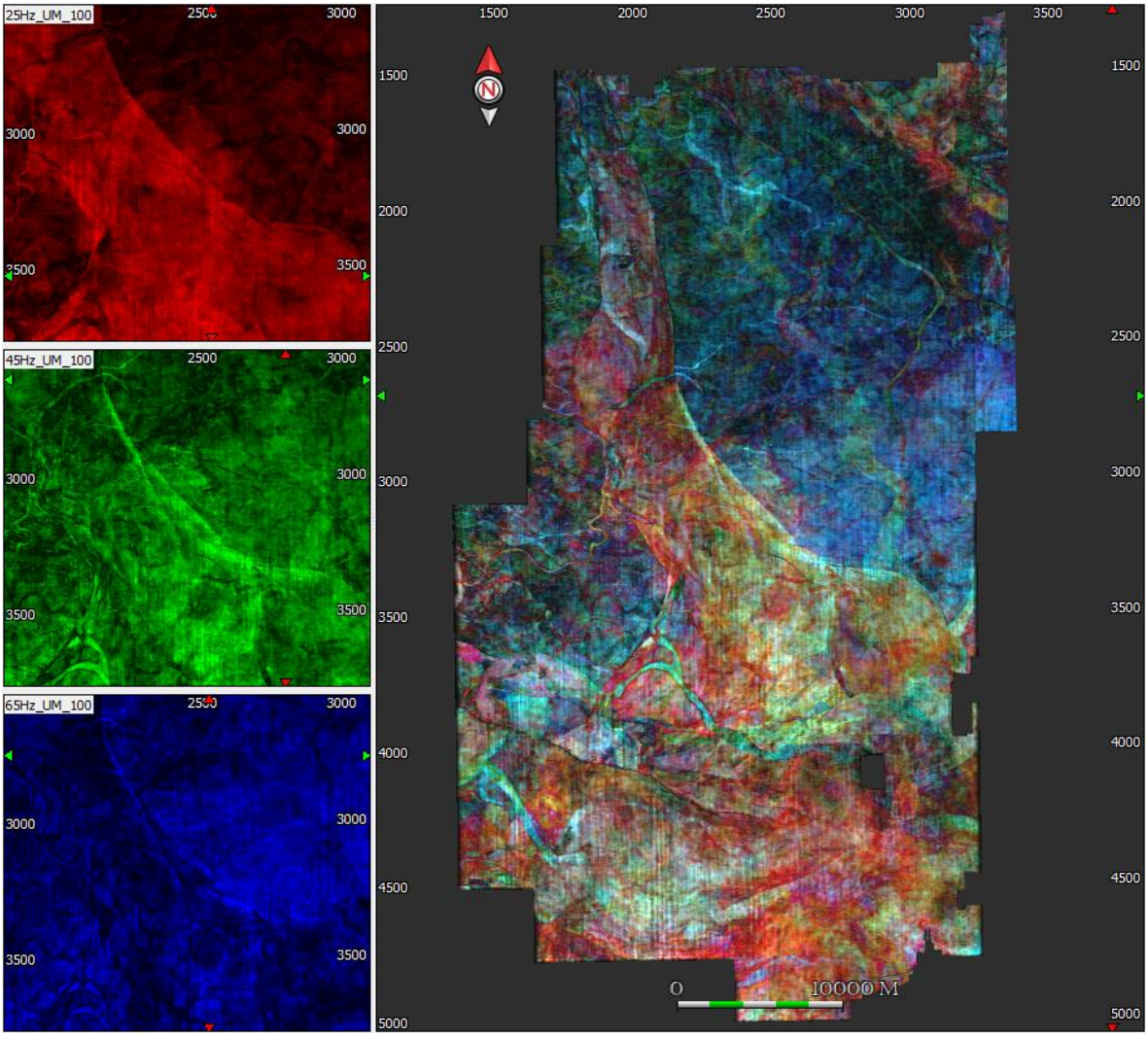

Figure 21. Massive channel system from stratal slices near top of UM, highlighted using spectral decomposition attribute. Data owned and controlled by SEI Inc, Interpretation by University of Texas at Austin.

The areas of interest have been defined after stratal slicing. Middle-to-outer shelf within the Chandeleur Sound seismic survey would be the main areas for further investigation and CO_2 capacity estimations. Ideal high-amplitude sand bodies have been found mostly in the Upper Miocene, including the channel system of Figure 21. They would be the intervals of interest for storage capacity calculations (Figure 22).

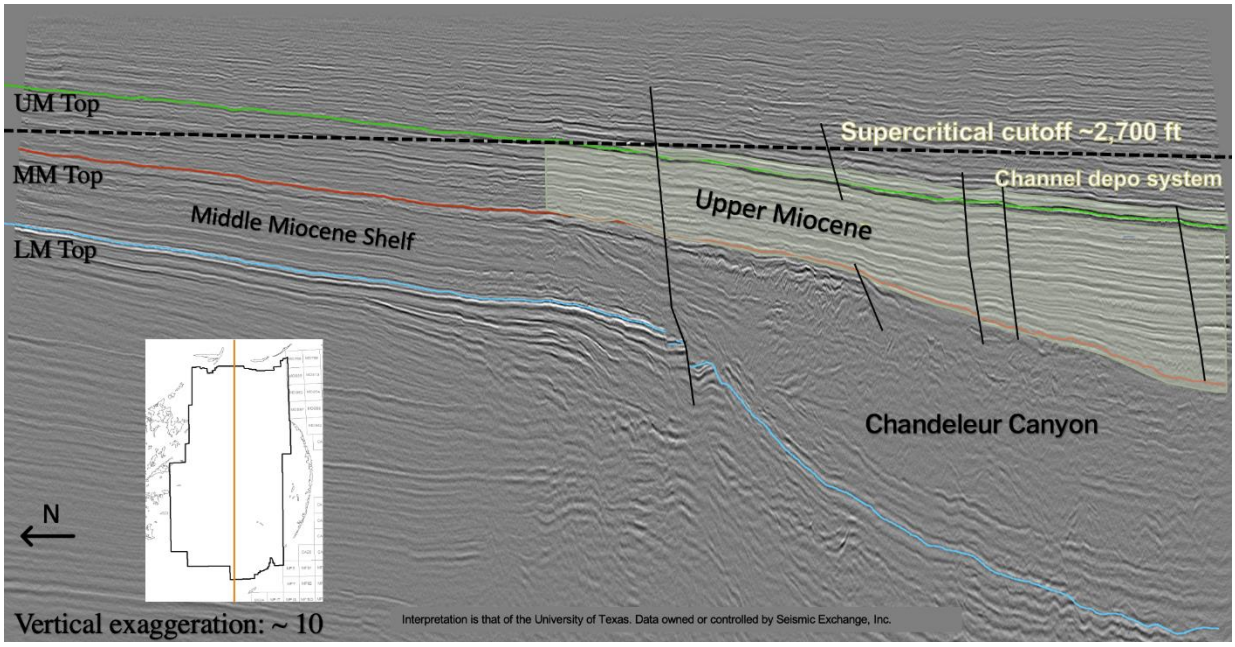

Figure 22. Seismic cross section showing ideal storage intervals defined after stratal slicing (light green) on seismic cross section. Data owned and controlled by SEI Inc, Interpretation by University of Texas at Austin.

3.2. WELL ANALYSIS

Publicly available digital well log data was used for analysis. 120 out of the 170 wells drilled in Chandeleur Sound have digital well logs. 48 wells have Gamma Ray log curves, and 22 wells have sonic logs. Figure 23 shows the distribution of the wells within the seismic survey, where the wells in yellow indicate wells with biostratigraphic markers. Wells are more concentrated in the middle and the southern part of the survey. There are only 6 usable wells with well logs on the northern shelf and only a few of them penetrated the Upper Miocene and reached the Middle Miocene. It is expected that this data would be only used for limited well-log correlation in the Upper Miocene and to calculate porosity and permeability for the Upper Miocene section.

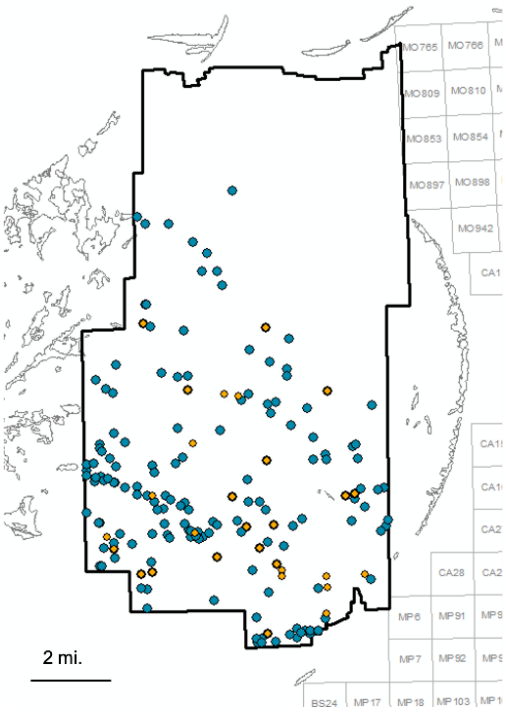

Figure 23. Well distribution within Chandeleur Sound seismic survey (Phillips, 2022). Noted that the wells in yellow indicate wells with biostratigraphic markers.

3.2.1. Well Correlation and Geological Interpretations

Sixteen wells with Gamma Ray log (GR) were used for stratigraphic correlation (well pick interpretation). To tie the wells with the seismic surfaces, I used 9 time-depth tables (TDs) which were applied on 11 wells, in order to display the wells in depth on the time seismic volume. The TDs were computed by previous researchers in GCCC-BEG. (Dunlap, 2022, unpublished data; DeAngelo, n.d., unpublished data). A new seismic depth volume, computed in-house by Dr. S. Bhattacharya, was also used (Bhattacharya, 2022, unpublished data) but the accuracy of the depth model remains unclear, due to the insufficiency of velocity data. However, by utilizing both time-depth tables and depth seismic volume, the relative well picks can be matched with the seismic reflections at the reservoir scale. The light blue and dark green pick on Figure 24 define the storage interval

within the Upper Miocene. The correlation technique is correlating the maximum flooding surfaces (MFS), where the GR point to the right the most. Fig. 20 shows the well log correlation of a linear well distribution from northwest to southeast (A - A') while Figure 25 shows northeast to southwest (B - B').

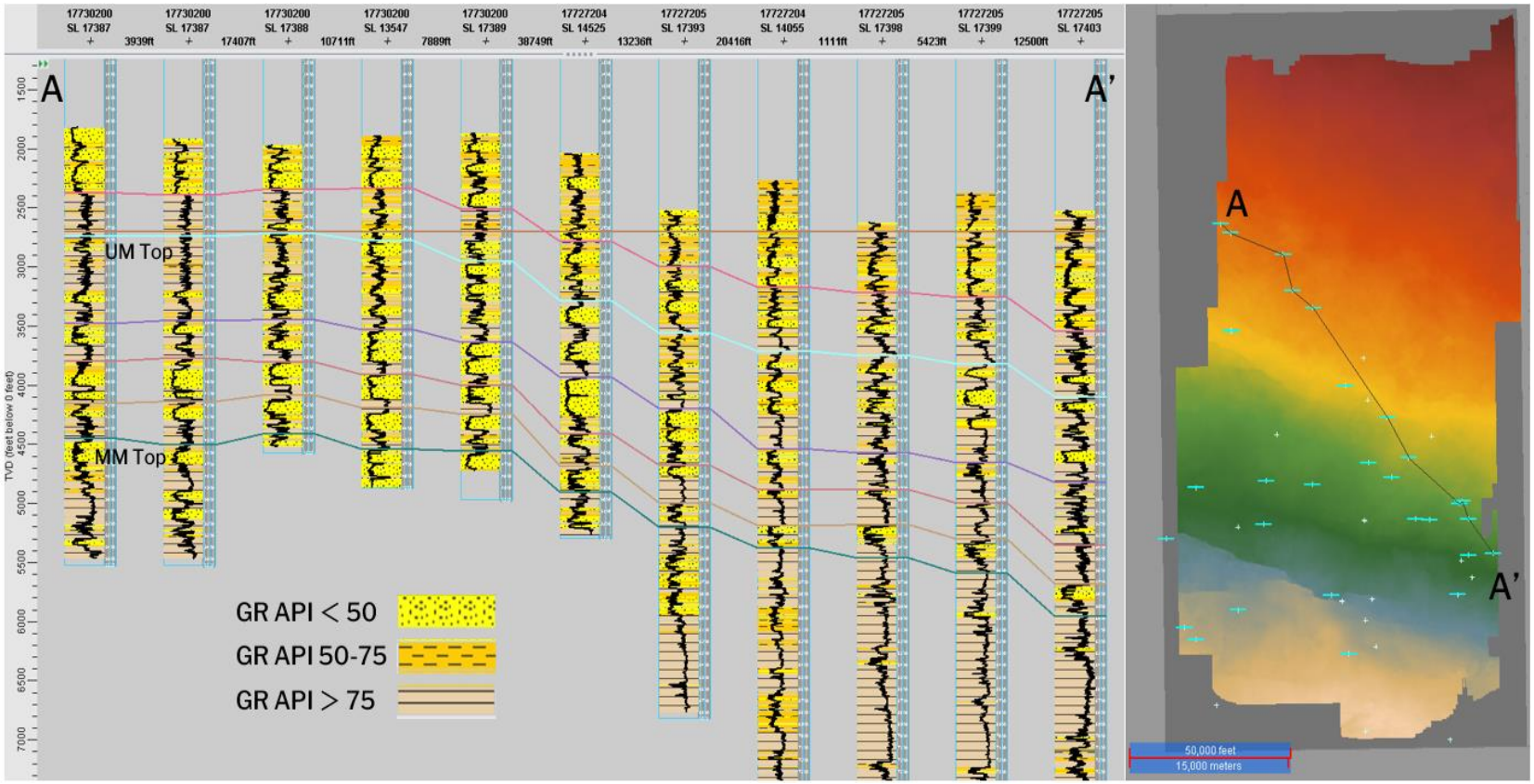

Figure 24. Structural correlation from A to A' using Gamma Ray log curves. The lithology strips show the general lithology of each well, while the cut-off value for clean sand is 50. Brown straight line is the supercritical cut-off (2,700 ft). Light blue line is the top of UM, dark green line is the bottom of UM.

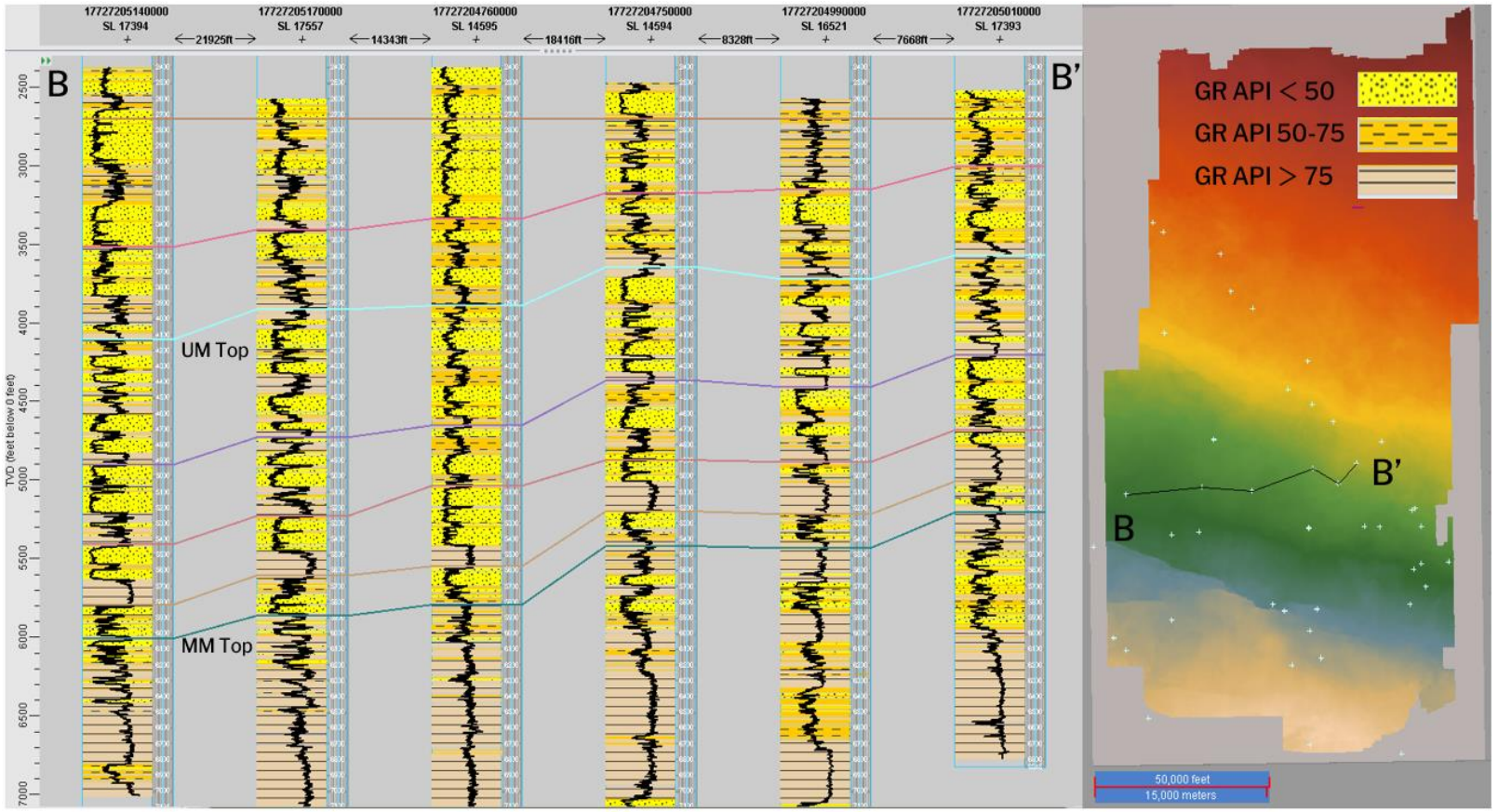

Figure 25. Structural correlation from B to B' using Gamma Ray, well picks and lithology strips classification refer to A to A' correlation.

A net sand map of Upper Miocene has been generated. The thickness of net sand from each well has been measured with a Gamma Ray cutoff of 50 API. Figure 26 shows the net sand distribution. Because of the lack of well control at the northeast Chandeleur survey, the area is marked as undefined thus not under our consideration for CO_2 storage.

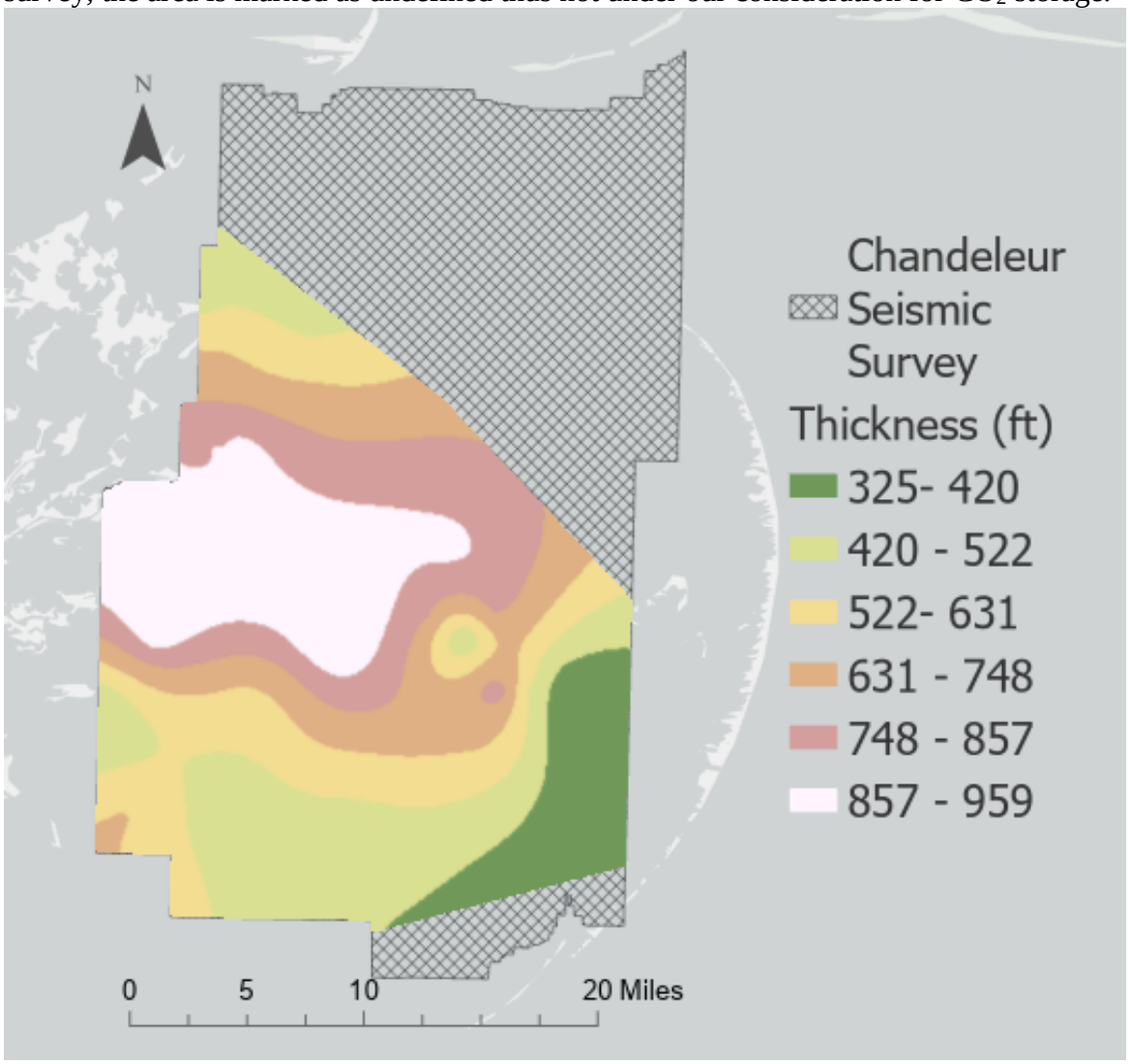

Figure 26. Net sand map for Upper Miocene (hatched indicates the areas without well control).

Cross sections with facies interpretations in the Upper Miocene (A - A' and B - B') were constructed based on Gamma Ray correlation. The interval of interest in Upper Miocene is thickening downward, towards the basin. One major shale interval is observed from the first three wells, which are more proximal (Figure 27 and Figure 28). This shale might be associated with an embayment. Seven major sandy intervals were defined and named as S1, S2, S3, S4, S5, S6, and S7, from bottom to top. To identify the net sands, a GR value of 50 API was used as the cut-off for clean sand. S1 contains one continuous sand body accumulating on top of Chandeleur Canyon and right below the Top of Middle Miocene pick. This sand body is thinning to the south. The upward coarsening feature makes S1 easy to be distinguished in most of the wells in A – A' correlation (Figure 24), which indicates deltaic progradation. S2 and S3 are also coarsening-upward sandy features which are continuous throughout the correlation. S4 can be identified with two bulky sand layers with a thin shale layer in between. S5 and S6 are not easily distinguishable. The interval between S5 and S6 can be classified as interbedded sand and mudstone, which appears to be sandier in the B - B' cross section and muddier in down-dip A - A'. S7 is the channel system that was identified from Spectral Decomposition. It was identified by the upward-coarsening feature above the top of Upper Miocene pick. Some thin and small sand bodies shown in the cross sections are likely to be onlapping features are which were formed by the transgression during the early Upper Miocene period (Hentz and Zeng, 2003), which have been seen on seismic cross sections. These features are not continuous throughout the correlations and would not be considered as reservoir candidates.

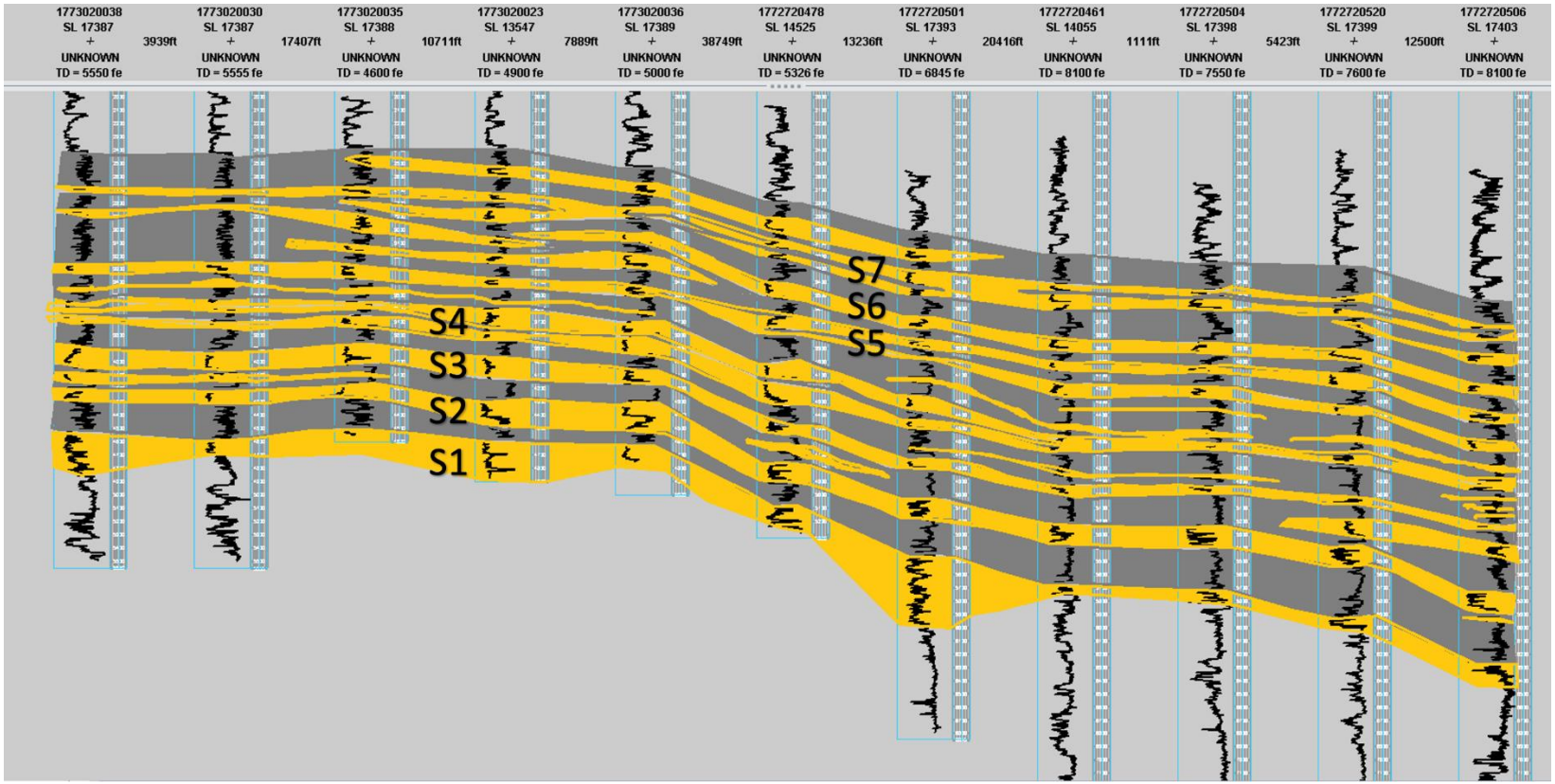

Figure 27. Cross section from A – A' with identified sandy reservoirs (Charlie Zheng, personal communication).

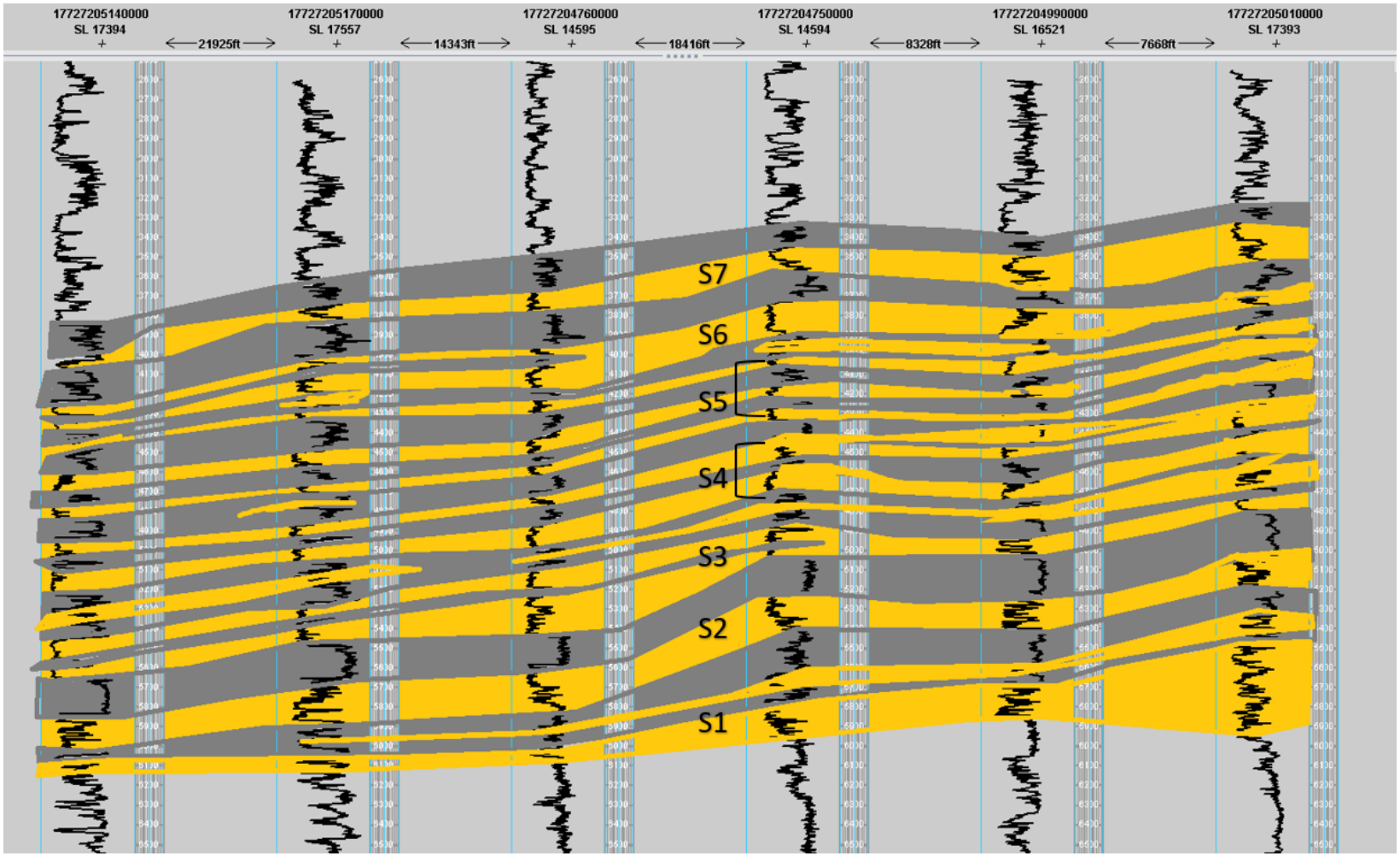

Figure 28. Cross section from B - B’ with identified sandy reservoirs.

The seven reservoirs that were picked from well correlation match with the high-amplitude areas in seismic as well as the geo-bodies extracted from stratal slices in terms of depth. However, some reservoirs have the extend much smaller in the seismic than in the well log correlation. Only one well (1772724780000) is overlapping with all the geo-bodies and is shown in Figure 29. The reason for this might be incorrect well correlation or reservoir quality decreasing. Nonetheless, it would be more realistic to calculate the reservoir areas based on stratal slices and geo-bodies. The area for seven reservoirs ranges from 260 to 480 km^2.

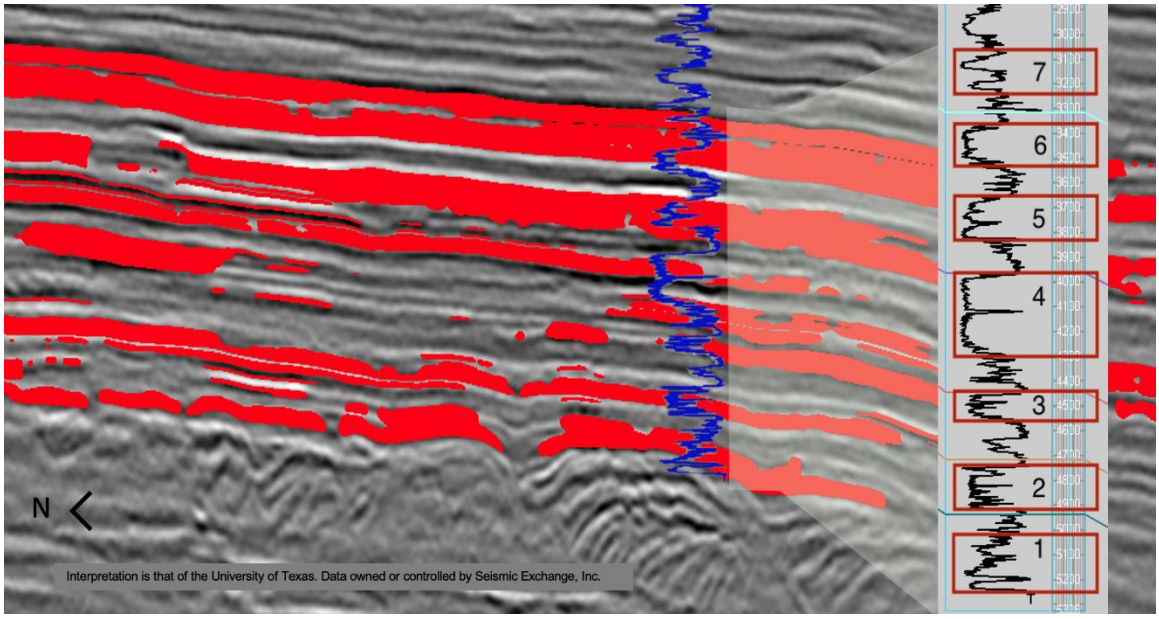

Figure 29. Identifying seven reservoirs on seismic cross section and well log (GR). Well used: 1772724780000.

3.2.2. Porosity Estimation

Nineteen wells with porosity curves (highlighted) were used for porosity estimation. Wells with Neutron Porosity (NPHI) and Density Porosity (DPHI) can be used for the effective porosity, using the equation below (Bigelow, 1992):

$$NPHIcorr = NPHI - (Vsh \times NPHIsh) \quad (2)$$

$$PHIa = \frac{NPHIcorr + DPHI}{2} \quad (3)$$

$$PHIe = PHIa - PHIsh \times Vsh \quad (4)$$

Where:

$NPHIcorr$ = Neutron Porosity corrected by Shale Volume

Vsh = Shale Volume

$NPHIsh$ = Neutron Porosity in shale, 0.4 was used in this calculation

$PHIa$ = Average Porosity

$PHIe$ = Effective Porosity

$PHIsh$ = Porosity in shale, 0.06 was used in this calculation

Two box plots were made showing the distribution of neutron and density porosity for the seven reservoirs (Figure 30).

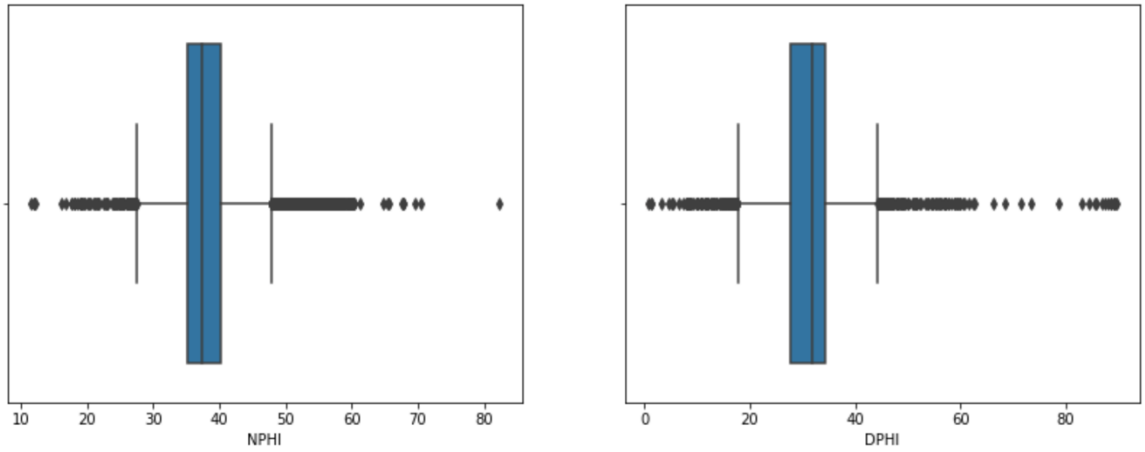

Figure 30. Box plots of Neutron Porosity (NPHI) and Density Porosity (DPHI) for the seven reservoirs.

If DPHI is not available, it can be calculated by bulk density (RHOB or Z_DEN) (Beaumont and Foster, 1999):

$$DPHI = \frac{\rho ma - \rho B}{\rho ma - \rho fluid} \quad (5)$$

Where:

ρma = Matrix density

ρB = Actual density values read from the log (Bulk Density)

$\rho fluid$ $\rho fluid$= Fluid density

To get the porosity of each reservoir defined in previous section, a 'reservoir' table was created showing the top and bottom depths of the reservoir S1 to S7 in all the 16 wells used for correlation. Six out of these wells have NPHI and DPHI logs, and 4 wells have NPHI and bulk density log throughout the UM interval. In a Jupiter Notebook, I imported the LAS files for the wells that have porosity log curves; then turn them into Pandas data frames and concatenate them into one data frame 'combined'. After, I merge 'reservoir with 'combined' so that every well has new columns indicating the depths of each reservoir interval. After that, I used a 'for' loop to find the intervals in each well that match the ideal reservoir intervals by extracting the depths that are bigger than the reservoir top depth and smaller than the bottom depth for each interval. Seven data frames that only contain the reservoir intervals were created, then were added into a list named 'S_list'. Then I used the equations listed above to calculate the effective porosity for every reservoir. The results are listed in Figure 31.

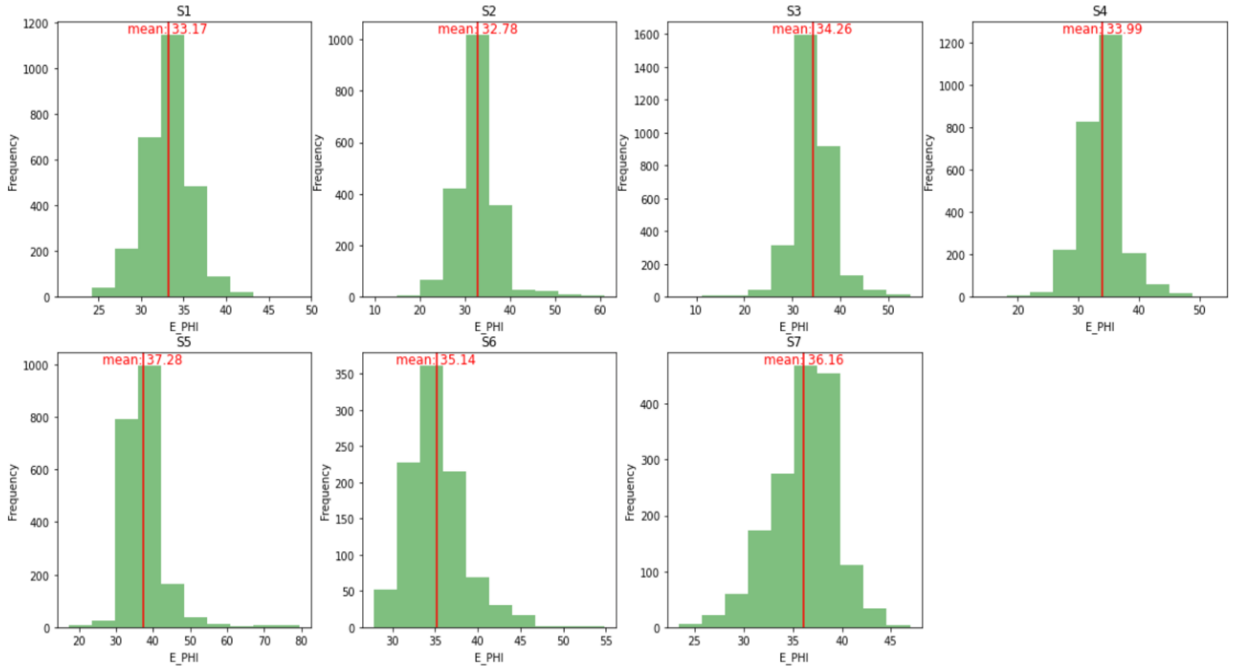

Figure 31. Histograms of effective porosity from seven reservoirs.

The effective porosity values for all reservoirs are all above 30%, which is unusually high. The reason for it might be the lack of petrophysical correction on the calculation (Uroza, personal communication). There is noise in the well log data that cannot be ignored: cycle skipping, depth matching, borehole washout, fluid salinity, tight spots, environmental corrections, etc. (Bhattacharya, personal communication). In order to get the most accurate wireline log value, we should take the local geologic condition into consideration, and detailed petrophysical analysis should be conducted.

The petrophysical analysis was done by Dr. Shuvajit Bhattacharya. He used three wells: 17730200300000, 17727205210000, and 17727205050000 and calculated the effective porosity for all sand bodies of the whole UM intervals of 20% (min), 29% (mean) and 32% (max), with a standard deviation of 5-7%. With the same three wells, the porosity

for each reservoir was computed (Table 1). I used the standard deviation of 6% for the maximum, and minimum effective porosity.

	S1	S2	S3	S4	S5	S6	S7
17730200300000	0.25	0.2	0.23	0.2	0.25	NaN	NaN
17727205210000	0.3	0.21	0.23	0.26	0.3	0.3	0.31
17727205050000	0.26	0.27	0.3	0.32	0.33	0.31	0.31
Mean	0.27	0.23	0.25	0.26	0.29	0.31	0.31
Min	0.21	0.17	0.19	0.20	0.23	0.25	0.25
Max	0.33	0.29	0.31	0.32	0.35	0.37	0.37

Table 1. Petrophysical analysis on three selected wells and their effective porosity for each reservoir unit (Bhattacharya, personal communication).

3.2.3. Permeability Prediction

After obtaining the porosity of the ideal reservoirs, the permeability needs to be estimated. Calibration with porosity and permeability measured on core would increase confidence. Unfortunately, there are no conventional cores or sidewall core plugs available among all the wells within Chandeleur seismic survey for porosity-permeability transform and subsequently permeability estimation. Two methods were used for this analysis:

1. Using the porosity and permeability transform from an unpublished project on the GOM shelf within the Middle Miocene interval (Bhattacharya, unpublished project). Due to the differences between compaction of the UM and MM, the permeability calculated from this Middle Miocene transform might be lower than Upper Miocene. The transform used can be expressed as (Equation 6) (Bhattacharya, unpublished project):

$$K = 0.0005e^{0.4424x} \quad (6)$$

Where:

K = Permeability in mD (millidarcy)

x = Porosity %

The original transform from the GOM shelf project, using the porosity and permeability data from Middle Miocene, data points and fitted line are illustrated in **Error! Reference source not found.**. This transformation was computed by Dr. Shuvajit Bhattacharya from BEG.

2. Apply the imperial porosity – permeability transformation proposed by Holtz (2002):

$$K = 7 \times 10^7 \times \varphi^{9.606} \quad (7)$$

Where:

K = Permeability in mD (millidarcy)

φ = Porosity

Table 2 concludes the permeability estimated from the two transforms above. Middle Miocene transform gives smaller values for permeability than Holtz's function. This could be due to more compaction in MM compared to UM. The permeability values computed from Offshore Middle Miocene project transformation would be used in future calculation such as storage capacity estimation, since it uses data from offshore Miocene in Gulf of Mexico, which could have similar properties with the seven reservoirs in this study. However, this transformation is tailored to Middle Miocene, so the permeability calculated could be underestimated since most of the reservoirs are within Upper Miocene in the Chandeleur Sound area.

		S1	S2	S3	S4	S5	S6	S7
Porosity	Mean	0.27	0.23	0.25	0.26	0.29	0.31	0.31
	Max	0.33	0.29	0.31	0.32	0.35	0.37	0.37
	Min	0.21	0.17	0.19	0.20	0.23	0.25	0.25
Permeability - GoM MM (mD)	Mean	77.01	11.32	36.84	49.48	216.19	362.24	451.92
	Max	1094.77	160.97	523.72	703.38	3073.48	5149.72	6424.65
	Min	5.42	0.80	2.59	3.48	15.21	25.48	31.79
Permeability - Holtz (mD)	Mean	241.42	44.97	130.91	168.01	535.27	778.54	910.16
	Max	1659.37	429.20	1008.64	1234.72	3198.60	4370.02	4980.17
	Min	21.59	2.35	9.76	13.51	59.41	94.94	115.27

Table 2. Permeability computed from two transformation – Offshore MM project and Holtz (2002).

3.3. TRAPPING MECHANISM AND CONFINING SYSTEM

The trapping mechanisms in CO_2 storage can be classified as physical trapping, which includes structural trapping and residual (capillary) trapping, and chemical trapping, including solubility trapping and mineral trapping (Mercer and Cohen, 1990; Trevisan et al., 2014; Agartan et al., 2015; Izgec et al., 2007). Supercritical CO_2 is buoyant relative to brine; therefore, it migrates upward through a porous and permeable system and stops when encountering a permeability barrier (Bennion and Bachu, 2008a). Structural traps such as an anticline structure or sealed fault block hold a column of CO_2 that is also limited in lateral migration. This type of trap is analogous to a hydrocarbon trap, and a thick column of mobile CO_2 can be retained.

Residual trapping occurs under the capillary forces within the pores inside the rock. Vertical movement of carbon dioxide is caused because supercritical CO_2 has lower density than brine. However, this vertical migration is limited because some fraction of the non-wetting phase fluid (CO_2) is trapped inside the pores by the capillary force (Ajayi et al., 2019; Hameli et al., 2022).

Dissolution trapping of CO_2 happens when CO_2 encounters undersaturated water and dissolved CO_2 and bicarbonate ions ($HCO3^-$) are produced. The amount of dissolution depends on salinity, temperature, and flow properties (Chang et al., 1981; Ajayi et al., 2019., Hameli et al., 2022). Mineral trapping occurs when dissolved CO_2 species in the solution react with cations in the fluid so that carbon-bearing minerals are precipitated.

The Upper Miocene within Chandeleur Seismic Survey is gently dipping south with a dip angle of much less than 1 degree. There are no structural traps visible from the seismic volume. A few fault blocks to the south and northwest could form traps that could retain a small amount of CO_2, but there has been no study on the offset and sealing capacity of the faults. The general lithology appears to be interbedded sandstone and shale throughout the UM. In this case, the main trapping mechanism for storing CO_2 in Chandeleur Sound would be residual/capillary trapping.

Trapping efficiency can be partially obtained from the hydrocarbon production data (IHS Markit, n.d.). The perforation top and bottom defined the interval where gas was found and produced from the well. Figure 32 combines the total gas production for each productive well, the perforation interval and thickness. The perforation top starts from around 4,000 feet in depth at the northern Chandeleur Sound seismic survey and getting deeper while going down-dip. The perforation interval is the thickest at central-to-west Chandeleur Sound, which correspond to the net sand map (Figure 26). However, many of these intervals do not fall within the interval of study in this research, especially of the wells located in southern Chandeleur Sound.

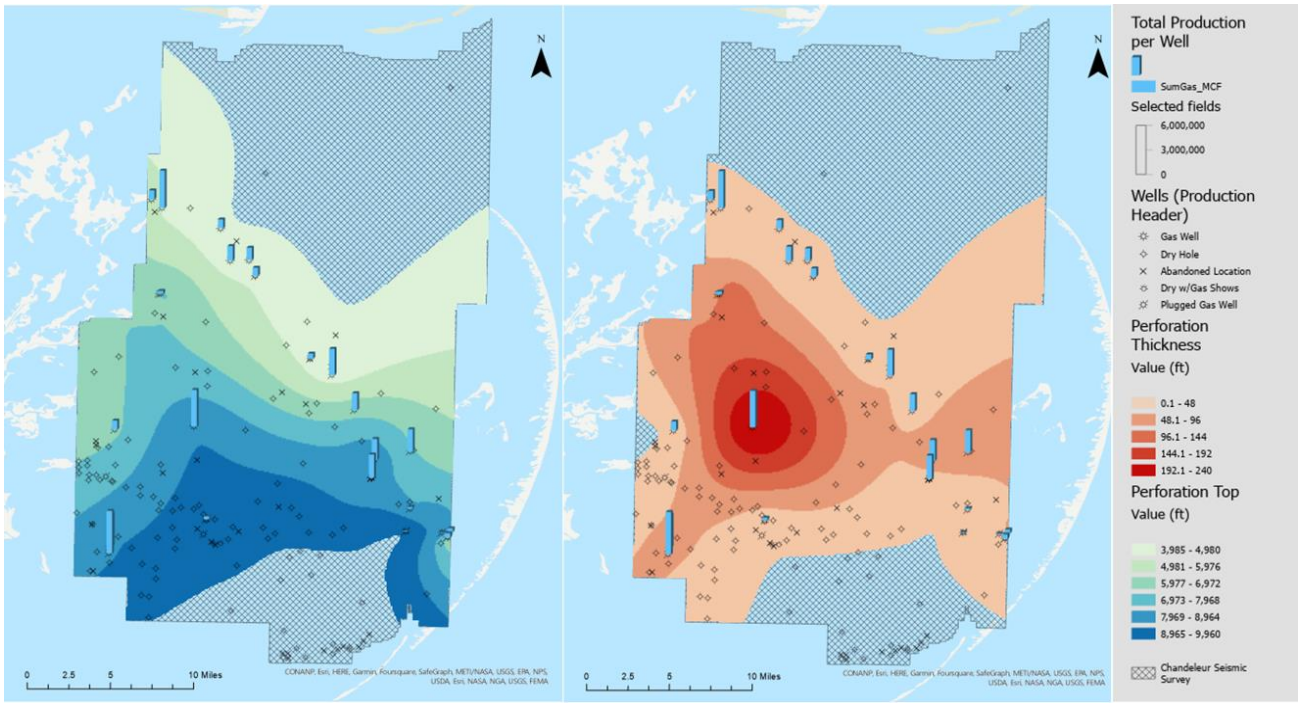

Figure 32. Gas production, depth of the perforation top (ft) and thickness of perforation interval (ft). Data retrieved from IHS Markit (n.d.).

Thirteen wells with gas production have Gamma Ray log curves. Ten of them were plotted for productive wells along with the perforation intervals (Figure 33), three wells were deviated from log curves and were not used. Well 17730200320000, 17727205140000, 17730200230000, 17730200340000 have perforation windows located on the sand bodies (GR API < 50) and overlaid by a shaly layer (GR API > 75). This indicate that the shaly layers are able to contain the hydrocarbon proficiently. However, only three wells (17730200230000, 17730200340000, 17727204780000) have perforation intervals within the interval of interest in this study. The rest of the well were drilled mainly into Middle Miocene.

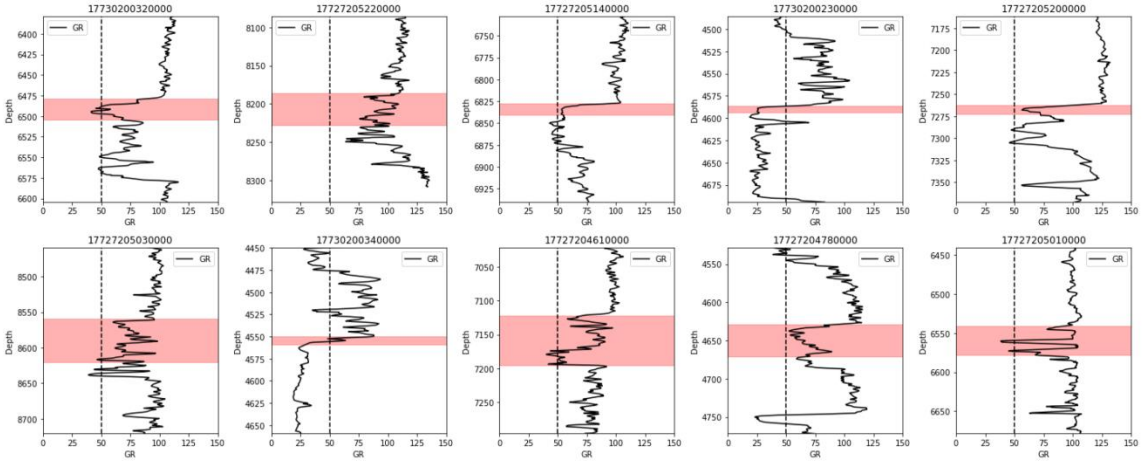

Figure 33. Perforation intervals of productive wells with Gamma Ray well logs. Red interval indicates perforation window. Dash line indicates GR cutoff where GR < 50 is clean sand.

To prevent the vertical migration of CO_2, a composite confining system has been proposed by Bump et al. (2023), which describes a multi-barrier system with discontinuous baffles. The study found that 5 to 15 mudstone barriers per a 100-meter section, with average length more than 1km, could retain an industrial scale of carbon dioxide within a few 10s of meters of vertical section (Bump et al., 2023). This study included physical modeling, reservoir scale numerical modeling for a deltaic system in Miocene, South Louisiana, which is similar to Chandeleur Sound in terms of depositional environment. With the theory of composite confining system, CO_2 storage in Chandeleur Sound could be secure even without conventional traps. From cross section A - A' and B - B' (Figure 27, Figure 28) we can conclude that all reservoir units have sufficient barriers which can form a complete composite confining system.

3.4. Storage Capacity Estimation

The final step of the geological section is to calculate the CO_2 storage capacity for Chandeleur Sound. There are different ways to estimate the capacity, but usually classified

as static and dynamic. Ruiz (2019) explored static methodologies: DOE – NETL function (Goodman et al., 2011), CO_2-SCREEN (CO_2 Storage Prospective Resource Estimation Excel Analysis), and direct natural gas production to CO_2 mass converting, as well as a dynamic EASiTool methodology and calculated a 15 – 23 Mt capacity for a 200 ft thick sand in offshore Texas.

In this section, I used one static and one dynamic methodology and estimated the storage capacity for seven reservoirs defined in Section *3.2.1.*

3.4.1. Static Volumetric Measurement

The first method is the static volumetric measurement, which it is the conventional way to calculate how much CO_2 can be stored within an interval given the reservoir area, reservoir thickness, effective porosity, water saturation, CO_2 density, fluid formation volume factor and storage efficiency factor. The U.S. DOE NETL methodology was summarized by Goodman et al. (2011). The equation for volumetric calculation for saline aquifer is expressed as Eq. 8.; total porosity was calculated using Eq.9 (Hartman, 1999).

$$GCO2net = (At\ hnet)\ \varphi tot\ \rho\ Enet = Vnet\ \varphi tot\ \rho\ Enet \quad (8)$$

$$\varphi\text{tot} = \sqrt{\frac{NPHI^2 + DPHI^2}{2}} \quad (9)$$

Where:

A_t = Reservoir area (m^2)

h_{net} = Net sandstone thickness (m)

V_{net} = Total volume = A_t* h_{net} (m^3)

φ_{tot} = Total porosity

ρ = CO_2 density (kg/m^3)

E_{net} = Net storage efficiency factor in a saline aquifer, which is a product of several efficiency factors (Goodman et al., 2011):

$$E_{net} = E_{An/At} E_{Hn/Hg} E_{\varphi e/\varphi tot} E_v E_D \quad (10)$$

Where:

$E_{An/At}$ = net-to-total area

$E_{Hn/Hg}$ = net-to-gross thickness

$E_{\varphi e/\varphi tot}$ = effective-to total porosity

E_v = volumetric displacement efficiency

E_D = microscopic displacement efficiency

Wallace et al. (2014) have used this equation and E_{net} of 4.5% calculated a static storage capacity of 172 Gt for a Miocene saline aquifer located at Texas coast of the north Gulf of Mexico (Wallace et al., 2014).

According to Goodman et al. (2011), the storage efficiency factors (E_{net}) for clastic saline formation in terms of all the factors listed in Equation 10 are 0.51% - 5.4% (2%) (P10 – P90 (P50)). I used 2.0% as for the static capacity calculation for the seven reservoirs in Chandeleur Sound.

Goodman et al. (2011) also summarized the capacity estimation for oil and gas reservoirs:

$$G_{co_2} = A h_n \varphi_e (1 - S_{wi}) B \rho_{co2std} E_{oil/gas} \quad (11)$$

Where:

A, h_n are areas and net thickness, same as ones in Eq. 8.

φ_e = effective porosity

S_{wi} = average initial water saturation within A and $h_n h_n$

B = fluid formation volume factor

ρ_{co2std} = standard density of CO_2

$E_{oil/gas}$ = CO_2 storage efficiency factor, the volume of CO_2 stored in and oil or gas reservoir per unit volume of original oil or gas in place.

Since the seven reservoirs in Upper Miocene cover multiple wells and the gas production in every well varies significantly, the efficiency factor in terms of oil/gas ($E_{oil/gas}$) is hard to acquire. Equation 11 is not suitable for capacity estimation in this study. The parameters and results for static storage capacity using Equation 8 with storage efficiency factor of 2% are shown in Table 3. The total capacity calculated from DOE method is 627.86 million metric tons.

Name	Density (kg/m^3)	Total Porosity	Thickness (m)	Area (km^2)	Estimated Capacity (Mt)
S1	703	33.46%	42.16	278.59	55.26
S2	700	33.28%	53.34	283.51	70.46
S3	696	34.87%	49.02	301.02	71.63
S4	691	34.37%	64.01	261.81	79.60
S5	685	34.68%	61.72	477.52	152.15
S6	681	35.39%	47.55	450.55	103.26
S7	673	36.54%	47.85	405.78	95.50

Table 3. Static capacity estimation parameters and results using DOE method (Goodman et al., 2011).

3.4.2. Dynamic Capacity Estimation with EASiTool

GCCC has developed its own tool – Enhanced Analytical Simulation Tool (EASiTool) for dynamic storage capacity estimation (Ganjdanesh and Hosseini, 2017; Hosseini et al., 2018). Unlike the procedure for static capacity, EASiTool takes the pressure into account and calculates the capacity, well rate, plume extents, as well as NPV for the project given certain input variables. The variables for capacity estimations have been gathered from the previous steps. Due to the high uncertainty of the reservoir parameters, I performed the 'Sensitivity Analysis', which allows users to input value ranges for multiple parameters. Sensitivity analysis allows users to know which parameter affect the capacity differences the most. Table 4 summarize all the variables needed for static and EASiTool calculations. For depth and thickness, I used trimmed mean in Excel and used 1st and 3rd quartiles for minimum and maximum value to exclude the outliers. From depth, temperature (depth in km * 25 +15), and hydrostatic pressure (depth in km * 10.5) were calculated. The temperature changes with the increase of depth are based on the geothermal gradient (Bachu, 2007). It was assumed that the surface temperature at Chandeleur Sound is 25 Celsius degrees. The lithostatic pressure was calculated by depth * 1 psi/ft, which is 22.6 Mpa/km. The frac pressure is assumed to be 80% of the lithostatic pressure (Stuart, 1960; Du Rochet, 1981). The injection pressure should always stay lower than the frac pressure in order to prevent rock from breaking, thus the maximum injection pressure was calculated using depth (km) * 17. The areas of reservoirs are 'projected area' of the sand bodies, based on amplitude extractions (RMS Amplitude slices) and well control.

I left the 'Rock Compressibility' and the permeability parameters as default, which are 4e-10 - 6e-10 (5e-10) 1/Pa (Hosseini, n.d.). I use the same values for salinity in all the reservoirs (0.8 – 2 (1)). I set the 'Max Number of Injectors' to 100 for S1 – 6 and 81 for S7, in order to observe a trend for capacity to the number of injection wells.

I used both 'Open' and 'Closed' for 'Boundary Condition' and compare the results from sensitivity analysis. According to the tool developers, the boundary condition applies to the basin. If a basin has closed boundary, EASiTool will assume that the pressure front and plume would not go beyond the basin. For open-boundary basin, the change of basin area does not change the results in terms of capacity, injection rate and the impact of other parameters (Hosseini, n.d.).

		S1	**S2**	**S3**	**S4**	**S5**	**S6**	**S7**
Porosity	Mean	0.27	0.23	0.25	0.26	0.29	0.31	0.31
	Max	0.33	0.29	0.31	0.32	0.35	0.37	0.37
	Min	0.21	0.17	0.19	0.20	0.23	0.25	0.25
Permeability - GoM MM (mD)	Mean	77.01	11.32	36.84	49.48	216.19	362.24	451.92
	Max	1094.77	160.97	523.72	703.38	3073.48	5149.72	6424.65
	Min	5.42	0.80	2.59	3.48	15.21	25.48	31.79
Depth (m)	Mean	1694.48	1574.25	1473.84	1359.75	1242.23	1188.36	1099.29
	Max	1984.25	1805.18	1693.16	1632.20	1562.10	1392.94	1260.35
	Min	1379.22	1289.30	1199.39	1069.85	995.17	931.16	835.15
Thickness (m)	Mean	42.16	53.34	49.02	64.01	61.72	47.55	47.85
	Max	57.91	60.20	60.58	82.30	90.30	79.25	55.63
	Min	30.48	48.77	30.48	44.58	38.86	32.77	36.58
Temperature (°C)	Mean	57.36	54.36	51.85	48.99	46.06	44.71	42.48
	Max	64.61	60.13	57.33	55.81	54.05	49.82	46.51
	Min	49.48	47.23	44.98	41.75	39.88	38.28	35.88
Pressure (Mpa)	Mean	17.79	16.53	15.48	14.28	13.04	12.48	11.54
	Max	20.83	18.95	17.78	17.14	16.40	14.63	13.23
	Min	14.48	13.54	12.59	11.23	10.45	9.78	8.77
Max Injection Pressure (Mpa)	Mean	28.81	26.76	25.06	23.12	21.12	20.20	18.69
	Max	33.73	30.69	28.78	27.75	26.56	23.68	21.43
	Min	23.45	21.92	20.39	18.19	16.92	15.83	14.20
Reservoir Area (km^2)	Reservoir Area	278.59	283.51	301.02	261.81	477.52	450.55	405.78

Table 4. Inputs for EASiTool storage capacity estimation. Porosity, permeability, depth, thickness, temperature, max injection pressure and salinity have mean, maximum and minimum values for sensitivity analysis.

Figure 34 shows the inputs and capacity estimation results for S1 in EASiTool. The tornado diagrams for each reservoir are shown in Figure 35. Under open-boundary condition, the tornado diagrams look alike: the permeability has the biggest positive impact on the storage capacity, followed by 'Frac Pressure' (maximum injection pressure) and thickness. For closed-boundary condition, the frac pressure has the largest positive effect on capacity for most reservoirs. This suggests that if the rock has higher fracture pressure (difficult to break) more CO_2 can be injected. Thickness, porosity and permeability also plays an important part on capacity under closed-boundary condition. while 'Pressure' (initial hydrostatic pressure of the reservoir) has negative impact on storage capacity under both conditions. Another observation from Figure 34 (and the results from other reservoirs) is that even setting the maximum injector number to 81, the storage capacity does not increase to much after the maximum injection well reach 50 under both boundary conditions. I set the maximum injection well to 49 and estimate capacity using the mean values for each parameter. Table 5 summarizes the final results for dynamic storage capacity estimation.

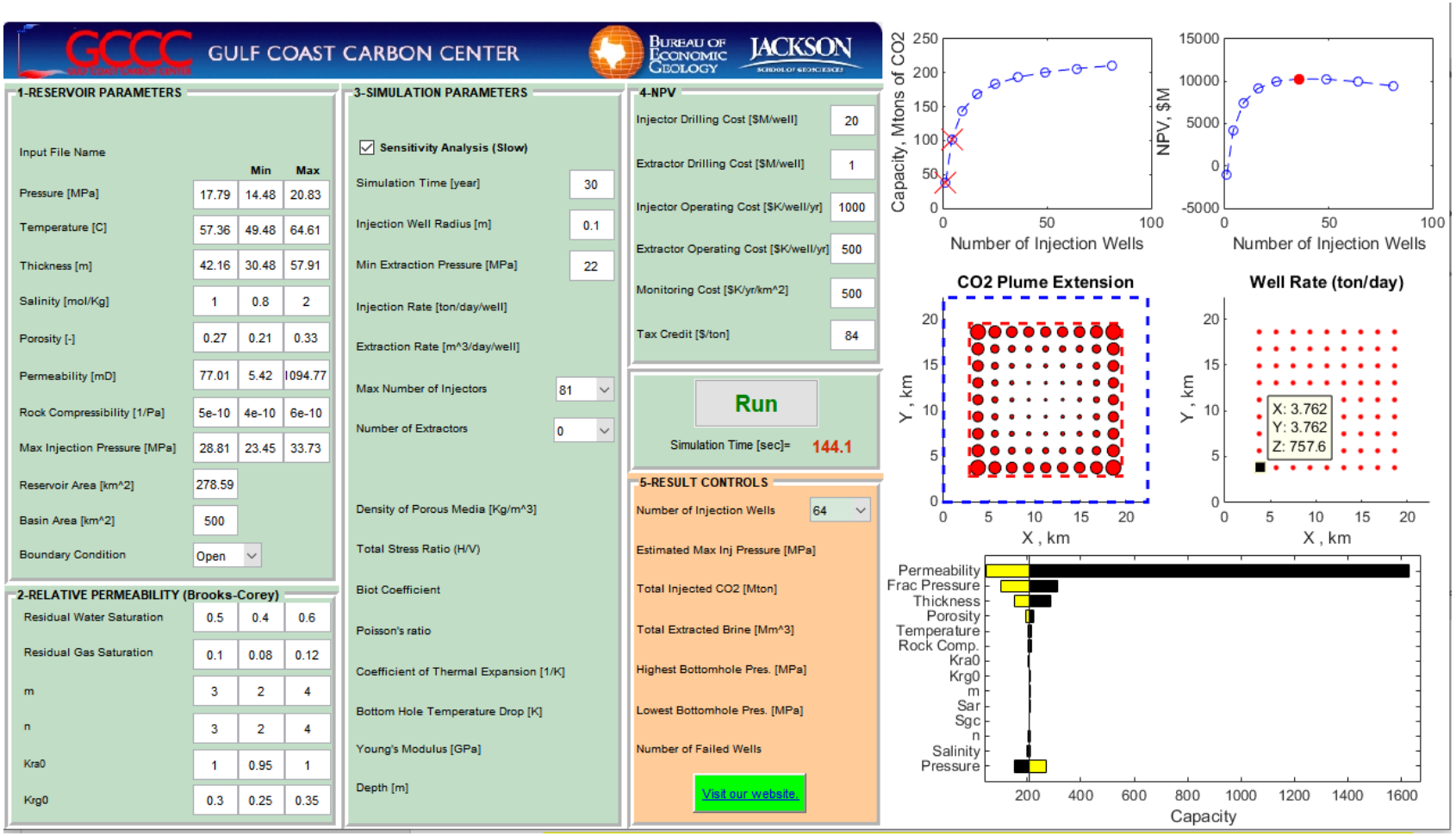

Figure 34. Sensitivity analysis for S1 using EASiTool.

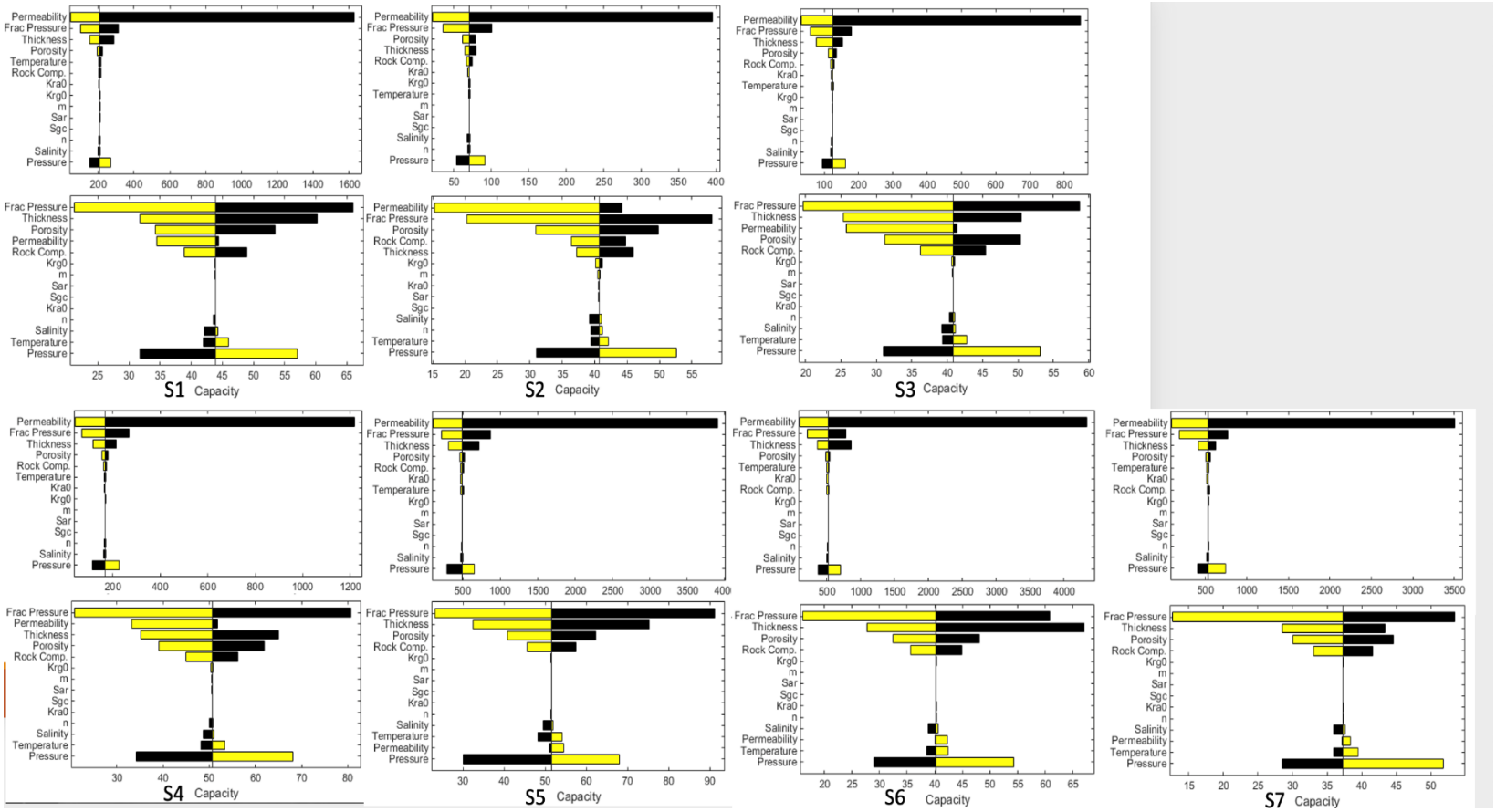

Figure 35. Tornado diagrams for sensitivity analysis. For each reservoir, top diagram indicates open-boundary condition while bottom diagram indicates closed-boundary condition

	CAPACITY (MILLION METRIC TONS)	
	Open Boundary	**Closed Boundary**
S1	198.60	43.97
S2	62.71	41.14
S3	113.50	41.00
S4	157.00	50.77
S5	463.40	51.53
S6	492.10	40.27
S7	512.40	37.33
TOTAL	1999.71	306.01

Table 5. Summary of dynamic storage capacity (EASiTool) for seven reservoirs under open and closed boundary conditions.

3.5. RESULTS AND DISCUSSIONS

Seismic interpretation and well logs analysis have been done for CO_2 storage capacity estimation. I have performed stratal slicing and attribute mapping on the seismic data. Three attributes were used: Sum Negative Amplitude, RMS Amplitude, and Spectral Decomposition. From the seismic analysis, it is concluded that southern Upper Miocene is the primary interval of interest. Well correlations along the dip and strike were done. A net sand map for Upper Miocene was constructed and indicates that central UM has the thickest sandy interval, with more than 750 ft of clean sand. An estimation of the geologic characteristics of Chandeleur Sound concluded that there are seven continuous sandy units that can be used as storage reservoirs. Storage capacity estimation was done for each reservoir using two approaches – static and dynamic, which gave various capacity value for each reservoir. In this section, I summarized the results from DOE – NETL static capacity calculation and EASiTool dynamic capacity estimation. The values for each reservoir with two methods are shown in Figure 36.

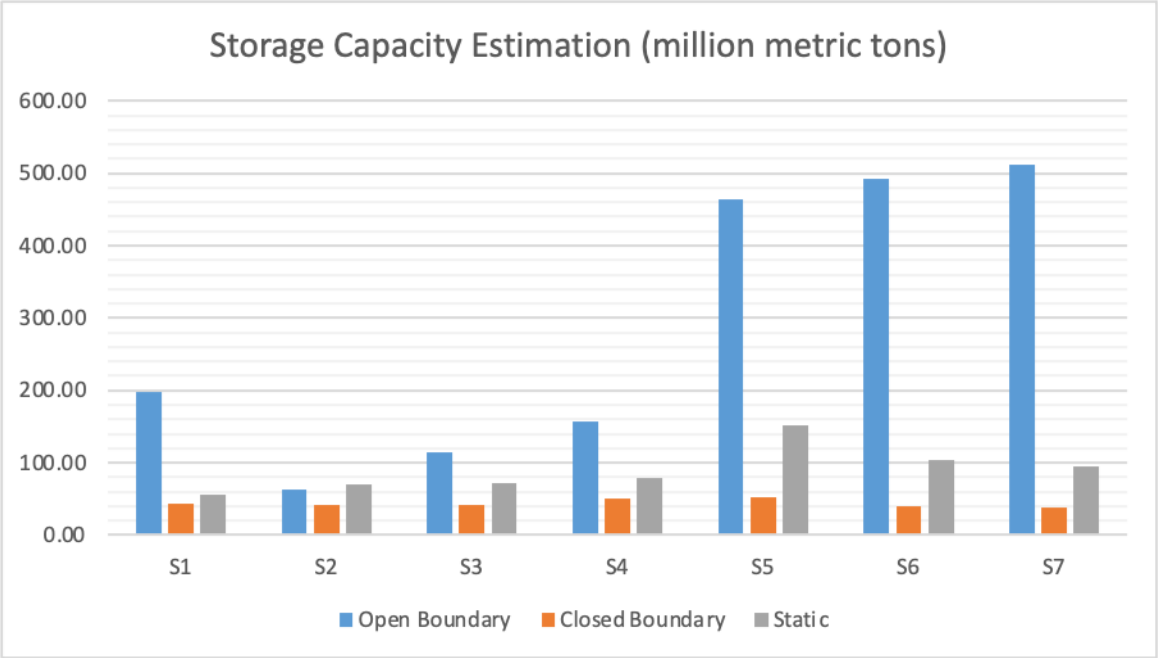

Figure 36. Comparing storage capacity from dynamic EASiTool method (open and closed boundary) and static volumetric method.

By comparing the results from all scenarios, the dynamic method with open-boundary condition gives the highest values for storage capacity while closed-boundary condition gives the lowest values. Realistically, the reservoirs are more likely to be closed boundary. From the stratal slices, the edge of a sand body could be seen as boundary, because the reservoir presence and quality are decreasing beyond the bright, high-amplitude areas. The heterogeneity within the sand bodies could also act as the impediment, preventing CO2 plume from extending freely like no boundary existed. In conclusion, 306.01 Mt is the most realistic and would be used for economic viability assessment in Chapter 4.

However, even the most conservative assumption could be an overestimation. They are major uncertainties due to lack of data. First of all, the values of porosity solely come from three wells. With the large areas of the reservoirs (260 to 480 square kilometer), more

wells would be needed to perform petrophysical analysis. Secondly, neither the Holtz (2002) or GoM MM porosity-permeability transformation is tailored to the area and interval of interest in this study. The lack of physical core data could lead to an overestimated permeability. Additionally, since the seismic volume is in time while the wells are in depth, the reservoirs mapped from seismic stratal slices and from the well logs are not tied perfectly. As mentioned in Section 3.2.1, the reservoir areas are much smaller in seismic than appeared in well logs. Hence, it is likely that the reservoir properties calculated from some wells are not correctly representing the reservoirs picked (S1 – S7). Moreover, there are risks from limited characterization of the confining system. There has been no assessment on faults' sealing capacity. Non-sealing faults could easily result in CO_2 leakage. Future work on geological characterization needs to be more precise, and more data such as physical cores need to be collected.

4. Economic Viability

From the last section, it is concluded that Chandeleur Sound Upper Miocene interval is geologically viable for large scale CCS project. The estimated storage capacity under different boundary conditions ranges from 306 to 2,000 million metric tons. Assuming using 306 Mt as the most realistic value for capacity, with a span of 30 years of injection, 10 Mt of CO_2 can be injected and stored under Chandeleur Sound per year.

In this section, I focused on allocating stationary carbon sources to the sink (Chandeleur Sound) with the results from storage capacity estimation. I first evaluated the emitters on Gulf Coast in Louisiana and Mississippi, then I reviewed the costs associated with the whole CCS supply chain, focusing on the cost of pipeline transport. Finally, I proposed a pipeline from the suitable source to Chandeleur Sound, investigated the regulations on pipeline sitting, and estimated the capital costs of proposed the pipeline.

4.1. Carbon Sources Near Chandeleur Sound

The northern coast of Gulf of Mexico is heavily industrialized. In this section, I analyze the stationary carbon sources near the sink – Chandeleur Sound using the Facility Level Information on Greenhouse Gases Tool (FLIGHT) Database developed by EPA. Figure 37 shows the facilities near Chandeleur Sound in Louisiana and Mississippi, while the grey circles indicate the carbon dioxide equivalents (CO_2e) emission in Year 2021.

522 facilities in Louisiana and Mississippi account for around 200 million metric tons of CO_2 equivalent in year 2021. The data was reported to EPA by facilities as of August 12th, 2022. In Mississippi, power generation is the biggest carbon emitter, which emitted 26 out of 40 million metric tons of CO_2e in 2021. While chemicals take the lead in the state of Louisiana and has a total CO_2e emission of 42 million metric tons (Figure 38)The biggest emitters near Chandeleur Sound include CF Industries LLC, ExxonMobil

Baton Rouge Refinery and Chemical Plant, both in Louisiana along the Chemical Corridor, and Daniel Electric Generating Plant in Mississippi. Those emitters have more than 5 Mt carbon equivalent emission in 2021. CF Industries LLC has reported carbon capture from its ammonia manufacturing, which account for over 4 Mt of annual emission in this facility (EPA, 2022).

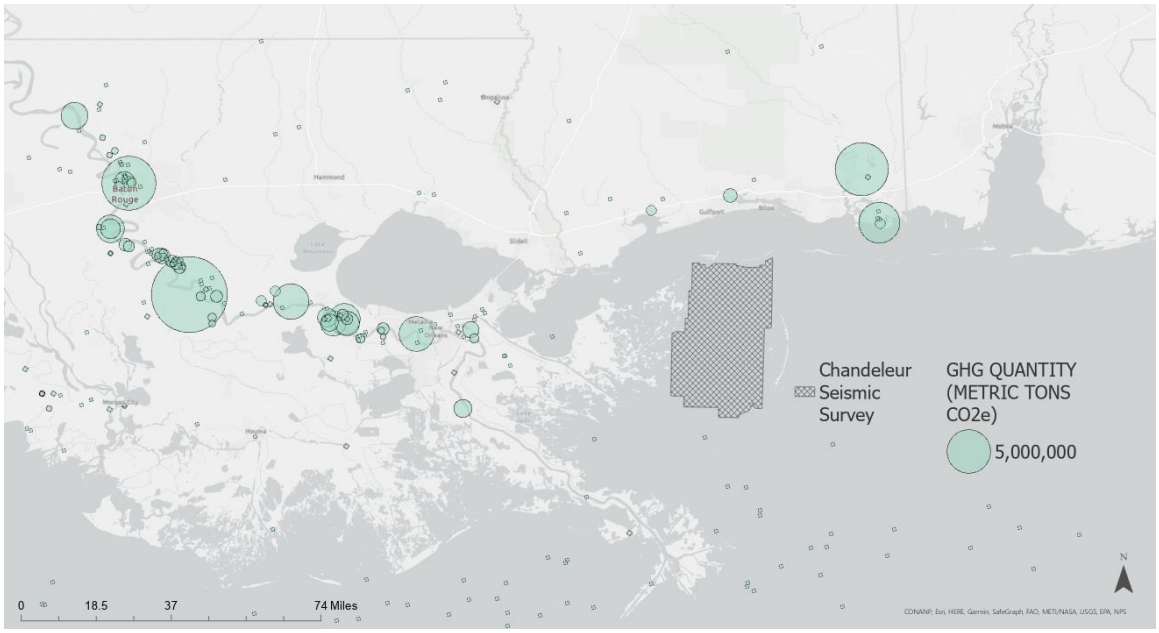

Figure 37. Point sources near Chandeleur Sound. The biggest circle indicates a CO_2e emission in 2021 of around 9 million metric tons.

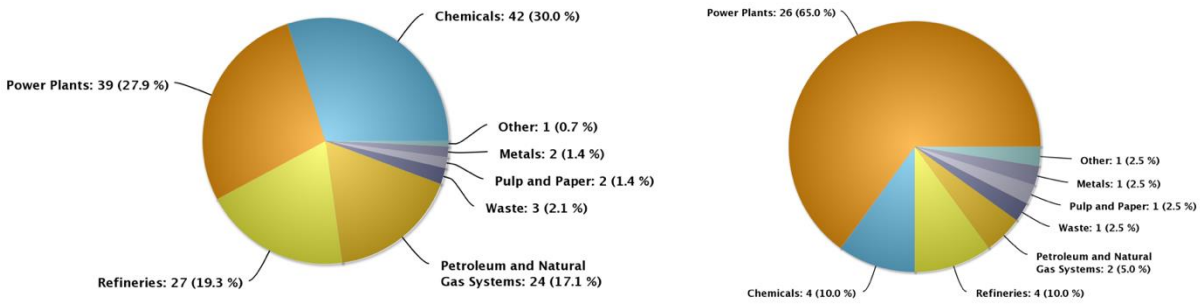

Figure 38. CO_2e emission by facility type in Louisiana (left) and Mississippi (right) (EPA, 2022).

4.2. CCS COSTS OVERVIEW

CCS has on most cases not been profitable due to high costs from different components. The costs associated with carbon capture and storage technology can vary widely depending on factors such as the location of the storage site, the type of capture technology used, and the size of the facility. For example, the cost of capturing CO_2 from power generation plants can range substantially, depending on the technology used and the location of the facility (NPC, 2019). Post-combustion capture, which involves capturing CO_2 after it is emitted from a power plant, tends to be more expensive than pre-combustion capture, which captures CO_2 before it is emitted. The cost of transporting and storing CO_2 can also vary widely, depending on factors such as the distance to the storage site and the type of storage formation. Pipeline, ship and rail are the common transport methods for carbon dioxide. Pipelines are suitable for high volume CO_2 transport while ships and rails are better options when it comes to smaller scale CCS projects (NPC 2019). However, as the technology and infrastructure improve, it is expected that the costs will decrease. Additionally, CCS can be cost-effective when paired with other technologies such as enhanced oil recovery, which can offset some of the costs.

In this section, I reviewed the costs analyses from different research for carbon capture, transport and storage from different literatures. I mainly focused on the costs for carbon transport via pipelines.

4.2.1. Capture

Carbon capture is the first step of CCS. The costs of capture vary largely depending on the facility type CO_2 concentration in the exhaust (NPC, 2019). Around 85-95% of CO_2 can be absorbed from a power plant with CCS system (Wilberforce et al., 2021). However, the CCS technology itself requires 10-40% more energy on the existing plant (Ben-Mansour et al., 2016; Plaza et al., 2012).

Carbon capture is costly. The technologies for capturing CO_2 from facilities can be classified as the following: absorption, membrane, adsorption, cryogenic processes and chemical looping (NPC, 2019; Al-Mamoori et al., 2017). Except capturing carbon dioxide form the stationary facilities, Direct Air Capture (DAC) is an emerging technology that allows carbon capture happen anywhere anytime. Since Chandeleur Sound is geologically viable for large amount of CO_2 to be injected, only stationary carbon emitters are be taken into consideration. DAC is not included in this study.

The biggest emitters near Chandeleur Sound include CF Industries LLC, ExxonMobil Baton Rouge Refinery and Chemical Plant, both in Louisiana along the Chemical Corridor, and Daniel Electric Generating Plant in Mississippi. Those emitters have more than 5 Mt carbon equivalent emission in 2021 (EPA, 2022). The carbon capture costs for power plant are generally higher than for ammonia production and refinery plants due to a lower CO_2 concentration in the exhaust. According to National Petroleum Council (2019), the unit capital costs for capturing CO_2 from ammonia plans ranges from $6-10 per

metric ton, while the number can increase to $43-72 for refineries and $33-155 for power generating plants depending on the fuel used (NPC, 2019).

4.2.2. Storage

Bump et al. introduce Common Risk Segment (CRS) mapping technique and mapped the basin-scale prospective for CO_2 storage in Gulf Coast regions, including onshore and offshore (Bump et al., 2021). It has concluded that the Gulf of Mexico has lower costs for CO_2 storage compared to other regions in the United States. Chandeleur Sound is defined as 'minimum to low costs' in terms of injecting into Middle and Upper Miocene (Bump et al., 2021).

The costs of storing carbon dioxide in saline aquifer depends on several components: geologic characteristics, the amount of CO_2 to be stored, and monitoring plans. Smith (2021) has studied thirteen reservoirs in the United States and estimated the storage costs range from $2.98 to $20.72 per tonne and the storage costs tend to be lower with higher CO_2 rate (Smith, 2021).

The latest nationwide storage costs estimation was done in house at Gulf Coast Carbon Center (Rodriguez Calzado, 2023). This study has taken regional pressure build-up and the area of sedimentary basin into consideration and concluded that the storage costs per ton of CO_2 range from $4.7 (P10) to $51.7 (P90), with the maximum storage capacity of 20 million metric tons over 20 years of injection (Rodriguez Calzado, 2023). For Gulf Coast Miocene interval, the average storage cost at 1 million tonne per annum (Mtpa) injection rate was estimated as $4 per ton CO_2, much lower than the national average (Rodriguez Calzado, 2023). However, the costs assessment in this research was focused on onshore storage. Higher storage costs associated with offshore drilling, operating and monitoring is expected in Chandeleur Sound.

4.2.3. Transport

Research conducted on natural gas pipelines can be used as a good analog for estimating the costs of CO_2 pipeline (Heddle et al., 2003; McCoy and Rubin, 2015; Parker, 2004, Rui et al., 2008). CO_2 pipelines and natural gas pipelines have some similarities in their design and construction, as they are both typically high-pressure pipelines that transport gases over long distances. However, there are also some important differences in their designs. CO_2 less explosive but more volatile and reactive than natural gas. Natural gas pipelines require a pressure below 1,480 pounds per square inch gauge (psig) while CO_2 pipeline usually operates at 1,200 to 2,200 psig (NPC, 2019). Additionally, CO_2 is often transported shorter distances than natural gas, which can reduce the overall cost of the pipeline.

Many researchers have used the costs of natural gas pipelines to construct costs model for CO_2 pipelines. The capital costs, which is the costs for pipeline construction (excluded operational and maintenance) vary with the pipeline diameter, length, regional difference (Heddle et al., 2003; Parker, 2004; McCoy and Rubin, 2008; Rui et al., 2011).

Heddle et al. (2003) research on the CO_2 transport costs includes storage options such as EOR, storing in depleted oil/gas fields, deep saline aquifer, and ocean storage. This study used the land construction and O&M costs for natural gas pipeline to estimate the CO_2 pipeline costs. It is worthwhile to point out that they have included the offshore pipeline, the transport method for CCS in Chandeleur Sound, in their research Figure 39 shows the pipeline diameter as a function of the mass CO_2 flow rate. This study concluded that the total annual costs (construction and O& M costs) per tonne CO_2 pipeline decreases when the mass flow rate increases (Heddle et al., 2003) (Figure 40).

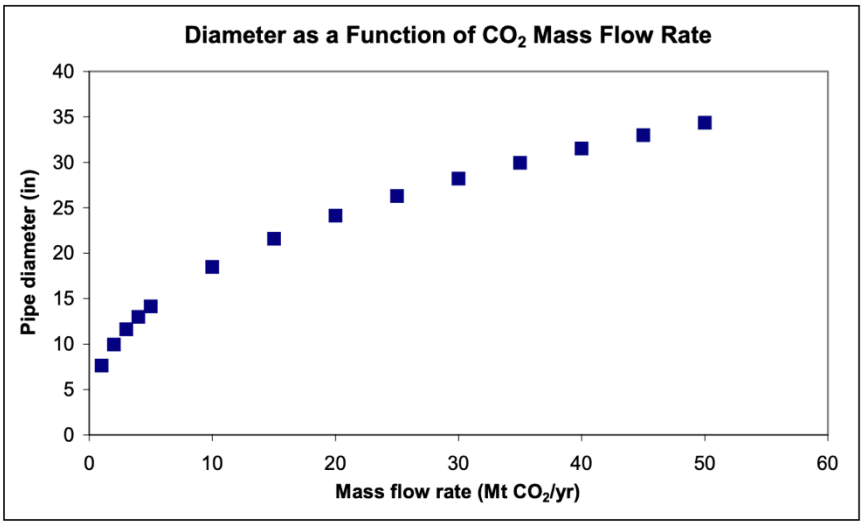

Figure 39. Pipeline diameter as a function of CO_2 mass flow rate (Heddle et al., 2003).

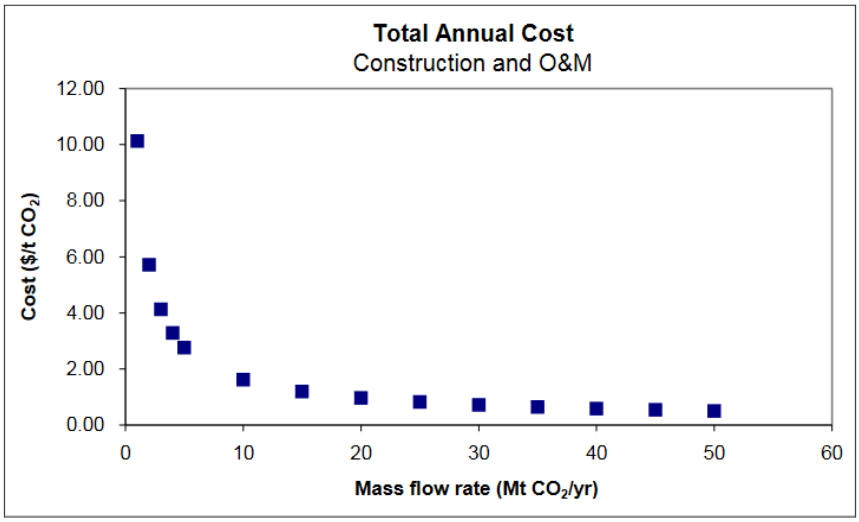

Figure 40. Pipeline total costs (construction and O&M) as a function of mass flow rate (Heddle et al., 2003).

McCoy and Rubin (2008) conducted research on how pipeline costs vary in six different regions defined by U.S. Energy Information Administration (EIA) (Figure 41) in the United States. They have concluded that the costs for 1 tonne of CO_2 in a 100-kilometer pipeline in the Midwest region is $1.16. and this cost is lower in Southwest region

(Chandeleur Sound and its nearby sources) due to lower labor costs (McCoy and Rubin, 2008).

Figure 41. Regions defined by EIA for segregating pipeline costs (McCoy and Rubin, 2008; DOE, 2022).

Parker (2004) used linear regression models and estimated the costs of hydrogen pipeline from existing gas pipeline data. The construction costs of natural gas pipelines as functions of four main capital costs components (materials, labor, ROW, miscellaneous) in terms of pipeline diameter and length are expressed as (Parker, 2004):

Materials (dia, length) = [330.5(dia)2 + 687(dia) + 26,960] (length) + 35,000

Labor (dia, length) = [343(dia)2 + 2,074(dia) +170,013] (length) + 185,000

Misc. (dia, length) = [8,417(dia) + 7,324] (length) + 95,000

Right of Way Cost (dia, length) = [577(dia)2 + 29,788] (length) + 40,000

Parker (2004) concluded that the material costs for hydrogen pipeline is 1.5 times higher than natural gas pipeline while the labor is 1.25 times more expensive for hydrogen pipeline (Parker, 2004). For CO_2 pipeline, the multipliers would be different. However, Parker (2004) does not consider the effect of regional differences on pipeline construction costs.

Rui et al. (2012) studied over 400 pipeline projects dated from 1992 to 2008 and has developed five regression models for pipelines in different sizes, lengths and regions. It is concluded that materials, labor, ROW and miscellaneous costs decrease while the diameter of the pipeline increases.

The FECM/NETL CO_2 Transport Cost Model was designed by the DOE Office of Fossil Energy and Carbon Management (FECM) and National Energy Technology Laboratory (NETL). This tool is an excel-based tool, incorporates models from Parker (2004), McCoy and Rubin (2008) and Rui et al. (2011) to estimate the costs for transporting liquid phase CO_2 by pipeline (FECM/NETL CO_2 Transport Model Description and User's Manual, 2022). Figure 42 summarizes the costs as the function of pipeline length, with 12-, 20- and 30-inches pipeline using the three models mentioned above.

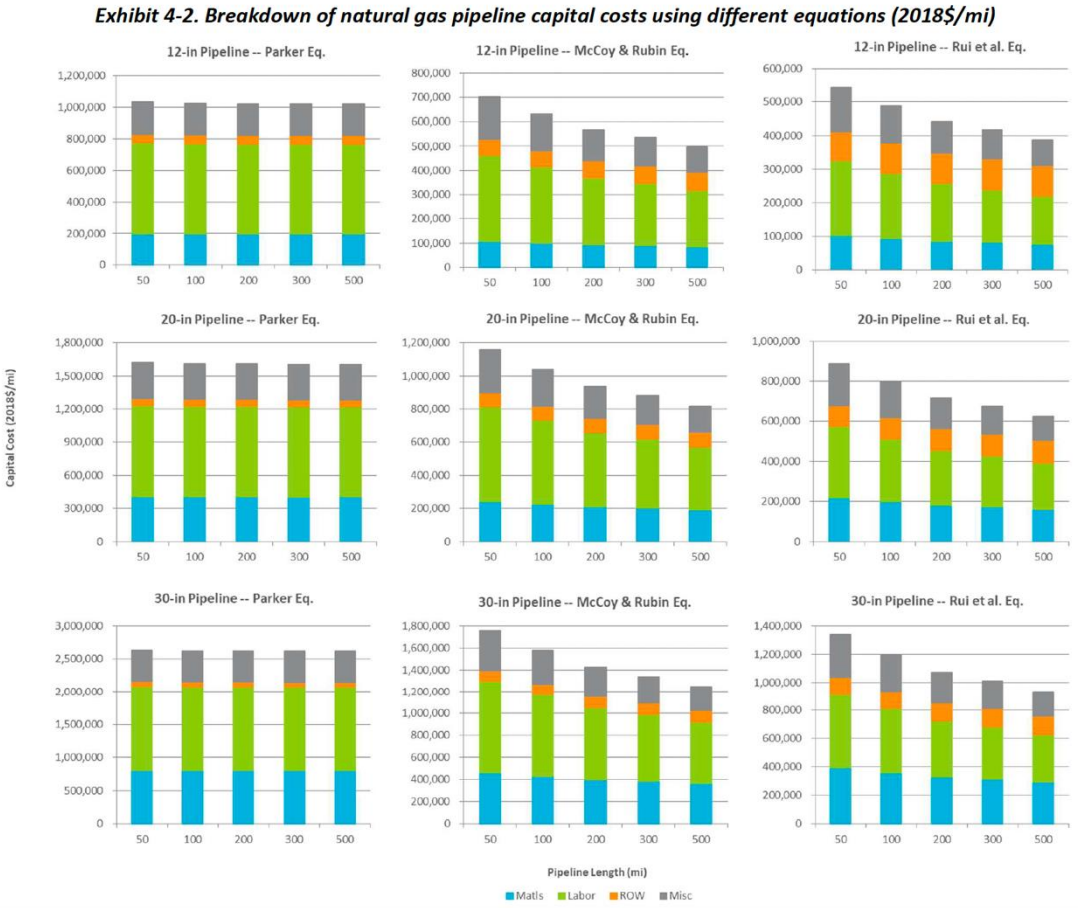

Figure 42. Comparing different models (Parker, 2004, McCoy and Rubin, 2008, and Rui et al., 2011) in FECM/NETL CO_2 Transport Costs Model (DOE, 2022).

4.3. REGULATIONS ON CO_2 PIPELINES

Pipeline is the only transport technique considered in this research. To gain the information on pipeline regulation, four government agencies were investigated along with their role on CO_2 or other types of pipelines. To install the pipeline on state water in Louisiana, right-of-way (ROW) needs to be obtained from the state agency which has the jurisdiction over the water body. The Louisiana Department of Natural Resources (LDNR) is the primary state agency responsible for managing the state's water resources and regulating the use of state-owned lands and waters. The LDNR website provides

information on the permits and approvals required for various types of activities, including pipeline construction and operation, and may provide guidance on the costs and compensation requirements associated with obtaining a right-of-way for a CO_2 pipeline on state water.

The Louisiana Public Service Commission is also responsible for pipeline especially pipeline sitting. The Louisiana Public Service Commission (LPSC) is a regulatory agency that oversees the utilities and transportation sectors in the state of Louisiana. In the context of pipelines, the LPSC has several roles and responsibilities, including regulate the rates, tariffs, and safety standards for CO_2 pipelines that operate in Louisiana. This includes reviewing and approving applications for new pipelines, as well as monitoring the safety and performance of existing pipelines. The LPSC is also responsible for reviewing the environmental impact of proposed pipelines in Louisiana, including assessing the potential impact on local ecosystems, water resources, and air quality. The LPSC conducts outreach and education efforts to inform the public about the benefits and risks of pipelines, and to solicit input from stakeholders on proposed projects. In addition, The LPSC works with other regulatory agencies at the state and federal level to ensure that pipelines in Louisiana are following all relevant laws and regulations.

Additionally, the Federal Energy Regulatory Commission (FERC) is the federal agency responsible for regulating interstate pipelines and may also provide guidance on the regulations and requirements related to the construction and operation of natural gas pipelines. The FERC website provides information on the regulatory process for pipeline projects, including the environmental and socioeconomic impact assessments and the public participation process. However, FERC does not regulate carbon dioxide pipelines.

The Department of Transportation (DOT) Pipeline and Hazardous Materials Safety Administration (PHMSA) is responsible for ensuring the safe and secure transportation of

hazardous materials, including carbon dioxide through pipeline in the United States. PHMSA plays an important role in ensuring that pipeline operators comply with the regulations and requirements for pipeline design, construction, operation, maintenance, and emergency response planning. PHMSA establishes and enforces the standards and regulations for CO_2 pipeline safety under the federal level. Specifications regarding CO_2 pipeline design and sitting can be found under 49 C.F.R. §195.

PHMSA specifies that the pipeline ROW should be selected to avoid areas that contain private dwelling, industrial buildings, and places of public assembly. Pipeline itself should not be located within 50 feet (15 meters) of any of those areas mentioned above unless it is provided at least 12 inches (305 millimeters) of cover (49 C.F.R. §195.210). That says, there is generally no absolute restriction in terms of where a pipeline cannot be built on, if additional mitigation plans are provided. High Consequence Areas (HCAs), which include commercially navigable waterways, high populated areas (at least 1,000 people per square mile), other populated areas and Unusually Sensitive Areas (USAs), was defined under 49 C.F.R. §195.450. USAs include drinking water and ecological resources. Figure 43 shows an example of USAs near Chandeleur Sound. Chandeleur Sound and its surroundings fit into every criterion under the HCA definition, extra attention and mitigation plans need to be provided to secure a safe, public acceptable CO_2 pipeline project.

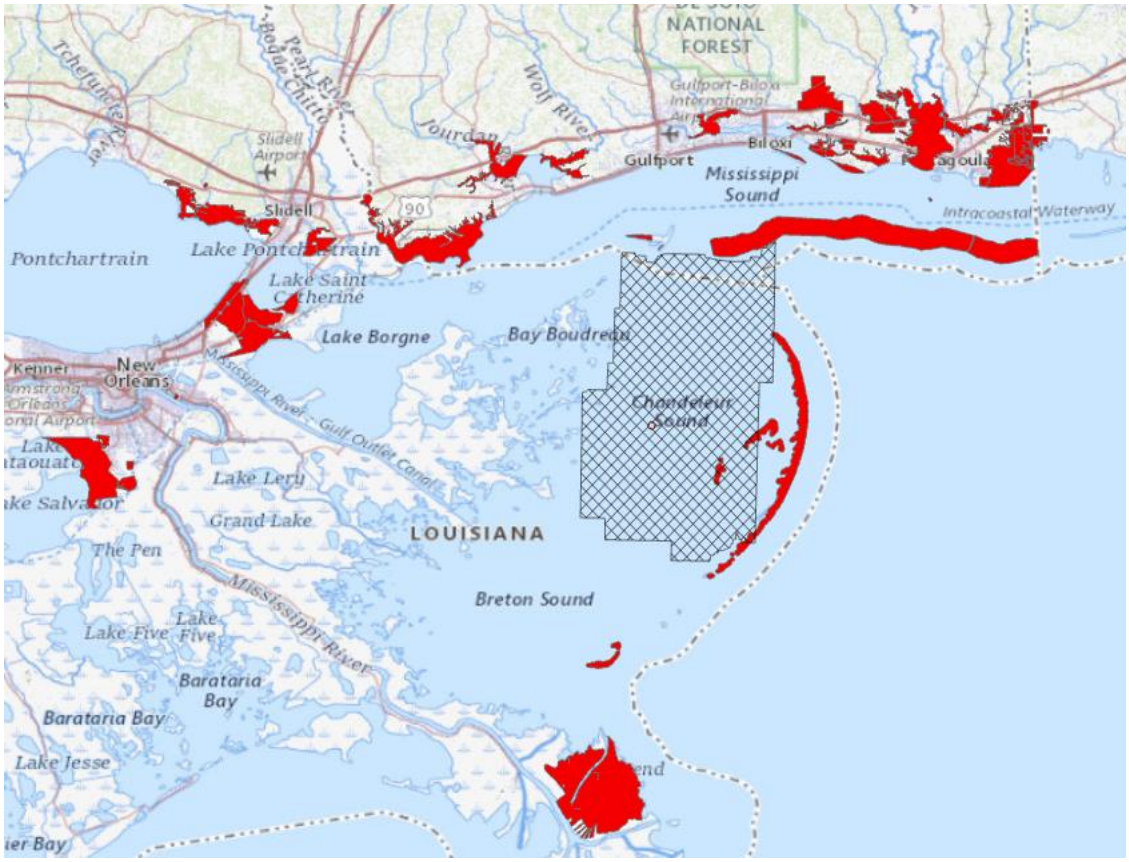

Figure 43. Marine protected areas in red (NOAA, 2022) as Unusually Sensitive Areas.

4.4. CHANDELEUR PIPELINE COSTS ESTIMATION

As the conservative estimation of storage capacity of Chandeleur is 306.01 million metric tons, if injection period is set to 30 years, the injection rate and carbon flow rate would be 10 Mt/yr. A CCS hub could be designed and shared with multiple sources within an industrial cluster. CCS hub allows multiple carbon sources to share the transportation infrastructure and store the CO_2 in one or multiple sinks (Global CCS Institute, 2016).

The first approach I used to calculate pipeline construction costs is using the FECM/NETL CO_2 Transport Costs Model. Assuming the CO_2 gathering hub is located at the biggest emitter: CF Industries Nitrogen, LLC, the storage hub is located at the central

Chandeleur Sound, where the net sand is the thickest. A straight-line pipeline from the source to sink has a length of 115.37 miles (Figure 44). With the length, CO_2 flow rate, and injection period confirmed, the FECM/NETL model calculated a pipeline diameter of 20 inches. Table 6 summarizes the capital costs in 2023 dollars for the proposed pipeline using three cost models. Parker's model gives the highest construction costs estimation, around 273 million dollars, while McCoy and Rubin's model has similar estimations on all the components of capital costs.

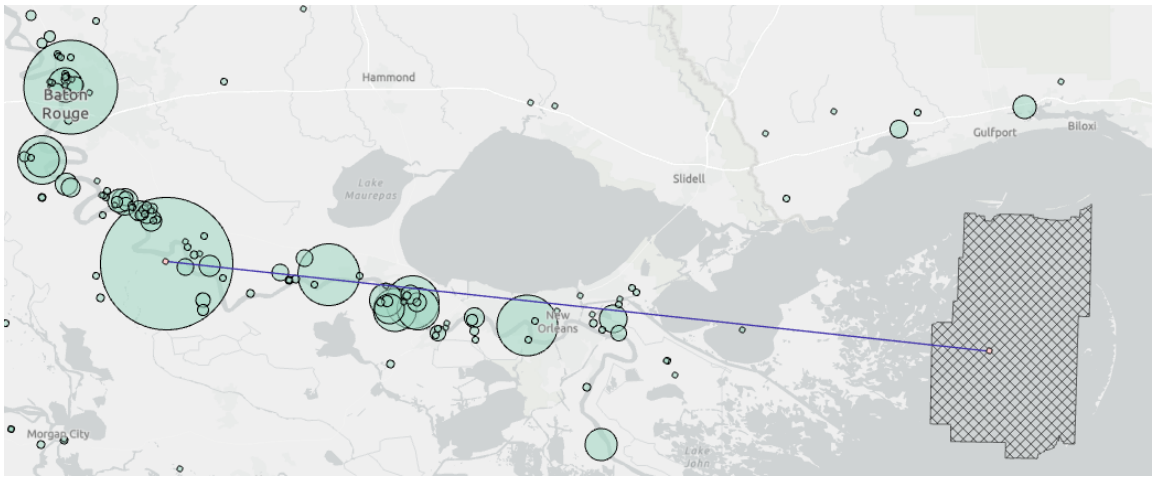

Figure 44. Straight-line pipeline from CF Industries Nitrogen LLC. To Chandeleur Sound.

	Parker	McCoy and Rubin	Rui et al.
Materials	$ 59,824,581	$ 32,870,731	$ 31,830,417
Labor	$ 121,002,768	$ 44,401,000	$ 43,077,299
ROW	$ 7,782,117	$ 10,584,751	$ 12,578,299
Miscellaneous	$ 40,091,569	$ 27,227,101	$ 25,065,154
CO2 Surge Tanks	$ 1,616,184	$ 1,616,184	$ 1,616,184
Pipeline Control System	$ 145,301	$ 145,301	$ 145,301
Pumps	$ 6,923,719	$ 6,923,719	$ 6,923,719
Contingency	$ 35,607,936	$ 18,565,318	$ 18,185,456
Capital Costs (2023$)	**$ 272,994,174**	**$ 142,334,104**	**$ 139,421,829**

Table 6. Breakdown of pipeline construction costs using three models.

The capital costs estimated from the FECM/NETL model are likely to be underestimations because the model does not include the offshore pipeline building scenarios. The second approach – Terrain Based Costs Model was used for pipeline capital costs estimation. Southeast Louisiana has a high variety of land cover type, which include barren land, agriculture land, swamp and marsh, and different level of populated areas. A pipeline costs metrics was proposed by Kinder Morgan (Layne, 2009). In order to compare the terrain-based costs with the value estimated from FECM/NETL mode, the unit cost ($/mi-in) for each terrain type was adjusted using the CPI Inflation Calculator from U.S. Bureau of Labor Statistics (2016) (Table 7).

Terrain	Capital Cost ($/in-mi)	Capital Cost in 2023$ ($/in-mi)
Flat, dry	$50,000.00	$70,845.35
Mountainous	$85,000.00	$120,437.10
Marsh, wetland	$100,000.00	$141,690.70
River	$300,000.00	$425,072.11
High population	$100,000.00	$141,690.70
Offshore (150 ft - 200 ft depth)	$700,000.00	$991,834.92

Table 7. Pipeline capital cost metrics, modified from Layne (2009).

The National Land Cover Database (NLCD) from the U.S. Geological Survey (USGS). This data contains the time-series land cover layers from 2001 to 2019 with a spatial resolution of 30 meter (USGS, 2021). I extracted the 2019 land cover data and grouped the types by the terrain type specified in the Kinder Morgan costs metrics table. I have classified barren land, all forest types, shrub or scrub, grassland or herbaceous, pasture or hay, and cultivated crops into the 'flat, dry' terrain type; all developed spaces into 'high population'; all wetland types into 'marsh, wetland', and open water into 'offshore'. The straight-line pipeline route with a length of 115.37 miles and a diameter of 20 inches results in $1,140,457,126.70in 2023's dollars.

The straight-line pipeline route has a long portion that is located offshore, as we can see from Figure 44, which could be the main reason that the terrain-based costs for this route is high.

A least cost path was generated based on the terrain type (Figure 45). This path automatically routes on the terrains with minimum total costs, while keeping the total length as short as possible. The length of the path is 122.06 miles.

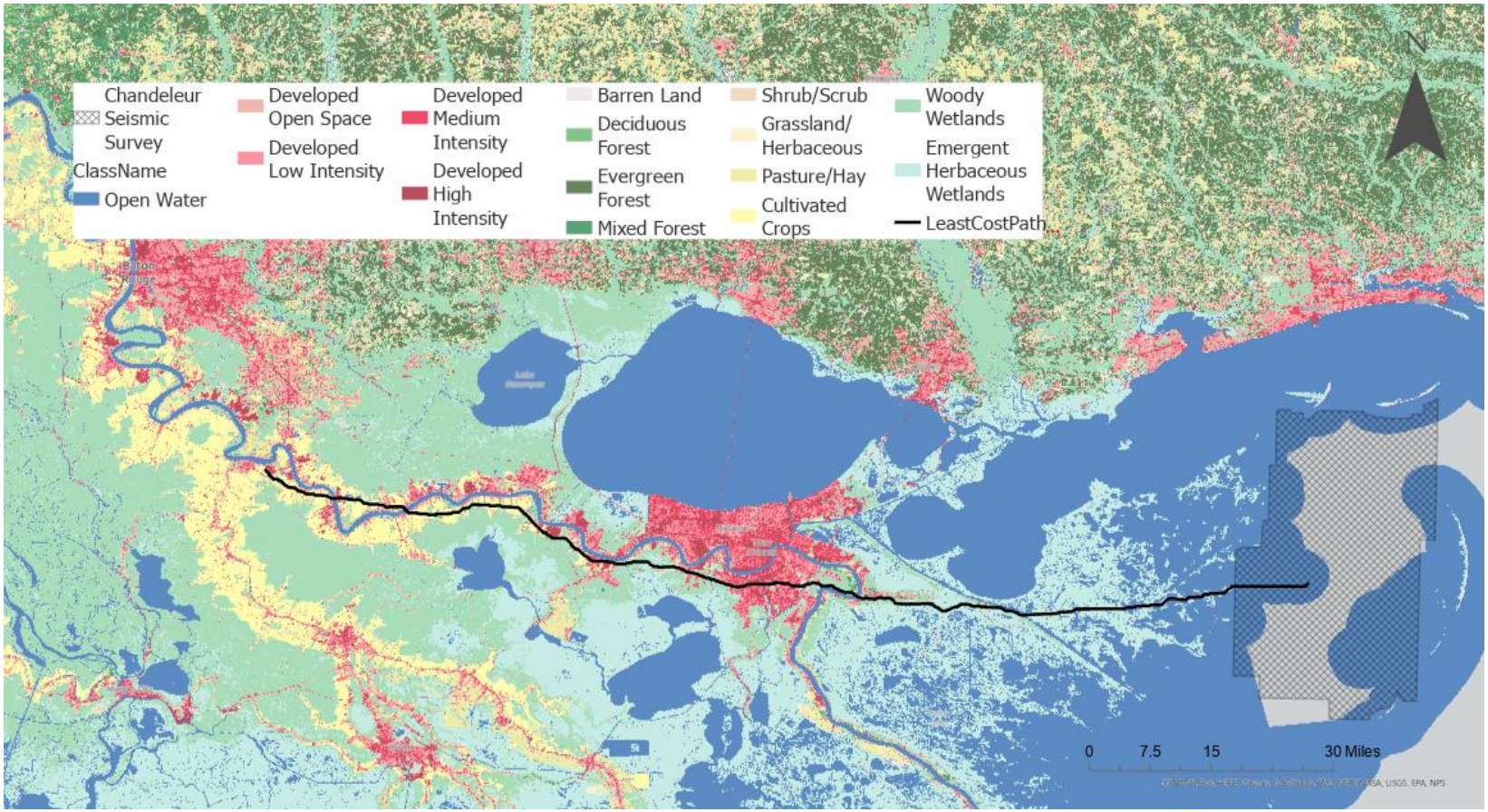

Figure 45. Least cost path from terrain-based pipeline costs metrics. Land cover data retrieved from USGS (2021).

The least costs path significantly reduced the costs compared to the straight-line path, with a total capital cost of $494,684,507.82. Table 8 summarize the construction costs on each land type from both straight line and least costs path approaches.

			Straight Line			**Least Cost Path**		
Land Cover	Terrain Type	Capital Cost in 2023$ ($/mi-in)	Cell Count	Length (mi)	Total Costs ($)	Cell Count	Length (mi)	Total Costs ($)
Open Water	Offshore	$991,834.92	2651	49.42	$980,329,634.93	705	13.14	$260,693,904.57
Developed Open Space	High population	$141,690.70	98	1.83	$5,185,879.62	472	8.80	$24,933,641.43
Developed Low Intensity		$141,690.70	511	9.53	$27,006,247.42	443	8.26	$23,401,701.60
Developed Medium Intensity		$141,690.70	474	8.84	$25,050,915.76	212	3.95	$11,199,008.44
Developed High Intensity		$141,690.70	238	4.44	$12,582,134.16	118	2.20	$6,233,410.36
Barren Land	Flat, dry	$70,845.35	21	0.39	$552,593.73	61	1.14	$1,611,178.10
Deciduous Forest		$70,845.35	1	0.02	$28,338.14	66	1.23	$1,743,241.88
Evergreen Forest		$70,845.35	2	0.04	$56,676.28	64	1.19	$1,690,416.37
Mixed Forest		$70,845.35	8	0.15	$212,536.05	227	4.23	$5,995,695.56
Shrub or Scrub		$70,845.35	1	0.02	$28,338.14	169	3.15	$4,463,755.72
Grassland or Herbaceous		$70,845.35	10	0.19	$269,212.33	75	1.40	$1,980,956.68
Pasture or Hay		$70,845.35	55	1.03	$1,459,414.21	976	18.19	$25,778,849.62
Cultivated Crops		$70,845.35	353	6.58	$9,323,248.06	1189	22.16	$31,404,766.59
Woody Wetlands	Marsh, wetland	$141,690.70	739	13.78	$39,049,956.92	340	6.34	$17,960,673.91
Emergent Herbaceous Wetlands		$141,690.70	1025	19.11	$54,154,185.54	1431	26.68	$75,593,306.97
Total			6189	115.37	$1,155,289,311.29	6548	122.06	$494,684,507.82

Table 8. Terrain based costs summary: straight line and least cost path.

4.5. DISCUSSION

Section 5 introduced the economic viability for CO_2 storage in Chandeleur Sound. There is no doubt that plenty of CO_2 sources can be considered. With the storage capacity calculated from previous section, a CCS hub can be built near the biggest emitter to gather CO_2 from itself and other facilities within the industrial cluster. The costs related to CCS was evaluated, focusing on the construction/capital costs on pipeline as the transport method. Two methods were used to estimate the pipeline costs: using the FECM/NETL CO_2 Pipeline Costs Model and a Terrain-based Costs Metrics. Table 9 summarizes the total costs, unit cost in terms of length and diameter, and unit cost in terms of per tonne CO_2.

	2023$	Total Cost ($)	Unit Cost ($/mi-in)	Unit Cost ($/tonne)
FECM/NETL CO_2 Transport Cost Model	**Parker**	$272,994,174.05	$118,312.46	$0.91
	McCoy and Rubin	$142,334,104.20	$61,685.93	$0.47
	Rui et al.	$139,421,829.44	$60,423.78	$0.46
Terrain Type	**Straight Line**	$1,155,289,311.29	$500,688.79	$3.85
	Least Cost Path	$494,684,507.82	$202,639.89	$1.65

Table 9. Capital costs for Chandeleur Sound CO_2 pipeline using different approaches.

Kaiser (2017) has studied twelve offshore FERC pipeline projects over the 1995 – 2012 period. The projects have actual or estimated construction costs range from $68.500 to $649.300 per mile-inch in 2023$ (Table 10).

Project	Year	Diameter (in)	Length (mi)	2014 Cost ($1000/mi)	2023 Cost ($1000/mi)	2023 Unit Costs ($/mi-in)
Stingray Vermillion (E)	1995	20	15.6	$1,086	$1,388.95	$69,447.50
Stingray Garden Banks (E)	1996	20	15.5	$1,103	$1,410.70	$70,535.00
Discovery	1997	30	105	$1,952	$2,496.54	$83,218.00
Garden Banks	1997	30	50.5	$1,860	$2,378.87	$79,295.67
Nautilus	1997	30	101	$1,607	$2,055.29	$68,509.67
Dauphin Island Phase 1 (E)	1997	24	65	$1,584	$2,025.88	$84,411.67
Destin	1998	36	73	$4,296	$5,494.43	$152,623.06
Mobile Bay Expansion	1998	24	56.6	$2,561	$3,275.43	$136,476.25
Main Pass Lateral (E)	1998	24	13	$1,583	$2,024.60	$84,358.33
Stingray East Cameron (E)	1998	16	12.9	$2,325	$2,973.59	$185,849.38
Destin (Gemini)	1999	24	31	$2,494	$3,189.73	$132,905.42
Texas Eastern	2000	24	9.7	$2,130	$2,724.19	$113,507.92
Gulfstream	2002	36	430	$2,719	$3,477.50	$96,597.22
Ocean Express (E)	2002	24	46.1	$3,272	$4,184.77	$174,365.42
Islander East (E)	2003	24	22.8	$4,776	$6,108.33	$254,513.75
Seafarer (E)	2005	26	29.4	$2,595	$3,318.91	$127,650.38
Triple T	2007	24	6.2	$8,293	$10,606.44	$441,935.00
Algonquin	2007	24	16.4	$12,185	$15,584.17	$649,340.42
Gulfstream IV	2008	20	17.7	$5,303	$6,782.34	$339,117.00
South Timbalier (E)	2012	30	20	$3,321	$4,247.44	$141,581.33

Table 10. FERC offshore pipeline projects and their unit costs. (E) indicates estimated costs. Source: FERC Reports. Modified from Kaiser (2017).

The costs for Chandeleur Sound pipeline can be compared with the FERC pipelines (Figure 46).by comparing the unit costs ($/mi-in), Rui et al. and McCoy and Rubin's models gave the results lower than the lowest value in FERC projects' costs. Parker's cost is the closest to the median value. Terrain based-Least Cost Path (LCP) estimated the unit cost beyond 75% percentile while Terrain (straight line) is too high and considered an outlier.

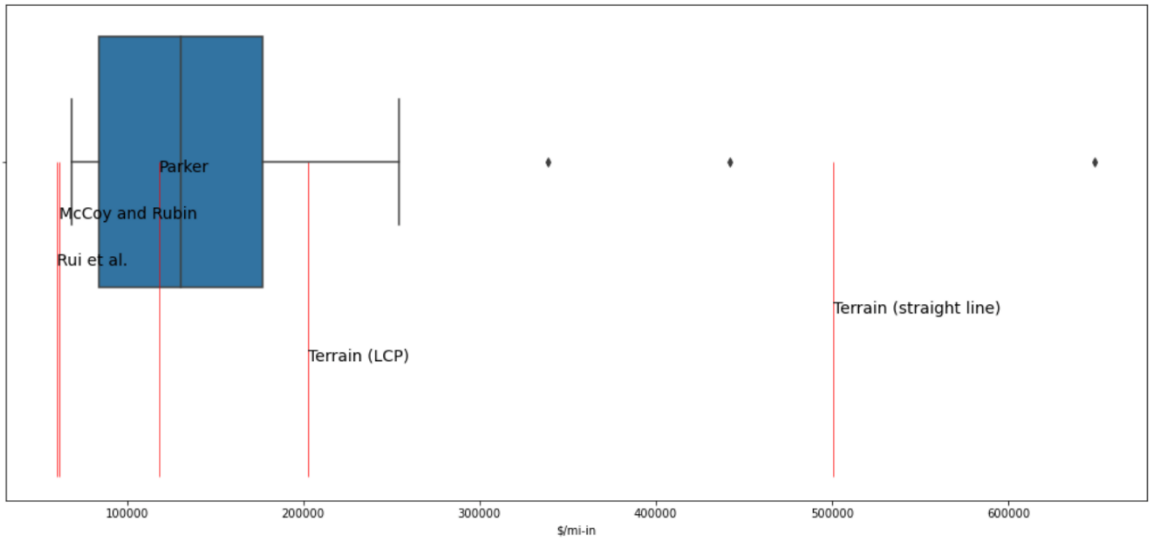

Figure 46. Box plot of FERC offshore pipeline construction costs, with estimated Chandeleur Sound pipeline costs (red lines).

Pipeline costs estimation for Chandeleur Sound from all approaches have limitations. The capital costs per tonne CO_2 estimated from FECM/NETL model are all below $1/tonne, which are considered as underestimations because the model has assumed the pipelines are onshore. The Terrain-based cost model has its shortcomings. First, the matching between NLCD land cover types and the Kinder Morgan costs metrics is general. For example, in the land cover layer, rivers and offshore regions are both classified as 'open water', while the costs for these two types are different in the cost metrics. Second, the costs related to regulation restriction are not included when routing the pipeline. In addition, neither of the methods considered the costs associated with CCS hub building.

Taking into consideration the preliminary nature of the assessment on construction costs for CO_2 pipelines in Chandeleur Sound study area, it is important to note that actual costs could be higher than estimated. The potential high capital costs, combined with risks such as corrosion, permissive water levels, and high operating costs, have led to the abandonment of several projects in the past (Onyebuchi et al., 2018). Despite these

challenges, carbon transport via pipelines remains a promising technology for reducing global emissions, especially with the increasing need for carbon capture and storage solutions. As the industry continues to advance in both technology and policy, addressing challenges and improving operational efficiencies will be crucial for ensuring the success and sustainability of carbon transport via pipelines. Studies have shown that existing pipelines, such as natural gas pipelines, can be repurposed for CO_2 transport (JGC, 2019). Implementing pipeline networks for large-scale CCS projects has proven to be more cost-effective, reducing operational costs and mitigating risks (Zapantis et al., 2019). Moreover, recent policy developments have increased the Q45 incentive to $85 per tonne for capturing CO_2 from point sources and storing it in saline aquifers (Inflation Reduction Act of 2022). With the advancement of technologies and policies supporting CCS and the use of existing pipelines, carbon transport via pipelines offers a safe and efficient solution for reducing global emissions. As we continue to work towards a more sustainable future, the role of carbon transport via pipelines will remain crucial in our efforts to combat climate change.

5. Conclusions and Future Work

5.1. CONCLUSIONS

In this research, I have assessed the geological viability for CO_2 storage in Chandeleur Sound. Seismic and well logs analysis have been done proving that there is sufficient storage capacity in this area. Stratal Slicing was performed on the 3D seismic survey. Methods such as RMS Amplitude and Sum Negative Amplitude determined that the southern shelf of Upper Miocene tend to have sand-prone high amplitude reflections. Spectral Decomposition showed the detailed morphology within the seismic survey and revealed some channel system where sand is likely to be deposited. One major channel system above the horizon of Top of Upper Miocene, possibly to be the ancient Tennessee River Delta has a bright reflection. Low amplitude appears in northern Upper Miocene and Middle Miocene shelf, especially in the mass transport complex within Middle Miocene Canyon. Ideal storage intervals observed from seismic are the southern Upper Miocene shelf, with sand-prone lobate geometries, and the major channel system near the top of Upper Miocene. The areas for the high-amplitude strata shown in attribute maps are estimated to be 280 to 480 square kilometers.

Well analysis enabled more detailed information for the ideal storage intervals. Well logs correlations have been done and net sand maps have been constructed. From the dip-oriented well log correlation cross section, it is clear that the sand bodies tend to thin to the south (basin-ward). The net sand map showing the whole Upper Miocene interval estimates that most sand clustered at the middle to southwest of Chandeleur Sound. Seven continuous sand bodies were observed and named to be the reservoir candidates. Three wells were chosen for petrophysical analysis. The values of effective porosity for seven reservoirs range from 23% to 31%. With the porosity values obtained, permeability can be

calculated using an unpublished transformation, and the value range from 11 to 452 millidarcy. Due to the limited number of wells, the geology condition at the northern Chandeleur Sound remains unknown. The primary trapping mechanism for CO_2 would be residual trapping. Bump et al. (2023) has shown that a composite confining system can retain large amount of carbon dioxide. The shale layers on top of each sand body can prevent CO_2 from migrating vertically.

Static and dynamic storage capacity analysis were done using the CO_2 storage capacity for the whole interval (including S1, S2, S3, S4, S5, S6, S7) ranges from 306 million metric tons to 2 gigaton. The boundary condition is the main variable affecting the capacity. The estimation of 306.06 Mt under closed-boundary condition was be used in economic analysis.

Chandeleur Sound does not lack of carbon sources to match with the storage capacity. Stationary carbon sources data is obtained from the EPA Flight Database. CF Industries Nitrogen LLC. is the largest emitter near Chandeleur Sound, and it has been selected as the carbon gathering hub. It has assumed that 10 Mt of CO_2 would be transported in a 20-inch, around 120-mile-long pipeline from the hub to central Chandeleur Sound each year, throughout a 30-year period. The total capital costs of the pipeline ranges from $140 million to $1.16 billion based on the method used. This translates to a unit cost for construction ranges from $60, 423 to $500,689 per mile-inch or $0.46 to $3.85 per metric ton CO_2 transported.

5.2. FUTURE WORK

Future works on assessing CO_2 storage viability in Chandeleur Sound is needed. For geologic characterization, I recommend creating more time-depth tables to tie the wells and seismic volume. It would be beneficial to conduct fault offset analysis and seal capacity

estimation in order to provide a more accurate security for the storage system. In this study, only three wells have been used for petrophysical porosity calculation. More wells could be used for petrophysical analysis in order to obtain more accurate reservoir properties. For future CCS costs estimation, in-depth analysis on capture and storage is encouraged. Moreover, more CO_2 transport methods such as transporting by ships could be taken into consideration. It is crucial to conduct detailed analysis on state level regulations in terms of pipeline sitting. Last but not least, Environmental Justice (EJ) has become a big topic in terms of CCS. EJ considerations should be included in future work.

Appendix

Horizon	Age (Ma)	177272012900	177302001400	177270023600	177270015600	177270012800	177270012900	177272049000	177270017300	177262002000	##########
Upper Miocene	5.33										
Bigenerina A	7.39							4640			
Marcie's "UM" p	N/A	3774	3086	3400	3901	4472	4530	4740	4647	4995	5017
Discorbis 12	9.18					5360	5220		5020		
Textularia L	9.71			5130						6120	
Bigenerina 2/C.	10.63				5470	6050	5970		6250	6960	
Middle Miocene	11.63	6080	4940	5218	6239	7570	7730	7420	8360	8713	7640
Textularia W	12.02				6670						
Fohsella lobata	12.24										9870
Fohsella fohsi	12.65	8570				9060			9690		
Bigenerina hum	12.98			6330	7600						
Fohsella periphe	13.16	9020		6990							
Cristellaria opim	14.46			7600							
Lower Miocene	15.97	9155	7023	7616							

Table i. Paleo-stratigraphic markers and their depths on wells (feet) within Chandeleur Sound (Phillips, personal communication).

References

Agartan, E., Trevisan, L., Cihan, A., Birkholzer, J., Zhou, Q., & Illangasekare, T. H. (2015). Experimental study on effects of geologic heterogeneity in enhancing dissolution trapping of supercritical CO_2. Water Resources Research, 51(3), 1635-1648. doi: 10.1002/2014WR015778.

Ajayi, T., Gomes, J.S., & Bera, A. (2019). A review of CO_2 storage in geological formations emphasizing modeling, monitoring and capacity estimation approaches. Pet. Sci., 16, 1028-1063.

Al Hameli, F., Belhaj, H., & Al Dhuhoori, M. (2022). CO_2 Sequestration Overview in Geological Formations: Trapping Mechanisms Matrix Assessment. Energies, 15(20), 7805. doi: 10.3390/en15207805

Al-Mamoori, A., Krishnamurthy, A. A., Rownaghi, A., & Rezaei F. (2017). Carbon Capture and Utilization Update. Energy Technol. 5, 834.

Bachu, S. (2003). Screening and ranking of sedimentary basins for sequestration of CO_2 in geological media in response to climate change. Env Geol 44, 277–289. doi: 10.1007/s00254-003-0762-9

Bachu, S. (2008). CO_2 storage in geological media: Role, means, status and barriers to deployment. Energy Conversion and Management, 49(8), 2178-2190.

Bachu, S., Bonijoly, D., Bradshaw, J., Burruss, R., Holloway, S., Christensen, N. P., & Mathiassen, O. M. (2007). CO_2 storage capacity estimation: Methodology and gaps. International Journal of Greenhouse Gas Control, 1(4), 430-443. doi: /10.1016/S1750-5836(07)00086-2.

Bachu, S., Bonijoly, D., Bradshaw, J., Burruss, R., Holloway, S., Christensen, N. P., & Mathiassen, O. M. (2007). CO_2 storage capacity estimation: Methodology and gaps. International Journal of Greenhouse Gas Control, 1(4), 430-443.

Beaumont, E. A., & Foster, A. H. (1999). Treatise of Petroleum Geology/Handbook of Petroleum Geology: Exploring for Oil and Gas Traps. The American Association of Petroleum Geologists. Pages 9-1 - 9-154.

Beckham, E. C. (2018). CO_2 storage in deltaic environments of deposition: integration of 3- dimensional modeling, outcrop analysis, and subsurface application. (Master's Thesis). The University of Texas at Austin.

Ben-Mansour, R., Habib, M., Bamidele, O., Basha, M., Qasem, N., Peedikakkal, A., Laoui, T., & Ali, M. (2016). Carbon capture by physical adsorption: materials, experimental investigations and numerical modeling and simulations–a review. Appl. Energy, 161, 225-255.

Bennion, D. B., Bachu, S. (2008a). Drainage and imbibition relative permeability relationships for supercritical CO_2/brine and H_2S/brine systems in intergranular sandstone, carbonate, shale, and anhydrite rocks. SPE Reservoir Evaluation & Engineering, 11 (3) (2008), pp. 487-496. doi: 10.2118/99326-PA

Berggren, W. A., Kent, D. V., Swisher III, C. C., & Aubry, M.-P. (1995). A revised Cenozoic geochronology and chronostratigra-phy, in W. A. Berggren, D. V. Kent, M. P. Aubry, and J. Har-denbol, eds., Geochronology, time scales and global strati-graphic correlation: Society for Sedimentary Geology Special Publication 54, p. 129–212.

Bhattacharya, S. (2022). Unpublished data.

Bhattacharya, S. (2023). Personal communication.

Bigelow, E.L. (1992). Introduction to Wireline Log Analysis. Western Atlas International Inc., Houston, Texas.

Bump, A., Bakhshian, S., Ni, H., Hovorka, S., Olariu, M. I., Dunlap, D., Hosseini, S. & Meckel, T. (2023). Composite Confining Systems: Rethinking Geologic Seals for Permanent CO_2 sequestration. Available at SSRN: https://ssrn.com/

Bump, A.P., Hovorka, S.D., & Meckel, T.A. (2021). Common risk segment mapping: Streamlining exploration for carbon storage sites, with application to coastal Texas and Louisiana. International Journal of Greenhouse Gas Control, 111, 103457. doi: 10.1016/j.ijggc.2021.103457.

Burke, L. A., Kinney, S. A., Dubiel, R. F., & Pitman, J. K. (2012). Regional map of the 0.70 psi/ft pressure gradient and development of the regional geopressure-gradient model for the onshore and offshore Gulf of Mexico basin, U.S.A. Gulf Coast Association of Geological Societies Journal, 1, 97–106.

Chang, Y.B., Coats, B.K., & Nolen, J.S. (1981). A compositional model for CO_2 floods including CO_2 solubility in water. In Proceedings of the Permian Basin Oil and Gas Recovery Conference, Midland, TX, USA, 12 March 1981. Midland, TX, USA: OnePetro. (March 1996).

Choudhary, P. (2016). Carbon Capture and Storage Program (CCSP) Final report 1.1.2011–31.10.2016.

Christie, C. H., & Nagihara, S. (2016). Geothermal gradients of the northern continental shelf of the Gulf of Mexico. Geosphere, 12(1), 26–34. doi: 10.1130/GES01163.1

Coleman, J.M., Prior, D.B., & Lindsay, J.F. (1983). Deltaic influences on shelf edge instability processes. SEPM Special Publication no. 33, 121-137.

DeAngelo, M. (n.d.). Unpublished data.

Department of Energy. (2022). FECM/NETL CO_2 Transport Model Description and User's Manual.

Department of Energy. (n.d.). 9.1.1. Carbon Dioxide Capture Approaches. https://netl.doe.gov/research/coal/energy-systems/gasification/gasifipedia/capture-approaches

Dewitz, J., & U.S. Geological Survey. (2021). National Land Cover Database (NLCD) 2019 Products (ver. 2.0, June 2021). U.S. Geological Survey data release. doi: 10.5066/P9KZCM54

Du Rochet, J. (1981). Stress fields, a key to oil migration. American Association of Petroleum Geologists Bulletin, 65, 74-85.

Dunlap, D. (2022). Unpublished data.

Eliis. (2021). PaleoScan User Guide.

Fisher, W.L., Galloway, W.E., Steel, R.J., Olariu, C., Kerans, C., & Mohrig, D. (2021). Deep-water depositional systems supplied by shelf-incising submarine canyons: Recognition and significance in the geologic record. Earth-Science Reviews, 214, 103531. doi: 10.1016/j.earscirev.2021.103531

Galloway, W. E., Ganey-Curry, P., Li, X., & Buffler, R. T. (2000). Cenozoic depositional history of the Gulf of Mexico basin. AAPG Bulletin, 84(11), 1743–1774. doi: 10.1306/8626C37F-173B-11D7-8645000102C1865D

Galloway, W. E., Whiteaker, T. L., & Ganey-Curry, P. (2011). History of Cenozoic North American drainage basin evolution, sediment yield, and accumulation in the Gulf of Mexico basin. Geosphere, 7(4), 938–973. doi: 10.1130/GES00647.1

Galloway, W.E. (2008). Depositional evolution of the Gulf of Mexico sedimentary basin. In K.J. Hsü (Ed.), Sedimentary basins of the world, Volume 5, The sedimentary basins of the United States and Canada (A.D. Miall, Ed.). Elsevier. 505-549.

Ganjdanesh, R., & Hosseini, S. A. (2017). Geologic carbon storage capacity estimation using enhanced analytical simulation tool (EASiTool). Energy Procedia, 114, 4690–4696. doi: 10.1016/j.egypro.2017.03.1624

Garcia, O. R. (2019). Geologic characterization and modeling for quantifying CO_2 storage capacity of the High Island 10-L field in Texas state waters, offshore Gulf of Mexico. (Master's thesis). The University of Texas at Austin.

Global CCS Institute. (2018). The global status of CCS Institute.

Global CCS Institute. (2022). Storing Carbon Dioxide. https://www.globalccsinstitute.com/about/what-is-ccs/storage

Goodman, A., Hakala, A., Bromhal, G., Deel, D., Rodosta, T., Frailey, S., & et al. (2011). US DOE methodology for the development of geologic storage potential for carbon

dioxide at the national and regional scale. International Journal of Greenhouse Gas Control, 5, 952–965. doi: 10.1016/j.ijggc.2011.05.005

Hartmann, D.J. (1999). Predicting reservoir system quality and performance. Exploring for Oil and Gas Traps, 9, 1-154.

Heddle, G., Herzog, H., & Klett, M. (2003). The economics of CO_2 storage. Massachusetts Institute of Technology Laboratory for Energy and the Environment, MIT LFEE 2003-003 RP, 115.

Hentz, T. and Zeng, J. (2003). High-Frequency Miocene Sequence Stratigraphy, Offshore Louisiana: Cycle Framewodk and Influence on Production Distribution in a Mature Shelf Province: *AAPG Bulletin*. 87 (2): 197-230

Holloway S., Savage D., 1993. The potential for aquifer disposal of carbon dioxide in the UK. Energy Convers Manage 34:925–32

Holtz, M. H. (2002). Residual gas saturation to aquifer influx: a calculation method for 3-D computer reservoir model construction. Presented at the SPE Gas Technology Symposium, Calgary, Alberta, Canada. 2002/1/1/. doi: 10.2118/75502-MS.

Hossain, S. (2020). Application of seismic attribute analysis in fluvial seismic geomorphology. Journal of Petroleum Exploration and Production Technology, 10, 1009–1019. doi: 10.1007/s13202-019-00809-z

Hosseini, S. A. (n.d.). EASiTool – User Manual – V4.0.

Hosseini, S. A., Ganjdanesh, R., & Kim, S. (2018). Enhanced Analytical Simulation Tool (EASiTool) for CO_2 Storage Capacity Estimation and Uncertainty Quantification (No. DE-FE0009301). The University of Texas at Austin.

International Energy Agency, 2019. STEPS: the Stated (Energy) Policies Scenario." Source: World Energy Outlook, Introduction, p. 29

International Energy Agency. (2019). World Energy Outlook 2019. Retrieved from https://www.iea.org/reports/world-energy-outlook-2019. CC BY 4.0 license.

International Energy Agency. (2022). Carbon capture, utilisation and storage. Retrieved from https://www.iea.org/fuels-and-technologies/carbon-capture-utilisation-and-storage.

IPCC, 2014. Climate Change 2014: Synthesis Report. Contribution of Working Groups I, II and III to the Fifth Assessment Report of the Intergovernmental Panel on Climate Change [Core Writing Team, R.K. Pachauri and L.A. Meyer (eds.)]. IPCC, Geneva, Switzerland, 151 pp. in IPCC ARS Synthesis Report website.

Izgec, O., Demiral, B., Bertin, H., & Akin, S. (2007). CO_2 Injection into Saline Carbonate Aquifer Formations II: Comparison of Numerical Simulations to Experiments. Transport in Porous Media, 73, 57-74. doi: 10.1007/s11242-007-9160-1.

Jenkins, C., Chadwick, A., & Hovorka, S. D. (2015). The state of the art in monitoring and verification—Ten years on. International Journal of Greenhouse Gas Control, 40, 312-349. doi: 10.1016/j.ijggc.2015.05.009

JGC Corporation. (2019). CO_2 transport demonstration. Presented at the Japan CCS Forum, June 2019.

Laughlin, K., Garossino, P., & Partyka, G. (2002). Spectral decomposition applied to 3D. AAPG Explorer, 23, 28–31.

Martin, R.G., & Bouma, A.H. (1978). Physiography of Gulf of Mexico. In A.H. Bouma, G.T. Moore, & J.M. Coleman (Eds.), Framework, Facies, and Oil Trapping Characteristics of the Upper Continental Margin. American Association of Petroleum Geologists Studies in Geology 7, 3-19.

McCoy, S., & Rubin, E. (2008). An engineering-economic model of pipeline transport of CO_2 with application to carbon capture and storage. International Journal of Greenhouse Gas Control, 2(2), 219-229.

Meckel, T., Trevino, R., Hovorka, S., (2018). Offshore CCS in the Gulf of Mexico, with Emphasis on the Inner-Shelf Cenozoic Stratigraphy of Texas, USA. 14th Greenhouse Gas Control Technologies Conference Melbourne 21-26 October 2018. (GHGT-14), SSRN: https://ssrn.com/abstract=3365784 or doi: 10.2139/ssrn.3365784

Mercer, J.W. and Cohen, R.M. (1990). A Review of Immiscible Fluids in the Subsurface: Properties, Models, Characterization and Remediation. Journal of Contaminant Hydrology, 6, 107-163. doi: 10.1016/0169-7722(90)90043-G

Nagihara, S., & Smith, M. A. (2008). Regional overview of deep sedimentary thermal gradients of the geopressured zone of the Texas–Louisiana continental shelf. AAPG Bulletin, 92(1), 1–14. doi: 10.1306/08070706111

National Oceanic and Atmospheric Administration (2022). NOAA's Marine Protected Areas Inventory.

National Petroleum Council. (2019). Meeting the Dual Challenge: A Roadmap to At-scale Deployment of Carbon Capture, Use, and Storage.

Onyebuchi, V.E., Kolios, A., Hanak, D.P., Biliyok, C., & Manovic, V. (2018). A systematic review of key challenges of CO_2 transport via pipelines. Renewable and Sustainable Energy Reviews, 81(Part 2), 2563-2583. doi; 10.1016/j.rser.2017.06.064

Parker, N. (2004). Using Natural Gas Transmission Pipeline Costs to Estimate Hydrogen Pipeline Costs. UC Davis: Institute of Transportation Studies. Retrieved from https://escholarship.org/uc/item/2gk0j8kq.

Partyka, G., Gridley, J., & Lopez, J. (1999). Interpretational applications of spectral decomposition in reservoir characterization. The Leading Edge, 18, 353-360.

Phillips, M. P. (2022). Carbon Storage Potential in the GOM [PowerPoint slides]. Institute of Geophysics, The University of Texas at Austin. https://www.beg.utexas.edu/files/gccc/2022/04%20PurkeyPhillips_Chandeleur_SECARB-GoMCarb%20Joint%20CCS%20Meet_May2022.pdf

Phillips, M. P. (2022). Personal communication.

Plaza, M., González, A., Pevida, C., Pis, J., & Rubiera, F. (2012). Valorisation of spent coffee grounds as CO_2 adsorbents for postcombustion capture applications. Applied Energy, 99, 272-279.

Rodriguez Calzado, E. (2023). Estimating CO2 Storage Capacity, Injectivity, and Storage Costs for Large-Scale CCS Deployment & Carbon Removal Goals. (Master's Thesis). The University of Texas at Austin.

Ruiz, I. (2019). Characterization of the High Island 24L Field for Modeling and Estimating CO_2 Storage Capacity in the Offshore Texas State Waters, Gulf of Mexico. (Master's thesis). The University of Texas at Austin.

Salvador, A. (1987). Late Triassic-Jurassic Paleogeography and Origin of Gulf of Mexico Basin. AAPG Bulletin, 71(4), 419–451. doi: 10.1306/94886EC5-1704-11D7-8645000102C1865D

Smith, E. (2021). The Cost of CO_2 Transport and Storage in Global Integrated Assessment Modeling. (Master's thesis). Massachusetts Institute of Technology.

Smith, E., Morris, J., Kheshgi, H., Teletzke, G., Herzog, H., & Paltsev, S. (2021). The cost of CO_2 transport and storage in global integrated assessment modeling. International Journal of Greenhouse Gas Control, 109, 103367. doi: 10.1016/j.ijggc.2021.103367.

Snedden, J., & Galloway, W. (2019). The Gulf of Mexico Sedimentary Basin: Depositional Evolution and Petroleum Applications. Cambridge University Press. doi: 10.1017/9781108292795

Stuart, C. A. (1960). Geopressures. Shell Oil Company, New Orleans, LA.

Text - H.R.5376 - 117th Congress (2021-2022): Inflation Reduction Act of 2022. (2022, August 16). https://www.congress.gov/bill/117th-congress/house-bill/5376/text

Trevisan, L., Cihan, A., Fagerlund, F., Agartan, E., Mori, H., Birkholzer, J. T., Zhou, Q., & Illangasekare, T. H. (2014). Investigation of mechanisms of supercritical CO_2 trapping in deep saline reservoirs using surrogate fluids at ambient laboratory conditions. International Journal of Greenhouse Gas Control, 29, 35-49. ISSN 1750-5836. doi: 10.1016/j.ijggc.2014.07.012.

U.S. Environmental Protection Agency (2022). Facility Level Information on Greenhouse Gases Tool (FLIGHT). Retrieved from https://ghgdata.epa.gov/ghgp/main.do?site_preference=normal

Ulfah, M. (2021). Plume Migration and Pressure Evolution Analyses for Recommendations in Offshore CO2 Storage Acreage Leasing Policy. (Master's Thesis). The University of Texas at Austin.

Uroza, C. (2022). Personal communication.

Vail, E. R., Todd, R. G., & Sangree, J. B. (1977). Seismic stratigraphy and global changes of sea level, Part 5: Chronostratigraphic significance of seismic reflections. In C. E. Payton (Ed.), Seismic Stratigraphy (pp. 99-116). American Association of Petroleum Geologists.

Wallace, K. J., Meckel, T. A., Carr, D. L., Treviño, R. H., & Yang, C. (2014). Regional CO_2 sequestration capacity assessment for the coastal and offshore Texas Miocene interval. Greenhouse Gas Science and Technology, 4, 53-65. doi: 10.1002/ghg.1380

Wilberforce, T. A., Olabi, A. G., Sayed, E. T., Elsaid, K., & Abdelkareem, M. A. (2021). Progress in carbon capture technologies. Science of The Total Environment, 761, 143203. doi: 10.1016/j.scitotenv.2020.143203

Wu, X., (2004). Upper Miocene depositional history of the Central Gulf of Mexico basin. (Ph.D. dissertation). The University of Texas at Austin.

Zapantis, A., Townsend, A., and Rassool, D. (2019). "Policy Priorities to Incentivise Large Scale Deployment of CCS." Thought Leadership Report. Global CCS Institute.

Zeng, H. (1994). Facies-guided 3D seismic modeling and reservoir characterization. Ph.D. dissertation, University of Texas at Austin.

Zeng, H. (2010). Stratal slicing: Benefits and challenges. The Leading Edge, 29(9), 1040-1047.

Zeng, H., Backus, M. M., Barrow, K. T., & Tyler, N. (1998). Stratal slicing, part I: realistic 3D seismic model. Geophysics, 63(2), 502-513.

Zheng, C. Y. C. (2022). Personal communication.

49 C.F.R. §195.